Available online at www.sciencedirect.com
SCIENCE DIRECT®
Coordination Chemistry Reviews 249 (2005) 919–969
COORDINATION CHEMISTRY REVIEWS
www.elsevier.com/locate/ccr

Review

Lanthanides and actinides: annual survey of their organometallic chemistry covering the year 1999

Jochen Gottfriedsen, Frank T. Edelmann*

Chemisches Institut der Otto-von-Guericke-Universität Magdeburg, Magdeburg, Germany

Received 2 October 2004
Available online 16 December 2004

Contents

Keywords: Actinides; Lanthanides; Scandium; Cyclopentadienyl complexes; Crystal structures

* Corresponding author. Fax: +49 3916712933.
E-mail address: frank.edelmann@vst.uni-magdeburg.de (F.T. Edelmann).

doi:10.1016/j.ccr.2004.10.005

1. Introduction

The review presents complexes of the lanthanides and actinides, as well as scandium and yttrium complexes containing metal–carbon bonds as defined by Section 29 of Chemical Abstracts. Abstracts of papers presented at conferences, dissertations, highlights and patents have been excluded.

2. Scandium and yttrium, and lanthanides

2.1. Complexes without supporting cyclopentadienyl and cyclopentadienyl-like ligands

2.1.1. Alkyl, alkenyl, alkynyl and CO complexes

A reversible fixation of ethylene at a samarium center in a calixpyrrol–samarium complex was reported by Gambarotta and co-workers [1]. The reduction of Sm(III) complexes [(R_8-calixpyrrol)ClSm{Li(THF)}$_2${Li(THF)$_2$}(μ_3-Cl)] (R = Et or {–$(CH_2)_5$–}$_{0.5}$) with lithium gave dark green solutions in both cases (Scheme 1). The resulting complex is dependent from the aliphatic substitution at the calixpyrrol-ring. The compounds [(R_8-calixpyrrol)(L)Sm{Li(THF)}$_2$ {Li(THF)$_2$}(μ_3-X)(Et_2O)$_{1.5}$] (R = {–$(CH_2)_5$–}$_{0.5}$, X = Cl, L = THF; R = Et, X = $OCHCH_2$, L = Et_2O) react with ethylene forming the ethylene-bridged complexes {[(R_8-calixpyrrol)[(CH_2CHO)Li][Li(THF)]$_2$Sm](μ-CH_2CH_2)} (R = {–$(CH_2)_5$–}$_{0.5}$ or R = Et). The magnetical moment of the compound R = {–$(CH_2)_5$–}$_{0.5}$ shows the complete oxidation to a Sm(III) species.

Single-crystal X-ray determinations revealed a Sm–C–C–Sm center with a relatively long carbon–carbon distance of 1.487 Å (Fig. 1).

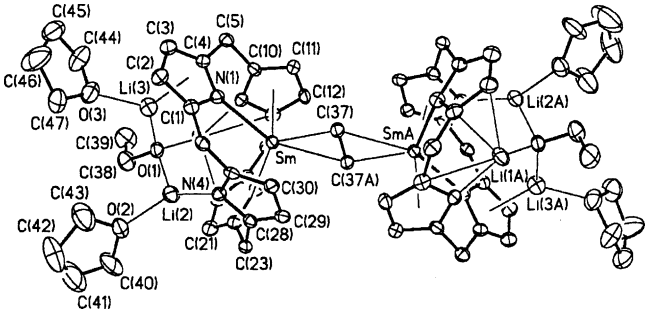

Fig. 1. Molecular structure of {[(Et_8-calixpyrrol)[(CH_2CHO)Li][Li(THF)]$_2$Sm](μ-CH_2CH_2)}.

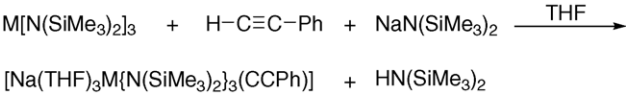

Scheme 2. Synthesis of [$Na(THF)_3M\{N(SiMe_3)_2\}_3$(C≡C–Ph)] (M = Ce, Sm, Eu).

Dehnicke et al. reported the reaction of ethynylbenzene with the trisamides M[$N(SiMe_3)_2]_3$ (M = Ce, Sm, Eu) in the presence of $NaN(SiMe_3)_2$ in THF under formation of the complexes [$Na(THF)_3M\{N(SiMe_3)_2\}_3$(CCPh)] [2] according to Scheme 2.

A single-crystal X-ray structure determination of [$Na(THF)_3Sm\{N(SiMe_3)_2\}_3$(C≡C–Ph)] revealed the presence of an ion pair in which the terminal carbon atom of the C≡C–Ph^- ligand is connected with the samarium atom of the Sm[$N(SiMe_3)_2]_3$ group. The sodium ion is side-on connected with the acetylido group (Fig. 2).

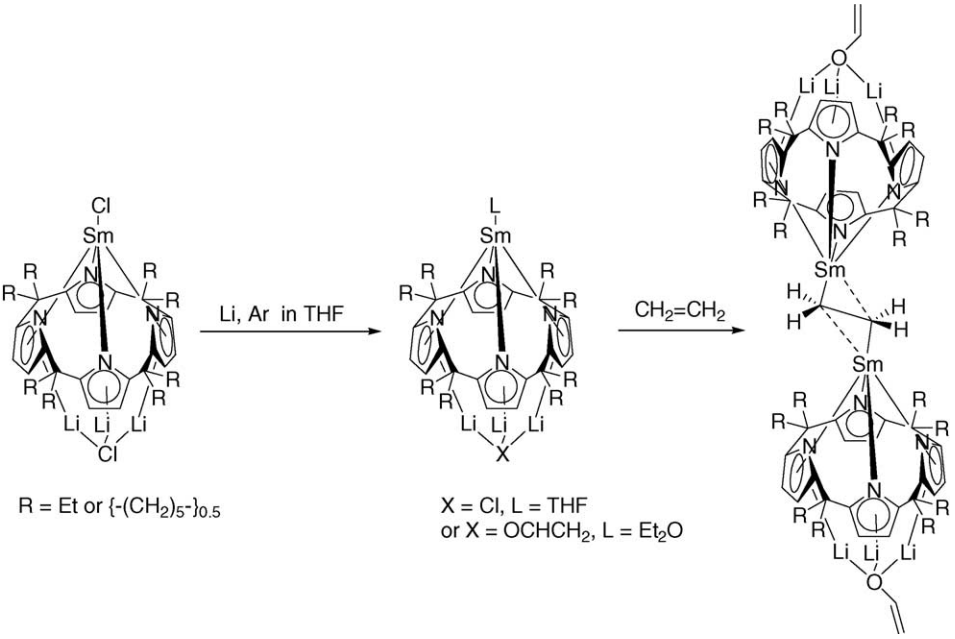

Scheme 1. Synthesis of {[(R_8-calixpyrrol)[(CH_2CHO)Li][Li(THF)]$_2$Sm](μ-CH_2CH_2)} (R = {–$(CH_2)_5$–}$_{0.5}$ or R = Et).

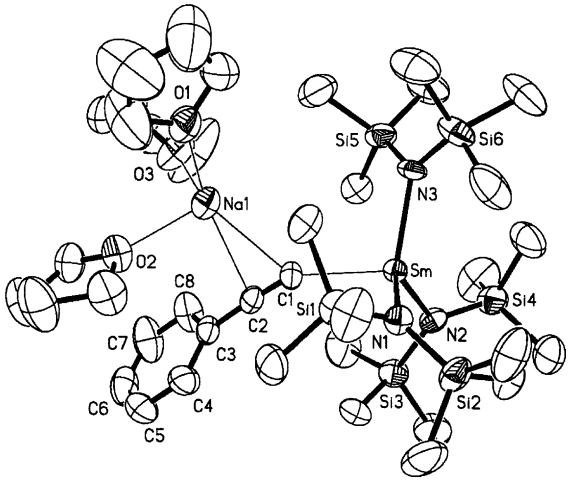

Fig. 2. Molecular structure of $[Na(THF)_3Sm\{N(SiMe_3)_2\}_3(C{\equiv}C{-}Ph)]$.

The distance between the Sm center and the terminal C of the acetylido ligand is 2.485 Å and is understandable as a strongly polar Sm···C bond. $[Na(THF)_3Sm\{N(SiMe_3)_2\}_3(C{\equiv}C{-}Ph)]$ does not polymerize methyl metacrylate but is catalyzing the ring opening polymerization of ε-caprolactone or δ-valerolactone.

Zang and Wang used a cerium acetylido compound (Scheme 3) for a C–C coupling reaction at a ring carbonyl center [3].

Bochkarev and co-workers reported the synthesis of homoleptic phenylethynyl derivatives of lanthanides by simple exchange reactions [4]. The reaction of LnI_2 or LnI_3 with PhC≡CNa in tetrahydrofuran was used for the preparation of the phenylethynyl derivatives $(PhC{\equiv}C)_2Ln(THF)_x$ (Ln = Sm, Yb; $x = 1, 2$) and $(PhC{\equiv}C)_3Ln(THF)_x$ (Ln = Pr, Nd, Dy, Ho, Er, Lu; $x = 1, 2$), respectively. They also reported studies of different reactions of the di- and triphenyllanthanides $Ph_2Yb(THF)_2$ and $Ph_3Ln(THF)_3$ (Ln = Ho, Tm, Yb) [5]. Reactions with H_2O, PhC≡CH, C_5H_6, HgX_2 and I_2 were performed. The phenyl derivatives of the lanthanides are highly reactive towards these agents and form the expected products in high yields.

The group of Kovba and co-workers published the characterization of the structure and the spectra of holmium complexes formed in the CO matrix [6]. The equilibrium geometry configurations and high-frequency IR spectra for the complex HoCO were characterized by ab initio quantum chemical calculations.

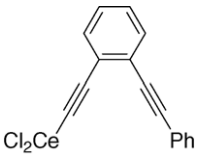

Scheme 3. Cerium acetylido compound.

2.1.2. Metallacarborane complexes

Xie et al. presented a series of metallacarborane complexes in different articles. The first organolanthanide compound containing an η^7-carboranyl ligand, $[\{[\eta^5{:}\eta^7\text{-}Me_2C(C_5H_4)(C_2B_{10}H_{11})]Er\}_2\{Na_4(THF)_9\}]_n$, has been achieved by treatment of $[\eta^5\text{-}Me_2C(C_5H_4)(C_2B_{10}H_{11})]ErCl_2(THF)_3$ or $[\{[\eta^5{:}\eta^6\text{-}Me_2C(C_5H_4)(C_2B_{10}H_{11})]Er\}_2(THF)_2$ with excess Na metal in THF [7]. The Na^+ ions in $[\{[\eta^5{:}\eta^7\text{-}Me_2C(C_5H_4)(C_2B_{10}H_{11})]Er\}_2\{Na_4(THF)_9\}]_n$ can be replaced by Er^{3+} ions, giving the tetranuclear cluster $[\{\eta^5{:}\eta^7\text{-}Me_2C(C_5H_4)(C_2B_{10}H_{11})\}Er_2(\mu\text{-}Cl)(THF)_3\}]_2$. The polymeric nature of $[\{[\eta^5{:}\eta^7\text{-}Me_2C(C_5H_4)(C_2B_{10}H_{11})]Er\}_2\{Na_4(THF)_9\}]_n$, has been confirmed by a single-crystal X-ray analysis, which reveals two $[\{[\eta^5{:}\eta^7\text{-}Me_2C(C_5H_4)(C_2B_{10}H_{11})]Er^{2-}$ structural motifs in each asymmetrical unit. The asymmetrical units are linked to each other via B–H–Er bonds to form an infinitive polymeric chain ((b) in Fig. 3).

The Me_2Si-bridged cyclopentadienyl/carboranyl ligand systems can be generated by reaction of $Me_2Si(C_5H_5)Cl$ with 1 equiv. of $Li_2C_2B_{10}H_{10}$ and subsequent hydrolysis, giving $Me_2Si(C_5H_5)(C_2B_{10}H_{11})$ [8]. $Me_2Si(C_5H_5)(C_2B_{10}H_{11})$ can be conventionally converted into the monoanion $Na[Me_2Si(C_5H_4)(C_2B_{10}H_{11})]$, the dianion $Li_2[Me_2Si(C_5H_5)(C_2B_{10}H_{10})]$, and the trianion $K_3[Me_2Si(C_5H_4)(C_2B_{10}H_{11})]$ by treatment with NaH, MeLi and K metal in THF at room temperature, respectively. $Na[Me_2Si(C_5H_4)(C_2B_{10}H_{11})]$ reacts with 1 equiv. of $LnCl_3$ in THF yielding the dichlorides $[\eta^5\text{-}Me_2Si(C_5H_4)(C_2B_{10}H_{11})]LnCl_2(THF)_3$ (Ln = Nd, Sm, Er, Yb). Single-crystal X-studies reveal a monomeric structure for the dichloro complexes (Fig. 4). The cyclopentadienyl ligand is bonded to the Yb center in η^5-fashion. The coordination sphere of the metal center is saturated by the two chlorine atoms and three THF molecules.

Treatment of $LnCl_3$ with 2 equiv. of $Na[Me_2Si(C_5H_4)(C_2B_{10}H_{11})]$ or reaction of the dichloro complexes $[\eta^5\text{-}Me_2Si(C_5H_4)(C_2B_{10}H_{11})]LnCl_2(THF)_3$ with an equimolar amount of $Na[Me_2Si(C_5H_4)(C_2B_{10}H_{11})]$ in THF results in the isolation of the monochlorides $Me_2Si(C_5H_4)(C_2B_{10}H_{11})]_2LnCl(THF)_2$ (Ln = Nd, Sm, Y, Gd, Yb). The solid-state structure of $[\eta^5\text{-}Me_2Si(C_5H_4)(C_2B_{10}H_{11})]_2SmCl(THF)_2$ reveals a distorted trigonal–bipyramidal geometry at the metal center with two η^5-bonded cyclopentadienyl rings, one chloride ion and two THF molecules (Fig. 5).

Interaction of $Li_2[Me_2Si(C_5H_5)(C_2B_{10}H_{10})]$ with $LnCl_3$ in THF in a molar ratio 1:1 or 2:1 or reaction of $Me_2Si(C_5H_4)(C_2B_{10}H_{11})]_2LnCl(THF)_2$ with 2 equiv. of MeLi in THF gives the same compounds $[\{\eta^5{:}\sigma\text{-}Me_2Si(C_5H_4)(C_2B_{10}H_{10})]\}_2Ln][Li(THF)_4]$ (Ln = Nd, Y, Er, Yb). The solid-state structure of $[\{\eta^5{:}\sigma\text{-}Me_2Si(C_5H_4)(C_2B_{10}H_{10})]\}_2Er][Li(THF)_4]$ shows well-separated, alternating layers of the discrete tetrahedral cation $Li(THF)_4^+$ and anion $[\{\eta^5{:}\sigma\text{-}Me_2Si(C_5H_4)(C_2B_{10}H_{10})]\}_2Er]^-$ (Fig. 6). In the anion, the Er center is η^5-bonded to each of two

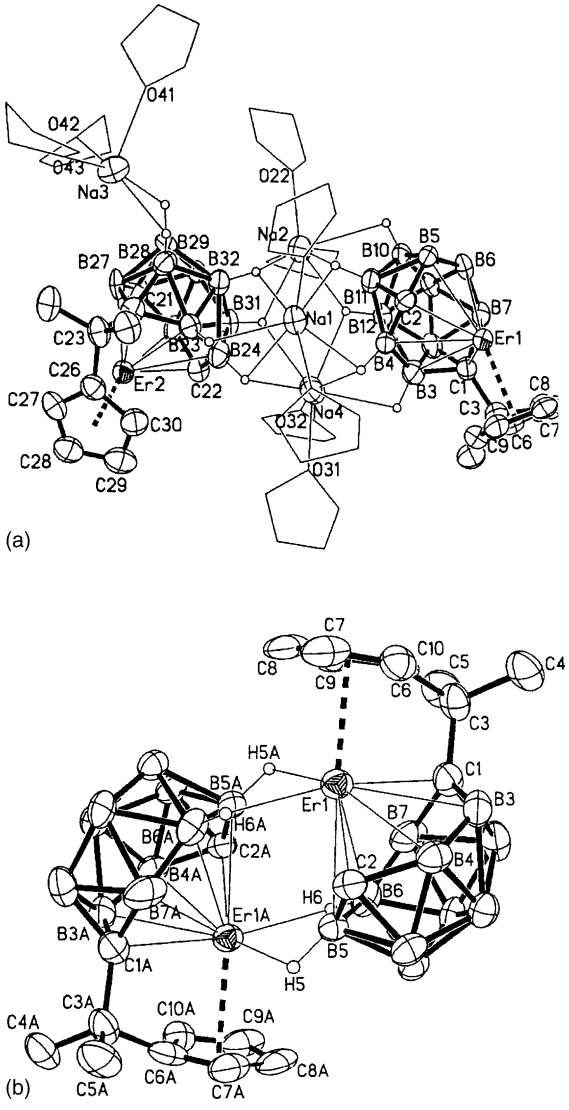

Fig. 3. (a) ORTEP illustration of $[\{[\eta^5{:}\eta^7\text{-}Me_2C(C_5H_4)(C_2B_{10}H_{11})]Er\}_2\{Na_4(THF)_9\}]_n$ showing one asymmetrical unit of the infinite polymeric chain and (b) closer view of the interactions of the Er metal with the neighboring carboranes.

cyclopentadienyl rings and σ-bonded to each of two carbon atoms from two carborane cages in a distorted-tetrahedral arrangement.

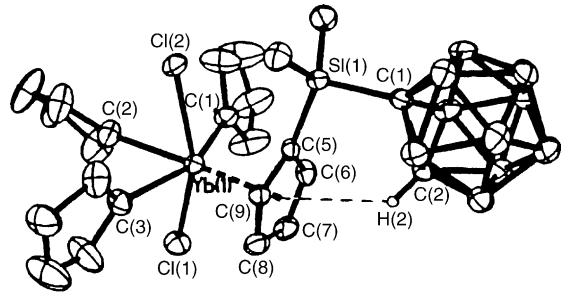

Fig. 4. Molecular structure of $[\eta^5\text{-}Me_2Si(C_5H_4)(C_2B_{10}H_{11})]YbCl_2(THF)_3$.

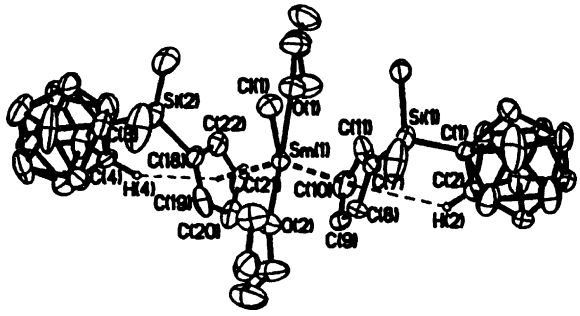

Fig. 5. Molecular structure of $[\eta^5\text{-}Me_2Si(C_5H_4)(C_2B_{10}H_{11})]_2SmCl(THF)_2$.

Treatment of $NdCl_3$ with an equimolar amount of $K_3[Me_2Si(C_5H_4)(C_2B_{10}H_{11})]$ in THF produces $[\eta^5{:}\eta^6\text{-}Me_2Si(C_5H_4)(C_2B_{10}H_{11})]Nd(THF)_2$. The samarium analogous $[\eta^5{:}\eta^6\text{-}Me_2Si(C_5H_4)(C_2B_{10}H_{11})]Sm(THF)_2$ was prepared from an unprecedented redox reaction of SmI_2 with 2 equiv. of $Na[Me_2Si(C_5H_4)(C_2B_{10}H_{11})]$ in THF. The reaction of $LnCl_3$ (Sm, Yb) with $K_3[Me_2Si(C_5H_4)(C_2B_{10}H_{11})]$ in THF afforded the organolanthanide(II) compounds $\{[\eta^5{:}\eta^6\text{-}Me_2Si(C_5H_4)(C_2B_{10}H_{11})]Ln(II)(THF)_2\}\{K(THF)_2\}$. The solid-state structure of $[\eta^5{:}\eta^6\text{-}Me_2Si(C_5H_4)(C_2B_{10}H_{11})]Sm(THF)_2$ revealed every Sm atom η^5-bonded to the cyclopentadienyl ring and η^6-bonded to the hexagonal C_2B_4 face of the $C_2B_{10}H_{11}$ cage and two THF molecules in a distorted-tetrahedral geometry (Fig. 7).

According to the cyclopentadienyl/carborane chemistry, the chemistry of ansa indenyl/carboranes was studied in detail [9]. The new versatile ligand $Me_2Si(C_9H_6)(C_2B_{10}H_{11})$ can conveniently be converted into the monoanion $[Me_2Si(C_9H_6)(C_2B_{10}H_{11})]^-$ and the dianion $[Me_2Si(C_9H_6)(C_2B_{10}H_{11})]^{2-}$ with 1 equiv. or excess amounts of NaH, respectively. Treatment of SmI_2 with $Na[Me_2Si(C_9H_6)(C_2B_{10}H_{11})]$ in THF gave the redox product $[\eta^5{:}\eta^6\text{-}Me_2Si(C_9H_6)(C_2B_{10}H_{11})]Sm(THF)_2$.

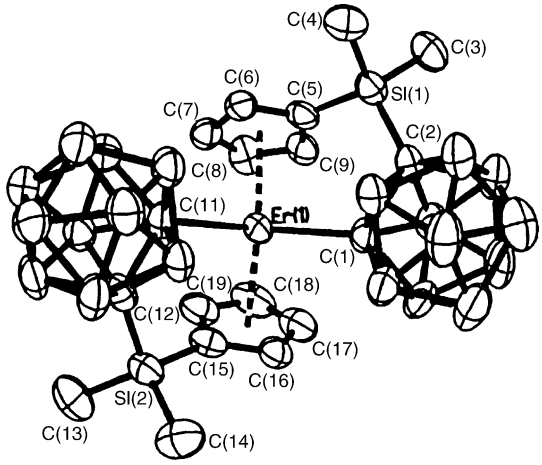

Fig. 6. Molecular structure of $[\{\eta^5{:}\sigma\text{-}Me_2Si(C_5H_4)(C_2B_{10}H_{10})]\}_2Er][Li(THF)_4]$.

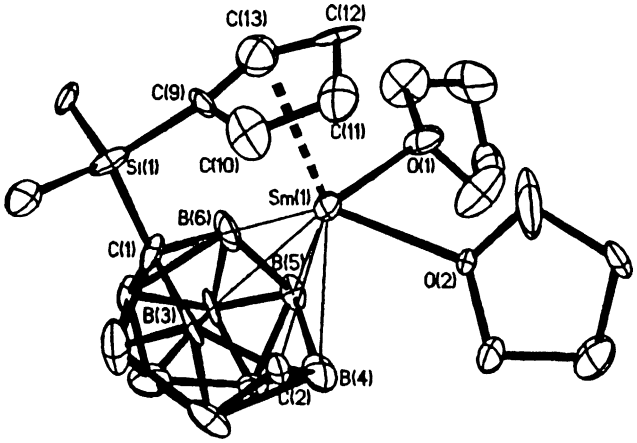

Fig. 7. Molecular structure of $[\eta^5{:}\eta^6\text{-}Me_2Si(C_5H_4)(C_2B_{10}H_{11})]Sm(THF)_2$.

As shown in Fig. 8, the Sm atom is η^5-bonded to the indenyl and η^6-bonded to the hexagonal C_2B_4 face of the $C_2B_{10}H_{11}$ cage and two THF molecules in a distorted-tetrahedral geometry. Reaction of SmI_2 with 1 equiv. of the sodium salt of the dianion $[Me_2Si(C_9H_6)(C_2B_{10}H_{11})]^{2-}$ afforded the C–H bond reduction product $[\{\eta^5{:}\sigma\text{-}Me_2Si(C_5H_4)(C_2B_{10}H_{10})\}_2Sm][Na(THF)_6](THF)_2$. Its solid-state structure consists of alternating layers of discrete tetrahedral anions and octahedral cations. Fig. 8 shows the structure of the anion, in which the Sm atom sits on a C_2 axis and is η^5-bonded to each of two indenyl rings and σ-bonded to two carbon atoms from two carborane cages in a distorted-tetrahedral geometry.

In contrast, reaction of YbI_2 with one or 2 equiv. $Na[Me_2Si(C_9H_6)(C_2B_{10}H_{11})]$ afforded $[\{\eta^5\text{-}Me_2Si(C_9H_6)(C_2B_{10}H_{11})\}Yb(\mu\text{-}I)(THF)_2]_2$ or $[\eta^5\text{-}Me_2Si(C_9H_6)(C_2B_{10}H_{11})]_2Yb(THF)_2$, respectively, which demonstrates the differences of Yb and Sm chemistry.

More studies on the versatile compound $Me_2Si(C_9H_7)(C_2B_{10}H_{11})$ lead to the indication that in this type of bridging ligand the carboranyl and cyclic organic groups

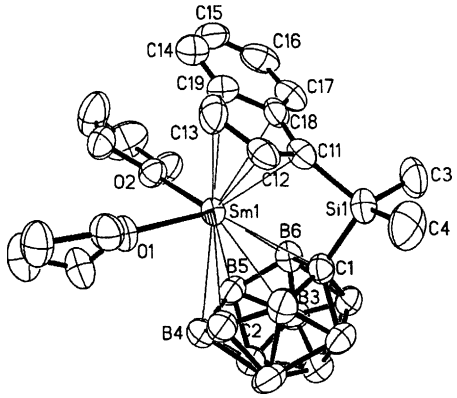

Fig. 8. Molecular structures of $[\eta^5{:}\eta^6\text{-}Me_2Si(C_9H_6)(C_2B_{10}H_{11})]Sm(THF)_2$ and $[\{\eta^5{:}\sigma\text{-}Me_2Si(C_5H_4)(C_2B_{10}H_{10})\}_2Sm][Na(THF)_6](THF)_2$.

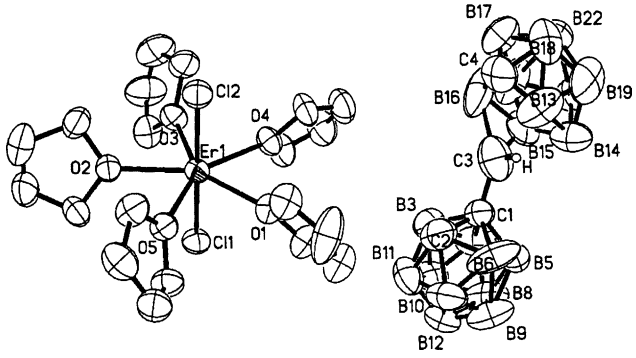

Fig. 9. Molecular structures of $[ErCl_2(THF)_5][\mu\text{-}CH\text{-}(closo\text{-}C_2B_{10}H_{11})\text{-}nido\text{-}CB_{10}H_{11}]$.

communicate with each other [10]. The authors discussed, that the acidity of the CH group of the carborane is dependent upon the substituents on the cyclopentadienyl ring, which in turn affects the properties of the resulting complex. Besides the known monoanion and dianion, they described the synthesis of the trianion $K_3[Me_2Si(C_9H_6)(C_2B_{10}H_{11})]$, available from $Me_2Si(C_9H_6)(C_2B_{10}H_{11})$ and K metal in THF. Reaction of $LnCl_3$ with 1 equiv. of $Na[Me_2Si(C_9H_6)(C_2B_{10}H_{11})]$ gave the dichloride complexes $[\eta^5\text{-}Me_2Si(C_9H_6)(C_2B_{10}H_{11})]LnCl_2(THF)_3$ (Ln = Nd, Er). They can further react with another equivalent of $Na[Me_2Si(C_9H_6)(C_2B_{10}H_{11})]$ to afford the monochloride complexes $[\eta^5\text{-}Me_2Si(C_9H_6)(C_2B_{10}H_{11})]_2LnCl(THF)_3$ (Ln = Ce, Nd, Sm, Er), which can also be prepared by treatment of $LnCl_3$ with 2 equiv. of $Na[Me_2Si(C_9H_6)(C_2B_{10}H_{11})]$ in one step. Furthermore, the authors described detailed reactivity studies of the monochloride and dichloride lanthanide complexes with NaH and K metal. For example, treatment of $[\eta^5\text{-}Me_2Si(C_9H_6)(C_2B_{10}H_{11})]ErCl_2(THF)_3$ with 2 equiv. of K metal at room temperature yielded $[\eta^5{:}\eta^6\text{-}Me_2Si(C_9H_6)(C_2B_{10}H_{11})]Er(THF)_2$. The new bis(carborane) compound $[LnCl_2(THF)_5][\mu\text{-}CH\text{-}(closo\text{-}C_2B_{10}H_{11})\text{-}nido\text{-}CB_{10}H_{11}]$ (Ln = Er, Y) was isolated. Fig. 9 shows the solid-state structure of $[ErCl_2(THF)_5][\mu\text{-}CH\text{-}(closo\text{-}C_2B_{10}H_{11})\text{-}nido\text{-}CB_{10}H_{11}]$. It consists of well separated, alternating layers of discrete cations $[ErCl_2(THF)_5]^+$ and bis(carborane) monoanions $[\mu\text{-}CH\text{-}(closo\text{-}C_2B_{10}H_{11})\text{-}nido\text{-}CB_{10}H_{11}]^-$. The cation adopts a pentagonal–bipyramidal geometry with two chloro ligands in the axial positions and the five THF molecules in the equatorial positions. The anion consists of two carborane cages that are connected through a C–C single bond.

2.2. Cyclopentadienyl complexes

2.2.1. Mono(cyclopentadienyl) complexes

Deacon and co-workers reported the structures of $CpSmBr_2(THF)_3$ and $CpSmI_2(THF)_3$ obtained through reaction of $Cp_2Sm(THF)$ with 1,2-dibromoethane and 1,2-

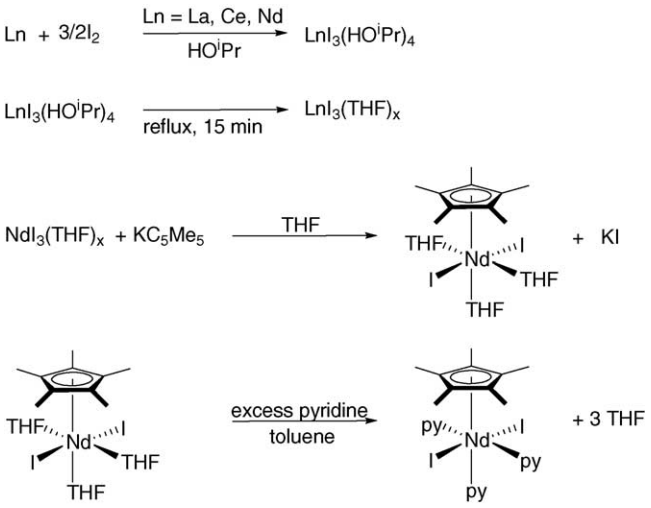

Scheme 4.

diiodoethane, respectively [11] (Eq. (1)).

$$2Cp_2Sm(THF) + XCH_2CH_2X \rightarrow CpSmX_2(THF)_3 + Cp_3Sm(THF) + CH_2CH_2 \quad (X = Br, I) \qquad (1)$$

$$2Cp_2Sm(THF) + C_2Cl_6 \rightarrow CpSmCl_2(THF)_3 + Cp_3Sm(THF) + C_2Cl_4 \qquad (2)$$

The reaction of $Cp_2Sm(THF)$ with C_2Cl_6 forms the corresponding $CpSmCl_2(THF)_3$ (Eq. (2)). The molecular structure shows a distorted pseudo-octahedral arrangement, in which the centroid of the Cp-ring and one THF molecule occupy the apical positions, while both halide ions are transoid in the equatorial plane. The distances of the centroids of the Cp-rings are nearly identical in both compounds (2.451 Å for $CpSmBr_2(THF)_3$ and 2.444 Å for $CpSmI_2(THF)_3$). The Sm–I bonds are significantly different [3.143 and 3.168 Å] and are relatively long as compared to other terminal Sm^{III}–I bond lengths. This and the likewise long Sm–THF distances show the relative steric bulk of the $CpSmI_2(THF)_3$ complex. Equal observations can be made for the dibromo compound.

Watkin and co-workers reported the synthesis of the mono(pentamethylcyclopentadienyl) derivative (η-C_5Me_5)$NdI_2(THF)_3$, produced by the reaction of $NdI_3(THF)_x$ with 1 equiv. of KC_5Me_5 in THF (Scheme 4) [12]. $NdI_3(THF)_x$ was generated from neodymium metal with 1.5 equiv. of elemental iodine in *iso*-propanol, followed by crystallization from THF.

Treatment of (η-C_5Me_5)$NdI_2(THF)_3$ with an excess of pyridine in toluene leads to displacement of the THF ligands and formation of the tris(pyridine) adduct (η-C_5Me_5)$NdI_2(py)_3$. According to a single crystal X-ray diffraction study, (η-C_5Me_5)$NdI_2(py)_3$ adopts a pseudo-octahedral geometry in the solid state, with the cyclopentadienyl ligand occupying one coordination site, the three

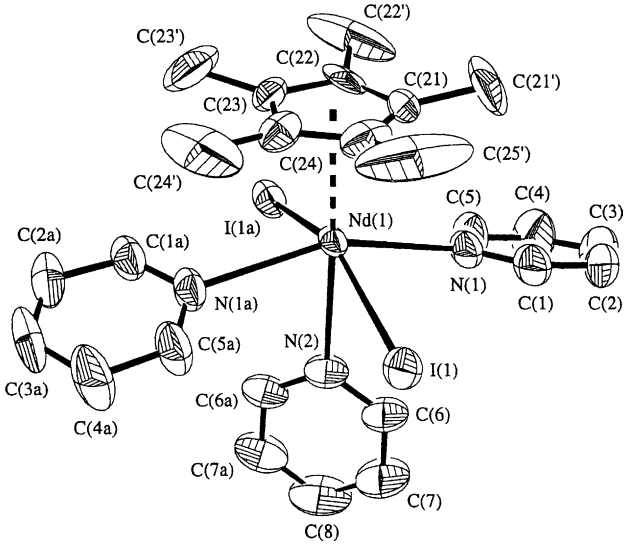

Fig. 10. Molecular structure of (η-C_5Me_5)$NdI_2(py)_3$.

pyridine ligands being arranged in a *mer*-conformation, and the iodide ligands *trans* to one another (Fig. 10). The Nd–I distance is 3.1603 Å, while Nd–N bond lengths to the pyridine ligands are 2.631 and 2.678 Å.

A series of optically active monocyclopentadienyl complexes of the lanthanides has been prepared by Mak and co-workers [13]. The (+)-neomenthylcyclopentadienyl complexes $Cp^RLnX_2(THF)_3$ [X = Cl, Ln = Sm, Gd, Yb, Y, Lu; X = I, Ln = Sm, Yb] have been prepared by metathetical reactions of the lanthanide halide with appropriate alkalimetal (+)-neomenthylcyclopentadienyl complexes. The syntheses of mono-(+)-neomenthylcyclopentadienyl lanthanide dichloride complexes were accomplished by the reaction of lanthanide trichlorides with 1 equiv. of sodium (+)-neomenthylcyclopentadienide in THF. ^{1}H NMR spectroscopic studies showed the coordination of three THF molecules.

$$LnCl_3 + NaCp^R + 3THF \rightarrow Cp^RLnCl_2(THF)_3 + NaCl \quad (Ln = Sm, Gd, Yb, Y, Lu)$$

Alternatively, lanthanide triiodides have been treated with 1 equiv. of potassium (+)-neomenthylcyclopentadienide in THF at r.t. to obtain the mono-(+)-neomenthylcyclopentadienyl lanthanide diiodides.

$$LnI_3 + KCp^R + 3THF \rightarrow Cp^RLnI_2(THF)_3 + KI \quad (Ln = Sm, Yb)$$

A single X-ray diffraction study of $Cp^RSmI_2(THF)_3$ revealed a pseudo-octahedral geometry with the iodine atoms bonded to the samarium in a *trans* fashion and the THF molecules in a *mer* conformation (Fig. 11). The bond lengths Sm–I (3.139 and 3.140 Å) and Sm–$Cp^{cetroid}$ (2.453 Å) are relatively long as compared to known bond lengths in analo-

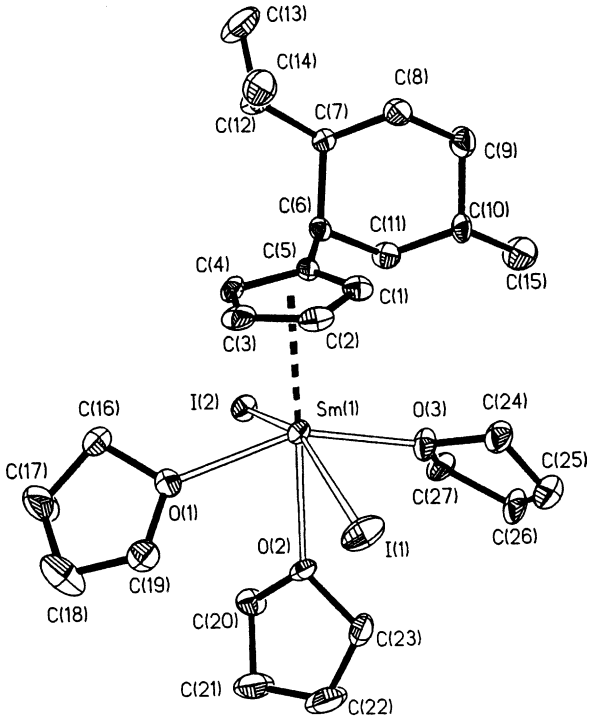

Fig. 11. Molecular structure of $Cp^RSmI_2(THF)_3$.

gous compounds, which demonstrates the sterical crowdedness in this compound. Optical rotation values of the mono-(+)-neomenthylcyclopentadienyl lanthanide dichlorides and -diiodides are all in the same range of 9–10°, which suggests that a similar coordination spere exists around the metal center among all of the mono-(+)-neomenthylcyclopentadienyl lanthanide dihalides.

Qian and co-workers presented the synthesis of mono-chelating ether side chain cyclopentadienyl lanthanide complexes with a symmetric tetradentate ligand [14]. $SmCl_3$ reacted with 3 equiv. of methoxyethylcyclopentadienyl potassium in tetrahydrofuran, followed by treatment with *trans*-(±)-2,2′-[1,2-cyclohexanediylbis(iminomethyl)]diphenole to give the binuclear mono(methoxyethylcyclopentadienyl)samarium complex $[\eta^5{:}\eta^1\text{-Cp}'\text{Sm}][(\mu{:}\eta\text{-OC}_{20}\text{H}_{20}\text{N}_2\text{O})]_2[\eta^5\text{-Cp}'\text{Sm}]$ ($Cp' = MeOCH_2CH_2C_5H_4$) (Scheme 5). X-ray structure determination studies showed that the molecule is a dimer, in which two $(MeOCH_2CH_2C_5H_4)Sm(\mu{:}\eta_1\text{-OC}_{20}\text{H}_{20}\text{N}_2\text{O})$ units are connected to two bridging oxygen atoms of the Schiff base ligands. The average Sm–C distance is 2.769 Å, while the Sm–O distance of the bridging oxygen is 2.401 Å.

The analogous dysprosium complex $[(MeOCH_2CH_2\text{-}C_5H_4)Dy(OC_{20}H_{20}N_2O)]_2$ can be obtained from the reaction of Cp'_2DyCl ($Cp' = MeOCH_2CH_2C_5H_4$) with

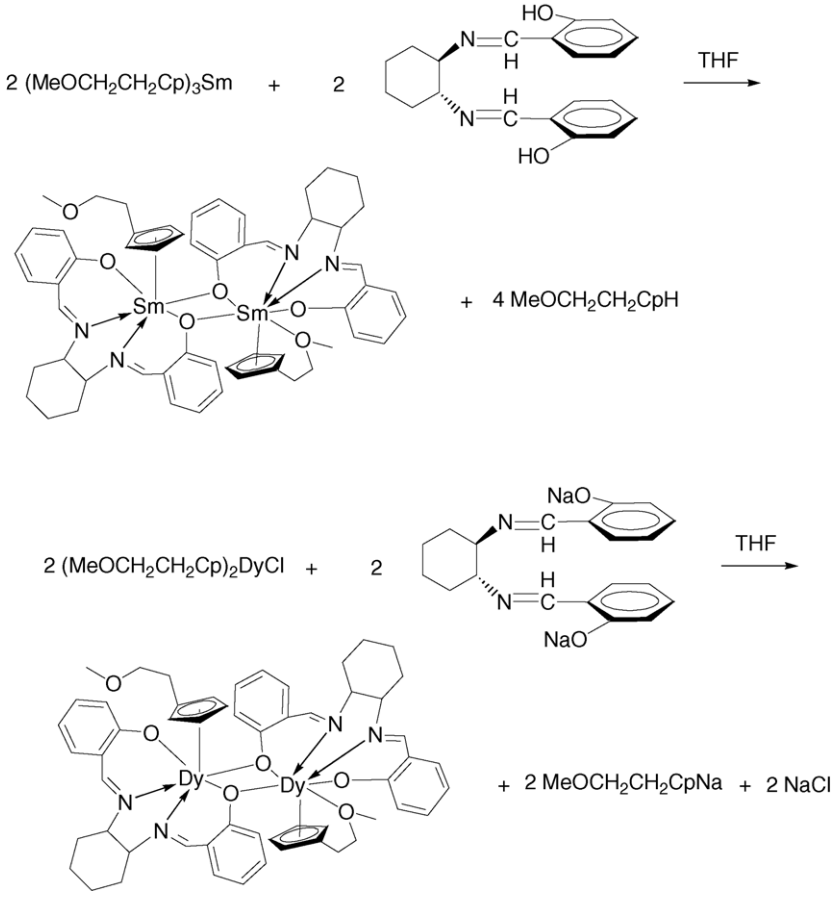

Scheme 5.

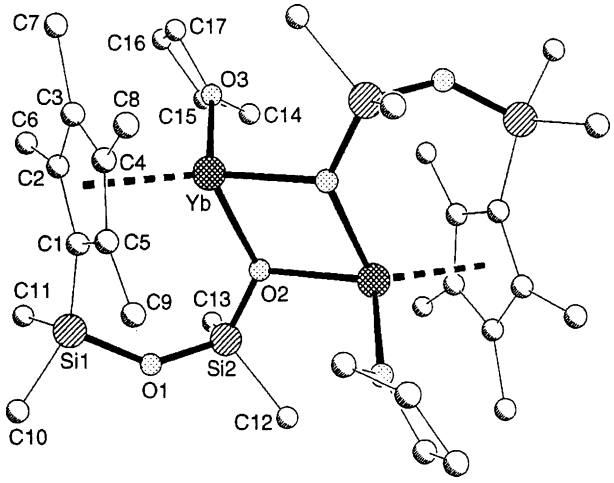

Fig. 12. Molecular structure of $[\{(\eta^5\text{-}C_5Me_4)SiMe_2OSiMe_2(\eta^1\text{-}O)\}Yb(THF)]_2$.

the disodium salt of *trans*-(±)-2,2′-[1,2-cyclohexanediylbis(iminomethyl)]diphenol.

Collin and co-workers synthesized a series of monocyclopentadienyl lanthanoid complexes with new asymmetric β-hydroxy-cyclopentadienyl ligands [15]. The novel ligands $C_5H_5CH_2CH(R)OH$ (R = Me, CH_2OMe, Ph) were obtained by the nucleophilic ring opening reaction of enantiopure epoxides by cyclopentadienyl anions (Scheme 6, Eq. (1)). Isomers **A** and **B** were isolated by flash chromatography. The metallation of these ligands by sodium or potassium metals or by butyllithium leads to the formation of the alkali metal derivatives $[C_5H_4CH_2CH(R)O]M_2$ (Li, Na, K) (Eqs. (2) and (3)). The complexes (*S*)-$C_5H_4CH_2CH(Me)OLaI(THF)_2$ and (*S*)-$C_5H_4CH_2CH(Me)OSmI(THF)$ were synthesized from the bis(potassium) salt and lanthanum or samarium iodides in THF (Scheme 6, Eq. (4)).

A comparable complex was synthesized by Bochkarev and co-workers [16]. The dimeric half sandwich complex $[\{(\eta^5\text{-}C_5Me_4)SiMe_2OSiMe_2(\eta^1\text{-}O)\}Yb(THF)]_2$ was obtained from the interaction of $(C_{10}H_8)Yb(THF)_2$ with $C_5Me_4SiMe_2OSiMe_2OH$ in THF at room temperature, affording H_2 and $C_{10}H_8$. (Scheme 7). The complex possesses inversion symmetry requiring the central four-membered ring $(Yb\text{-}O)_2$ to be planar with ytterbium oxygen distances of 2.274 and 2.319 Å and a Yb–Cp(centroid) distance of 2.41 Å (Fig. 12). 1,1,3,3-Tetramethyl-3-tetramethylcyclopentadienyl-disiloxane-1-ol was synthesized in two steps (Scheme 7).

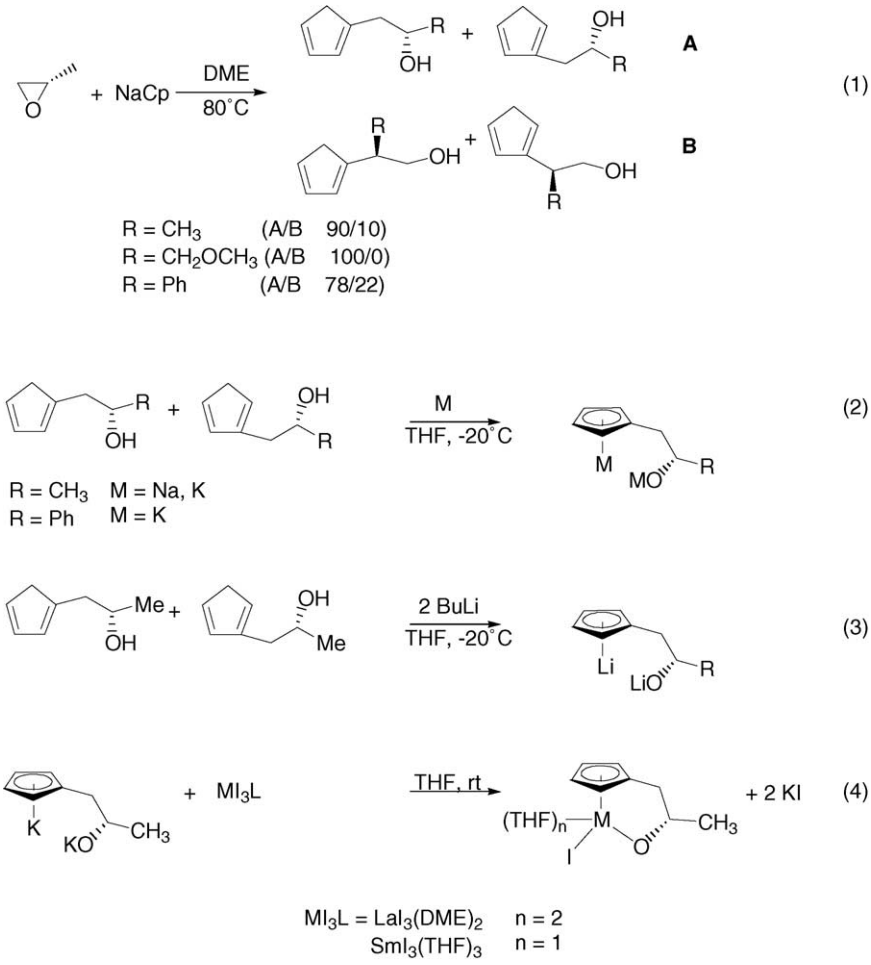

Scheme 6.

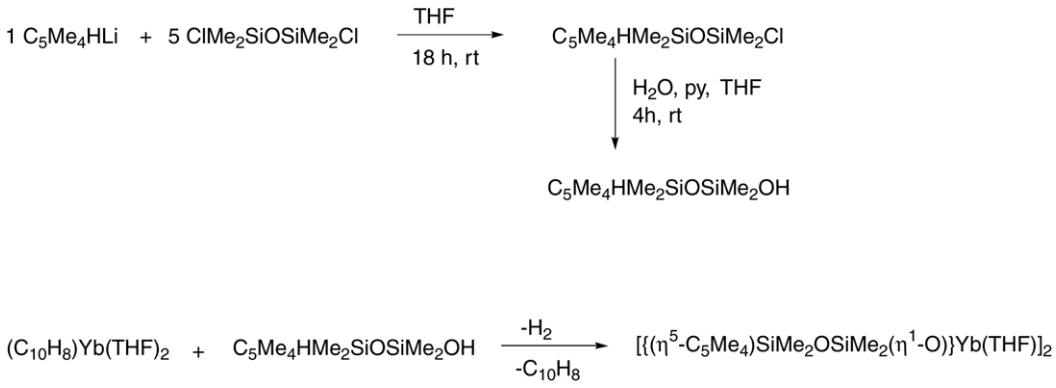

Scheme 7.

The synthesis of samarium mono(pentamethylcyclopentadienyl) aryloxide complexes was achieved by Watkin and co-workers [17]. The reaction of $SmCl_3$ with 3 equiv. of KO-2,6-*tert*-$Bu_2C_6H_3$ in THF leads to the tris(aryloxide) complex Sm(*O*-2,6-*tert*-$Bu_2C_6H_3)_3$(THF) which undergoes a clean metathesis reaction with one equivalent of LiC_5Me_5 to form the mono(pentamethylcyclopentadienyl) aryloxide derivative (η-C_5Me_5)Sm(*O*-2,6-*tert*-$Bu_2C_6H_3)_2$(THF) (Scheme 8, Eqs. (1) and (2)). Single-crystal X-ray diffraction studies showed that the complex features a three-legged piano-stool geometry with Sm–O distances to the aryloxide ligands of 2.133 and 2.188 Å and a Sm–O(THF) distance of 2.435 Å.

In contrast, the analogous reaction of LiC_5Me_5 with the 2,6-di-*iso*-propylphenoxide complex Sm(*O*-2,6-*iso*-$Pr_2C_6H_3)_3(THF)_2$ gave the lithium containing 'ate' complex [(η-C_5Me_5)Sm(*O*-2,6-*iso*-$Pr_2C_6H_3$)(μ-*O*-2,6-*iso*-$Pr_2C_6H_3)_2$Li(THF)] (Scheme 8, Eq. (3)). The complex possesses a similar three-legged piano-stool geometry like the *O*-2,6-*tert*-$Bu_2C_6H_3$ analogue, with two of the aryloxide oxygen atoms coordinated to a lithium metal center. A THF ligand completes the coordination sphere of the lithium. The Sm–O bond lengths to the lithium-coordinated aryloxide oxygens (2.250 and 2.247 Å) are somewhat longer than the distance to the terminal aryloxide (Sm–O = 2.144 Å), presumably owing to a loss of electron density at the oxygen upon forming the Sm–O–Li bridges.

Schaverien and co-workers performed single-crystal neutron diffraction studies on (C_5Me_5)Y(OAr)[$CH(SiMe_3)_2$] (Ar = *O*-2,6-*tert*-$Bu_2C_6H_3$) and (C_5Me_5)La[$CH(SiMe_3)_2]_2$ to get conclusive evidence of which nature the close intramolecular contacts between $CH(SiMe_3)_2$ and the lanthanoid center in these complexes are [18]. These intramolecular contacts are often described in the literature and can be caused by α_{CH}, α_{CSi}, β_{SiC} and γ_{CH} interactions. The molecular structures of both compounds as determined by neutron diffraction show distorted $CH(SiMe_3)_2$ groups with the metal–silicon and metal oxygen distances well within

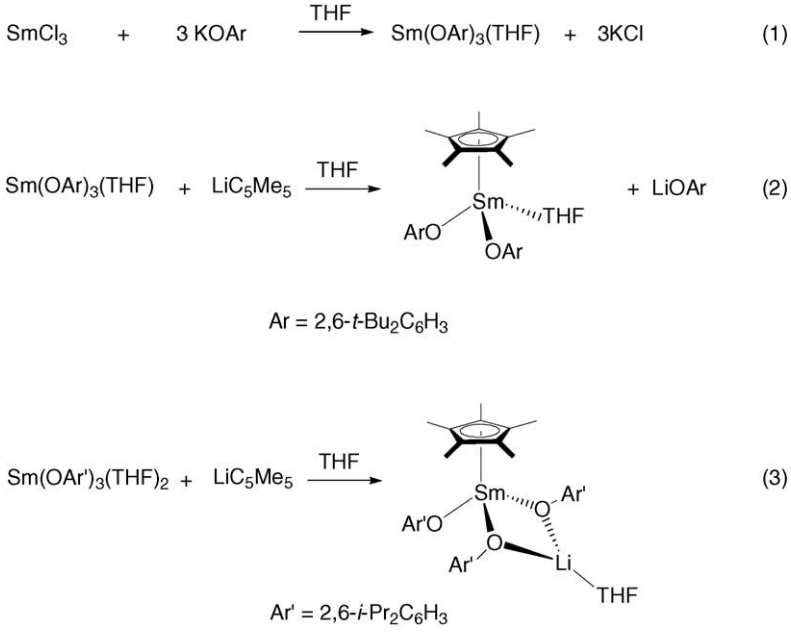

Scheme 8.

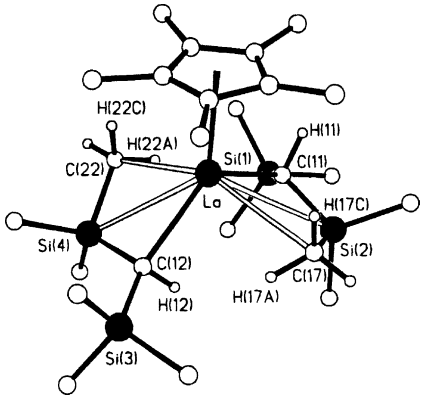

Fig. 13. Neutron diffraction studies of $(C_5Me_5)La[CH(SiMe_3)_2]_2$.

the sum of their van der Waals radii (Fig. 13). The yttrium complex shows interaction with the $CH(SiMe_3)_2$ group ($Y\cdots Si(1) = 3.281$ Å, $Y\cdots C(2) = 2.972$ Å). The coordinative unsaturation around the La in the lanthanum complex is relieved by interaction with two Si–Me bonds, one from each $CH(SiMe_3)_2$ group (La···Si(2) 3.346 Å, La···C(17) 2.964 Å, La···Si(4) 3.416 Å, La···C(22) 2.973 Å).

None of the short C–H···M intramolecular contacts shows a significant elongation of the C–H bonds. In contrast, the elongation of the agostic Si_β–C_γ bonds is significant (0.037 Å in average). The metal center interacts mainly with the β–Si–C bond, but not with the γ–C–H bonds. The results where supported by theoretical calculations.

Lin and Wang isolated partially hydrolyzed mono(cyclopentadienyl) lanthanide complexes [19]. The trichlorides of lanthanum, neodymium, samarium and gadolinium react with 1 equiv. of the cyclopentadienyl Grignard reagent in THF to give the mono(cyclopentadienyl) lanthanide species coordinated with magnesium dichloride and THF (Eq. (3)).

$$LnCl_3 + [C_5H_4C(CH_3)(C_3H_7)CH_2CH{=}CH_2]MgCl \rightarrow [C_5H_4C(CH_3)(C_3H_7)CH_2CH{=}CH_2]\,LnCl_2{\cdot}MgCl_2{\cdot}THF \quad (Ln = La,\ Nd,\ Sm,\ Gd)\ \text{in THF} \qquad (3)$$

Subsequent recrystallization of the neodymium and the gadolinium complexes from moist THF/hexane afforded the partially hydrolyzed complexes in which one chloride is exchanged by a hydroxy group (Eq. (4)).

$$[C_5H_4C(CH_3)(C_3H_7)(CH_2CH{=}CH_2]LnCl_2{\cdot}MgCl_2{\cdot}THF + H_2O \rightarrow [C_5H_4C(CH_3)(C_3H_7)CH_2CH{=}CH_2]Ln(OH)Cl{\cdot}2MgCl_2{\cdot}4THF \quad (Ln = Nd,\ Gd) \qquad (4)$$

Single-crystal X-ray determinations of the partially hydrolyzed Nd and Gd complexes reveal distorted geometries around the lanthanide with the lanthanoid center being coordinated to three magnesium-bonded chlorides in addition to the coordination to the hydroxy group, one chloride, and the cyclopentadienyl ligand. The THF molecules are coordinated to the magnesium atoms, which have a coordination number of six (Fig. 14). The Nd–O(1) distance is 2.442 Å.

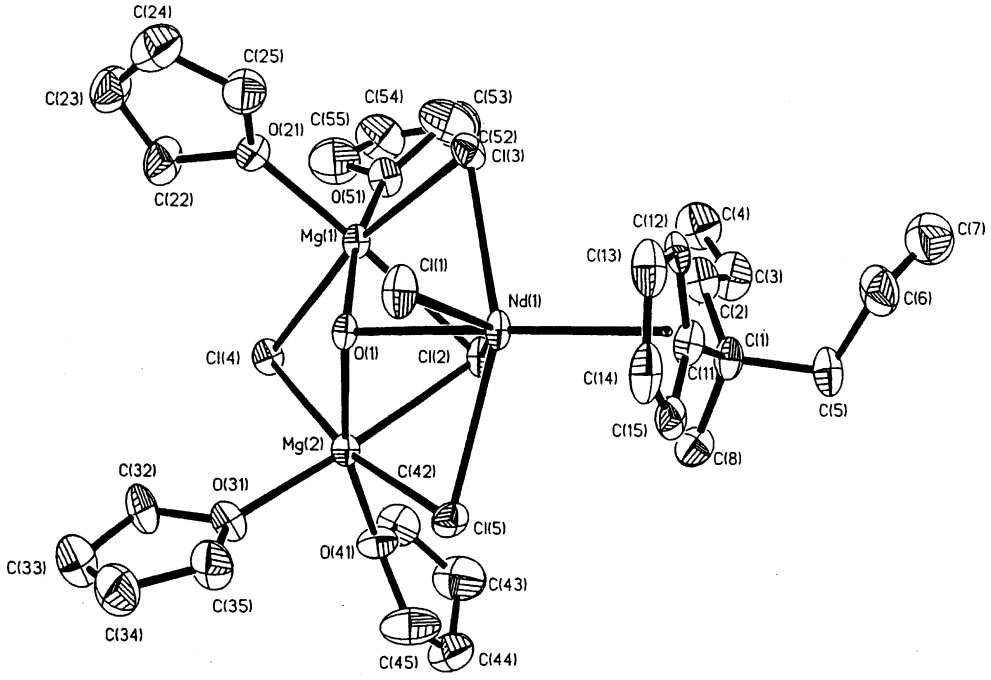

Fig. 14. Molecular structure of $[C_5H_4C(CH_3)(C_3H_7)(CH_2CH=CH_2]Nd(OH)Cl{\cdot}2MgCl_2{\cdot}4THF$.

$$Tl(C_5H_5) + Sm(Tp^{MeMe})_2 \xrightarrow{THF} Sm(\eta^3\text{-}Tp^{MeMe})(\eta^2\text{-}Tp^{MeMe})(\eta^5\text{-}C_5H_5) + Tl \quad (1)$$

$$2\,Sm(Tp^{MeMe})_2(C_5H_5) \xrightarrow{\Delta} Sm[HB(3,5\text{-}Me_2pz)_2(C_5H_4)](\eta^3\text{-}Tp^{MeMe}) + Sm(\eta^3\text{-}Tp^{MeMe})_2(\eta^2\text{-}3,5\text{-}Me_2pz) + C_5H_6 \quad (2)$$

Scheme 9.

The first mixed Tp/Cp (Tp = hydro-tris(pyrazolyl)borate) derivative of the lanthanides was reported by Marques, Takats and co-workers [20]. The reaction of TlCp with a slurry of $Sm(Tp^{MeMe})_2$ in THF (Tp^{MeMe} = hydro-tris-3,5-dimethylpyrazolylborat) resulted in the formation of thallium metal and $Sm(Tp^{MeMe})_2(Cp)$ (Scheme 9, Eq. (1)). NMR data indicate different coordination modes of the two Tp^{MeM} ligands.

Heating of $Sm(Tp^{MeMe})_2(Cp)$ overnight in a sealed tube at 165 °C gave two products. One is the result of an unprecedented transformation of the Tp ligand to the mixed pyrazolylborate $[HB(3,5\text{-}Me_2pz)_2(C_5H_4)]$ (Scheme 9, Eq. (2)). The second product is $Sm(Tp^{MeMe})_2(3,5\text{-}Me_2pz)$, which was also generated from the reaction of $Sm(Tp^{MeMe})_2(Cp)$ with 3,5-dimethylpyrazole. The thermally induced intramolecular C–H activation in $Sm(Tp^{MeMe})_2(Cp)$ is a useful method for the preparation of the new $HB(3,5\text{-}Me_2pz)_2(C_5H_4)$ ligand and opens the way for the synthesis of an extended family of heteroscorpionates with different organic functional groups.

Evans et al. reported the synthesis of the divalent lanthanide complexes $[[Zr_2(OiPr)_9]Ln(C_5H_5)]$ (Ln = Yb, Sm). $[\{[Zr_2(OiPr)_9]LnI\}_2]$ reacts with NaC_5H_5 to give the hexane soluble complexes [21]. $[[Zr_2(OiPr)_9]Sm(C_5H_5)]$ is the first reported soluble ($C_5H_5^-$) complex of Sm^{II}. The $[Zr_2(OiPr)_9]^-$ ligand is compatible with cyclopentadienyl reagents and enhances the solubility of divalent lanthanide organometallic species in comparison with $C_5H_5^-$ analogues.

$$[\{[Zr_2(OiPr)_9]LnI\}_2] + 2\,NaC_5H_5 \rightarrow [[Zr_2(OiPr)_9]Ln(C_5H_5)] + NaI$$

Both complexes do not form isolable adducts with THF, Et_2O or DME, but NMR spectra in [D_8]-THF show two distinct THF environments, suggesting coordination of THF in solution. Single X-ray determinations reveal that the samarium and ytterbium complexes are isostructural (Fig. 15 shows a ball-and-stick representation of the complexes).

The C–Ln bond length of 2.67–2.728 Å for the ytterbium complex and 2.803–2.825 Å for the samarium complex are in the normal range. Evans et al. also reported the synthesis and structure of unsolvated triple-decked bent metallocenes with COT as the bridging ligand, which are shown in Chapter 2.7.

Marks and co-workers synthesized a new series of constrained geometry organolanthanide catalysts and report their enhanced activity for aminoalkene hydroamination/cyclization (see Chapter 2.8) [22]. $[Me_2Si(C_5Me_4)(^tBuN)]LnN(SiMe_3)_2$ (Ln = Nd, Lu, Sm) and $[Me_2Si(C_5Me_4)(^tBuN)]LnCH(SiMe_3)_2$ (Ln = Yb, Lu) complexes were synthesized by reaction of the corresponding homoleptic amides or alkyls with $[Me_2Si(C_5Me_4H)(^tBuNH)$ (Scheme 10).

The amine elimination does not lie completely on the product side and must be driven to completion by $HN(SiMe_3)_2$ removal. Single-crystal X-ray determination of $[Me_2Si(C_5Me_4)(^tBuN)]SmN(SiMe_3)_2$ revealed a monomeric structure with a relatively long Sm–$N(SiMe_3)_2$ distance of 2.320 Å while the Sm–$N(^tBu)$ (2.257 Å) distance is substantially shorter than usual, presumably due to the chelating structure. The structure of $[Me_2Si(C_5Me_4)(^tBuN)]YbCH(SiMe_3)_2$ shows the typical close Ln–CH_3–Si contact of 2.657 Å which is observed in numerous organolanthanide $-CH(TMS)_2$ complexes.

The synthesis of cyclopentadienyl lanthanide pyrazolate complexes and their reactivity towards dimethylsilicone was reported by Huang and co-workers [23]. Reactions of Cp_3Ln (Cp = C_5H_5; Ln = Ho, Dy, Yb, Sm) with 2 equiv. of $HPzMe_2$ ($HPzMe_2$ = 3,5-dimethylpyrazole) in THF at room temperature yield complexes $CpLn(PzMe_2)_2$ (Ln = Ho, Dy) and $Cp_2Yb(PzMe_2)(HpzMe_2)$ and $Sm(PzMe_2)_3$, respec-

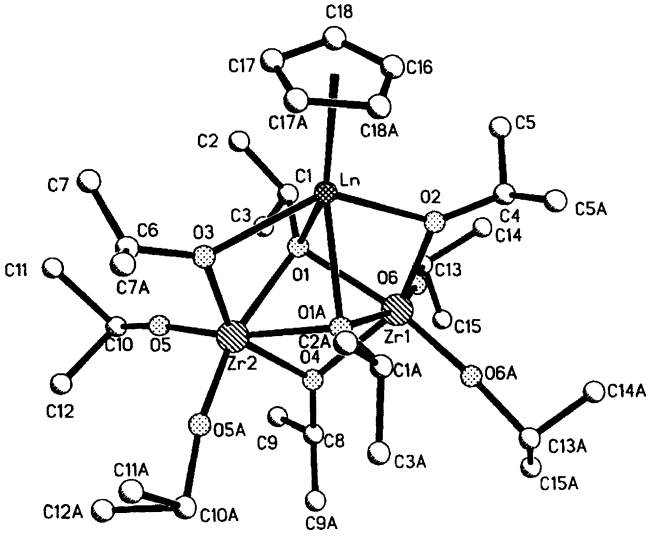

Fig. 15. Molecular structure of $[[Zr_2(OiPr)_9]Ln(C_5H_5)]$.

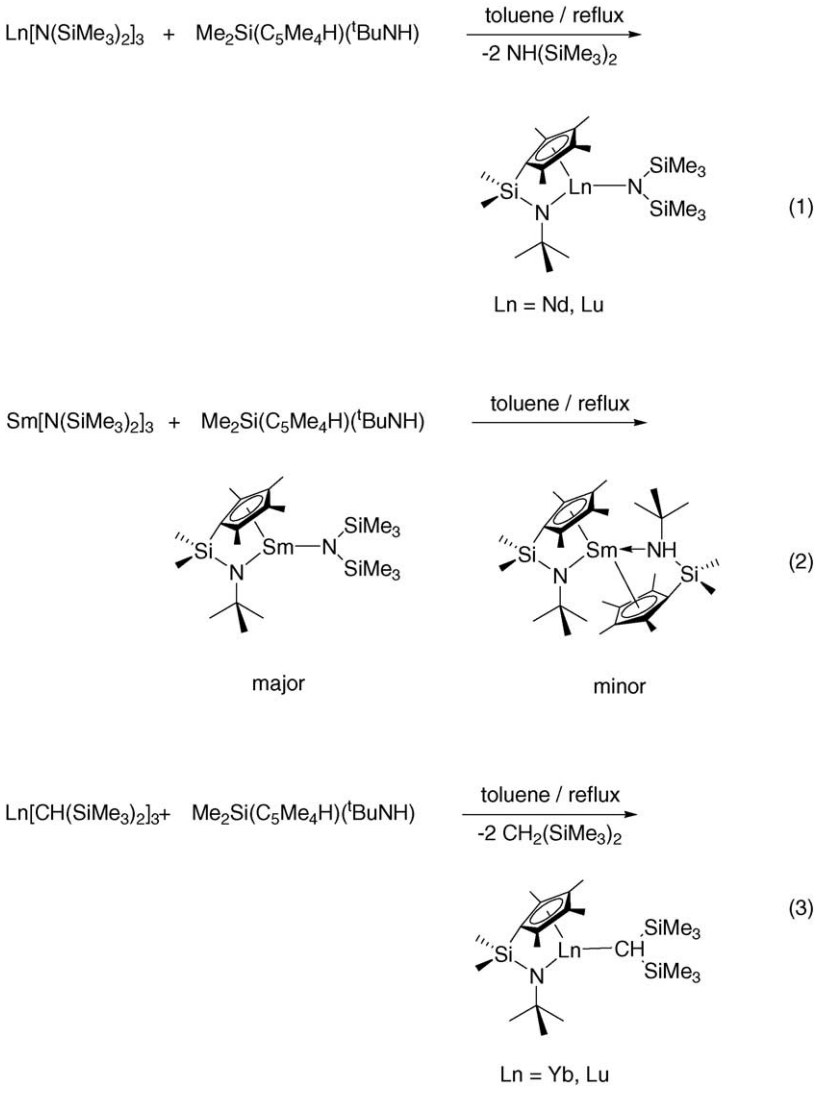

Scheme 10.

tively (Eq. (5)).

$$Cp_3Ln + 2HpzMe_2 \rightarrow CpLn(PzMe_2)_2 + CpH \quad (Ln = Ho, Dy) \quad (5)$$

$$CpLn(PzMe_2)_2 + (Me_2SiO)_n \rightarrow [CpLn(PzMe_2)(OSiMe_2PzMe_2)]_2 \quad (Ln = Ho, Dy) \quad (6)$$

The different products indicate that the number of cyclopentadienyl groups liberated from a Cp_3Ln moiety is influenced by the size of the lanthanide ion. $CpHo(PzMe_2)_2$ and $CpDy(PzMe_2)_2$ react with dimethylsilicone grease to give the corresponding $(Me_2SiO)_n$ insertion products $[CpLn(PzMe_2)(OSiMe_2PzMe_2)]_2$ (Ln = Ho, Dy) (Eq. (6)). Only the monocyclopentadienyl type organolanthanide pyrazolates show the insertion of dimethylsilicone into the Ln–N bond. X-ray diffraction studies reveal $[CpHo(PzMe_2)(OSiMe_2PzMe_2)]_2$ to be a centrosymmetric dimer in which each holmium is coordinated to one cyclopentadienyl group, two bridging oxygen atoms, and three nitrogen atoms, two from the chelating $PzMe_2$ ligand and one from the bridging 3,5-dimethylpyrazolyl-siloxide ligand to form a distorted octahedron (Fig. 16).

Dehnicke and co-workers reported the synthesis and structures of phosphoraneiminato complexes of ytterbium, yttrium and samarium. $YbCp_2Br$ ($Cp = C_5H_5$) and $LiNPPh_3$ were allowed to react in boiling toluene to give $[Yb_2Cp_3(NPPh_3)_3]$ with cyclopentadienyl and phosphoraneiminato ligands (Scheme 11, Eq. (1)) [24].

Single-crystal X-ray determinations of $[Yb_2Cp_3(NPPh_3)_3]$ show two Cp rings bonded to one ytterbium and one Cp ligand bonded to the second ytterbium atom which also binds one $(NPPh_3)^-$-group in terminal fashion (Fig. 17). The other two $(NPPh_3)^-$-groups are linked to ytterbium atoms to form a non-planar Yb_2N_2 four-membered ring.

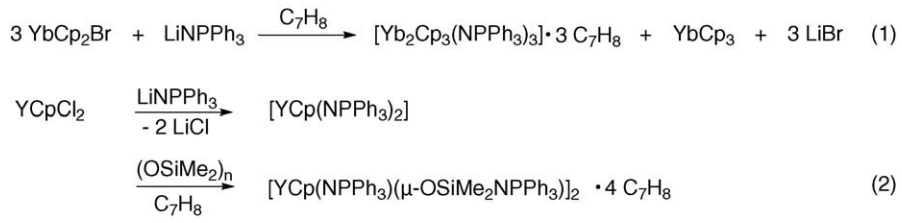

Scheme 11.

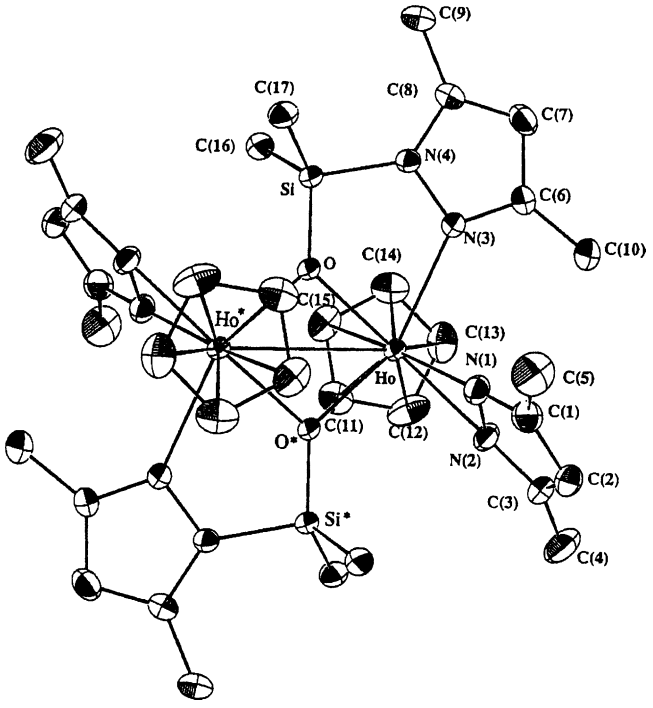

Fig. 16. ORTEP diagram of $[CpHo(PzMe_2)(OSiMe_2PzMe_2)]_2$.

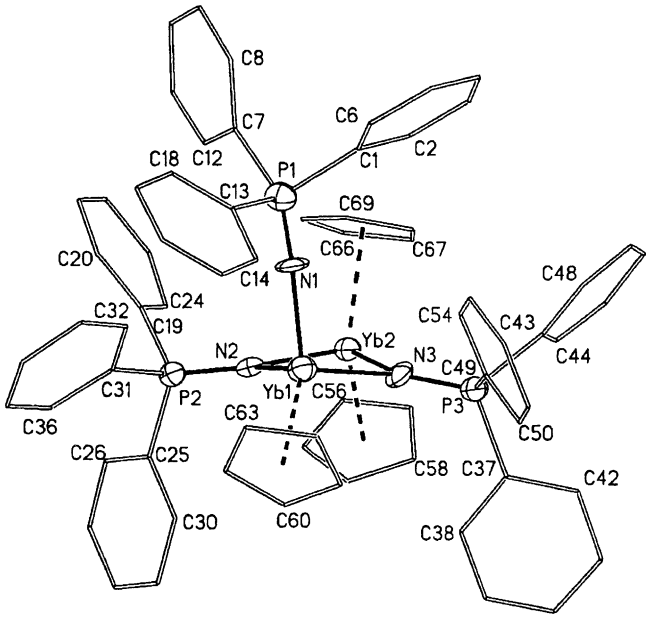

Fig. 17. Molecular structure of $[Yb_2Cp_3(NPPh_3)_3]$.

2.2.2. *Bis(cyclopentadienyl)complexes*

Winter and co-workers [25] prepared monomeric bis(cyclopentadienyl)(1,3-diphenyltriazenido)(4-*tert*-butylpyridine) complexes of erbium and lutetium via reaction of the tris(cyclopentadienyl)complexes with 1,3-diphenyltriazene in the presence of 4-*tert*-butylpyridine (Scheme 12). 4-*tert*-Butylpyridine is essential because of the insolubility of tris(cyclopentadienyl)erbium and -lutetium in toluene.

Three equivalents of 1,3-diphenyltriazene react with 1 equiv. of the tris(cyclopentadienyl) lanthanides in the presence of pyridine to afford tris(1,3-diphenyltriazenido)(pyridine)$_x$ lanthanoid complexes. A single-crystal X-ray determination of bis(cyclopentadienyl)(1,3-diphenyltriazenido)(4-*tert*-butylpyridine)erbium revealed a monomeric species with two η^5-cyclopentadienyl ligands, one bidentate 1,3-diphenyltriazenido ligand, and one 4-*tert*-butylpyridine donor (Fig. 18). The erbium–cyclopentadienyl(centroid) distances are 2.624 and 2.668 Å, while the erbium–nitrogen bond length within the 1,3-diphenyltriazenido ligand are 2.423 Å (N(1)), 2.447 Å (N(3)) and 2.958 Å (N(2)), indicating idealized bidendate bonding of the 1,3-diphenyltriazenido ligand, with N(2) not being bonded to erbium.

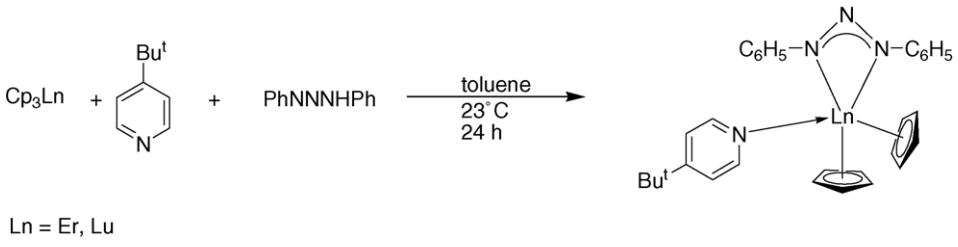

Scheme 12.

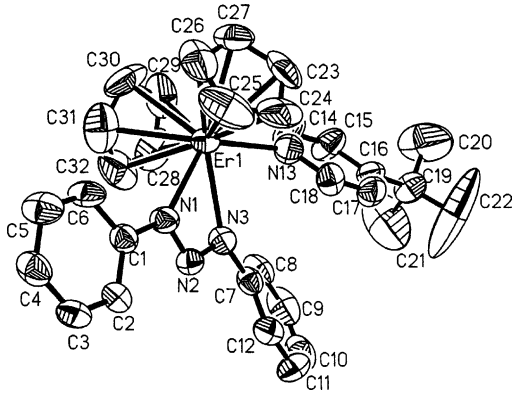

Fig. 18. Molecular structure of $(C_5H_5)_2Er(PhNNNPh)[4\text{-}(^tBu)C_5H_4N]$.

The reaction of the mono(pentamethylcyclopentadienyl) derivative $(\eta\text{-}C_5Me_5)NdI_2(py)_3$, which is described above, with $KC_5H_4SiMe_3$ in THF led to the mixed bis(cyclopentadienyl) complex $(\eta\text{-}C_5Me_5)(\eta\text{-}C_5H_4SiMe_3)NdI$ (py) [12]. Watkin et al. reported that the monomeric $(\eta\text{-}C_5Me_5)(\eta\text{-}C_5H_4SiMe_3)NdI(py)$ features a typical bent metallocene Cp_2MX_2 geometry with Nd–I and Nd–N distances of 3.066 and 2.555 Å, respectively, which is in both cases shorter than in $(\eta\text{-}C_5Me_5)NdI_2(py)_3$ (Fig. 19). Distances between the neodymium metal center and the ring centroids are 2.47 Å for the $\eta\text{-}C_5H_4SiMe_3$ ligand and 2.44 Å in the case of the $\eta\text{-}C_5Me_5$ moiety.

In addition to the mono(+)-neomenthylcyclopentadienyl complexes of the lanthanides described in Chapter 2.2.1, Leung et al. synthesized a series of dicyclopentadienyl complexes using (+)-neomenthylcyclopentadienyl ligands [13]. Treatment of 2 equiv. of $NaCp^R$ (Cp^R = (+)-neomenthylcyclopentadienyl) with anhydrous lanthanide trichlorides in THF at room temperature afforded the organolanthanide chlorides $[Cp^R{}_2Ln(\mu\text{-}Cl)]_2$ (Ln = Sm, Yb, Y, Lu).

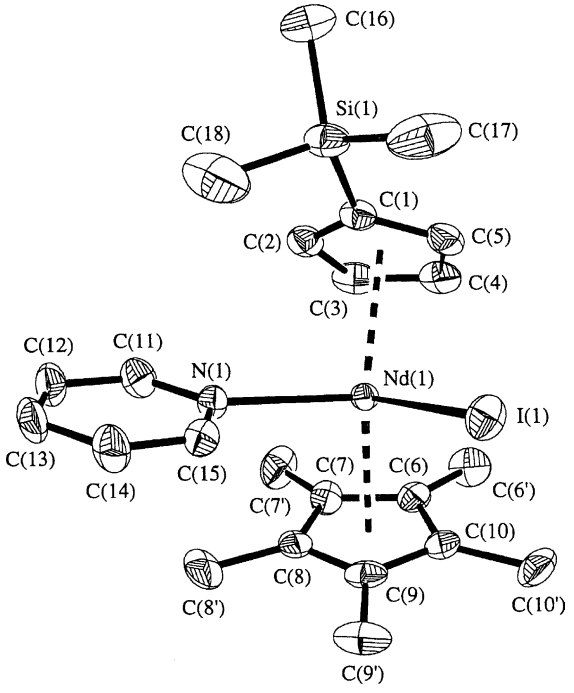

Fig. 19. Molecular structure of $(\eta\text{-}C_5Me_5)(\eta\text{-}C_5H_4SiMe_3)NdI(py)$.

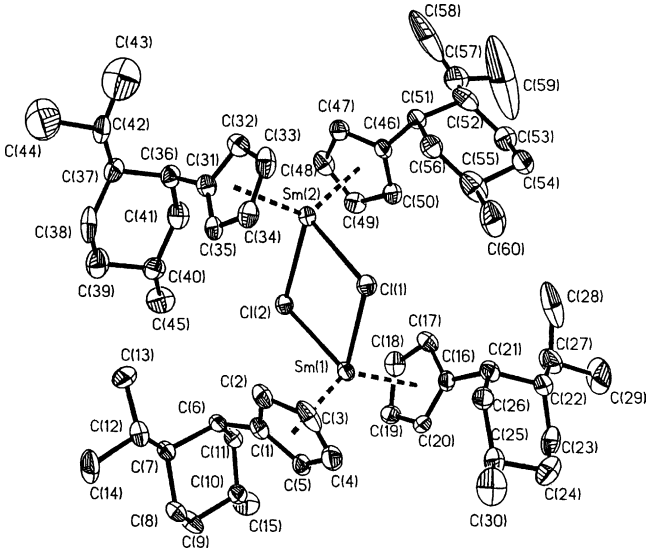

Fig. 20. Molecular structure of $[Cp^R{}_2Sm(\mu\text{-}Cl)]_2$.

$$LnCl_3 + 2NaCp^R \rightarrow [Cp^R{}_2Ln(\mu\text{-}Cl)]_2 + 2NaCl$$
$$(Ln = Sm, Yb, Y, Lu)$$

Single-crystal X-ray diffraction studies of $[Cp^R{}_2Sm(\mu\text{-}Cl)]_2$ and $[Cp^R{}_2Y(\mu\text{-}Cl)]_2$ revealed that both compounds are chloro-bridged dimers with an asymmetric plane described by Ln_2Cl_2 almost perpendicular to the plane described by the four cyclopentadienyl ring centroids (Fig. 20). The (+)-neomenthyl groups attached to the cyclopentadienyl rings in each $Cp^R{}_2Sm$ unit are positioned in a *trans* orientation with respect to each other in order to minimize the steric interaction. The four different bond distances of $Cp^{centroid}$–Ln lie in the range of 2.4–2.5 Å for the samarium cyclopentadienyl compound and 2.3–2.4 Å for the yttrium compound.

In addition to the mono(cyclopentadienyl) lanthanide pyrazolate complexes described above, Huang and coworkers synthesized the bis(cyclopentadienyl) erbium pyrazolate complex $Cp_2Er(PzMe_2)(THF)$ and the ytterbium complex $Cp_2Yb(PzMe_2)(HpzMe_2)$ [23]. Reaction of Cp_3Er ($Cp = C_5H_5$) with 1 equiv. of $HPzMe_2$ ($HPzMe_2$ = 3,5-dimethylpyrazole) in THF at room temperature gave the complex $Cp_2Er(PzMe_2)(THF)$ (Eq. (7)). Abstraction of only one cyclopentadienyl ligand occurred by reacting Cp_3Yb with 2 equiv. of $HPzMe_2$ in THF leading to the bis(cyclopentadienyl)monopyrazolate $Cp_2Yb(PzMe_2)(HpzMe_2)$ where the coordination sphere of the ytterbium is saturated by one $HpzMe_2$ molecule (Eq. (8)). Presumably, the formation of $Cp_2Yb(PzMe_2)(HPzMe_2)$ is due to the enhanced covalence of the Ln–Cp bond in the series

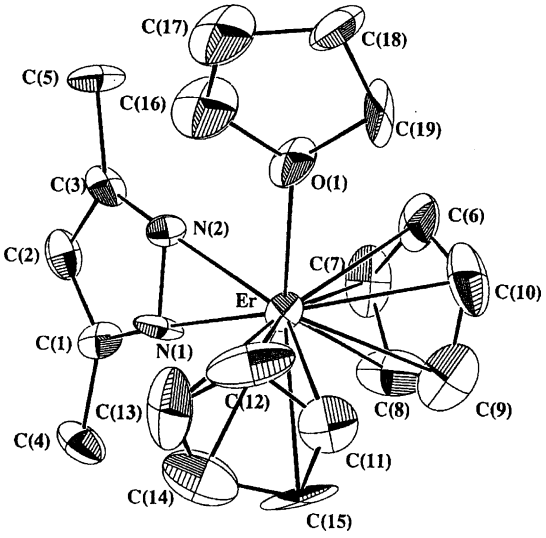

Fig. 21. Molecular structure of $Cp_2Er(PzMe_2)(THF)$.

Cp_3Ln (Ln = Sm, Dy, Ho, Yb), as a result of the lanthanide contraction, and because the acidity of CpH is relatively high. Thus, $HpzMe_2$ is not a strong enough acid to liberate the second Cp group from the more covalent Cp_3Yb moiety to give $CpYb(PzMe_2)$.

$$Cp_3Er + HpzMe_2 \rightarrow Cp_2Er(PzMe_2)(THF) + CpH \quad (7)$$

$$Cp_3Yb + 2\,HpzMe_2 \rightarrow Cp_2Yb(PzMe_2)(HpzMe_2) + CpH \quad (8)$$

The structures of $Cp_2Er(PzMe_2)(THF)$ and $Cp_2Yb(PzMe_2)(HPzMe_2)$ in the solid state (Fig. 21) show monomeric molecules with a coordination geometry which is typical for bent metallocenes. The Ln–Cp distances and angles lie in the typical range for such compounds.

Sizov and co-workers reported the synthesis and structural characterization of $(1,3\text{-}tert\text{-}Bu_2C_5H_3)_2Eu(THF)$ via the reaction of EuI_2 with 2 equiv. of $1,3\text{-}tert\text{-}Bu_2C_5H_3Na$ in THF (Eq. (9)) [26]. The mixed cyclopentadienyl complex $(1,3\text{-}tert\text{-}Bu_2C_5H_3)(C_5Me_5)Yb(THF)$ was obtained from the subsequent reaction of YbI_2 with C_5Me_5Na and $1,3\text{-}tert\text{-}Bu_2C_5H_3Na$ in THF (Eq. (10)).

$$ErI_2 + 2\,1,3\text{-}tert\text{-}Bu_2C_5H_3Na \rightarrow (1,3\text{-}tert\text{-}Bu_2C_5H_3)_2Eu(THF) + 2\,NaI \quad (9)$$

$$YbI_2 + C_5Me_5Na + 1,3\text{-}tert\text{-}Bu_2C_5H_3Na \rightarrow (1,3\text{-}tert\text{-}Bu_2C_5H_3)(C_5Me_5)Yb(THF) + 2\,NaI \quad (10)$$

$$YbCl_3 + 1,3\text{-}tert\text{-}Bu_2C_5H_3Li \rightarrow (1,3\text{-}tert\text{-}Bu_2C_5H_3)_2Yb(\mu^2\text{-}Cl)_2Li(THF)_2 \quad (11)$$

The reaction of $YbCl_3$ with $1,3\text{-}tert\text{-}Bu_2C_5H_3Li$ afforded the $(1,3\text{-}tert\text{-}Bu_2C_5H_3)_2Yb(\mu^2\text{-}Cl)_2Li(THF)_2$ *ate*-complex. Single-crystal X-ray determinations revealed the monomeric structures of $(1,3\text{-}tert\text{-}Bu_2C_5H_3)_2Eu(THF)$ and $(1,3\text{-}tert\text{-}Bu_2C_5H_3)(C_5Me_5)Yb(THF)$, respectively.

Trifonov et al. reported the synthesis of the trivalent ytterbium diazadiene complex $Cp_2Yb(DAD)$ ($Cp = C_5H_5$, DAD = *t*-BuN=CH–CH=N-*t*-Bu). $Cp_2Yb(DAD)$ was obtained using three different procedures [27], namely, by oxidation of $Cp_2Yb(THF)_2$ with diazadiene in THF, by reaction of Cp_2YbCl with $DAD^{2-}Na^+{}_2$ taken in a ratio 2:1, and by the reaction of $Cp_2YbCl(THF)$ with $DAD^{\bullet-}K^+$ taken in a ratio of 1:1 (Scheme 13).

The solid-state structure shows $Cp_2Yb(DAD)$ to be monomeric with Yb–Cp_{centr} distances of 2.324 and 2.334 Å and Yb–N distances of 2.31 Å in average (Fig. 22). $Cp_2Yb(DAD)$ exhibits a magnetic moment at room temperature of 4.8 μ_B, which is slightly higher than the average value observed for Yb^{III} derivatives (4.3–4.5 μ_B). This can be explained taking into account the radical-anionic character of the DAD ligand and its contribution to the total magnetic moment of the molecule.

Huang and co-workers reported the reaction of Cp_3Ln ($Cp = C_5H_5$, Ln = Yb, Dy, Sm, Y) with an equimolar amount of 2-mercapto-benzothiazole (HSBT) in THF at room temperature yielding the bis(cyclopentadienyl) complexes $Cp_2Ln(SBT)(THF)$ (Ln = Yb, Dy, Sm, Y) [28]. Spectroscopic data revealed that all complexes are monomeric and one THF

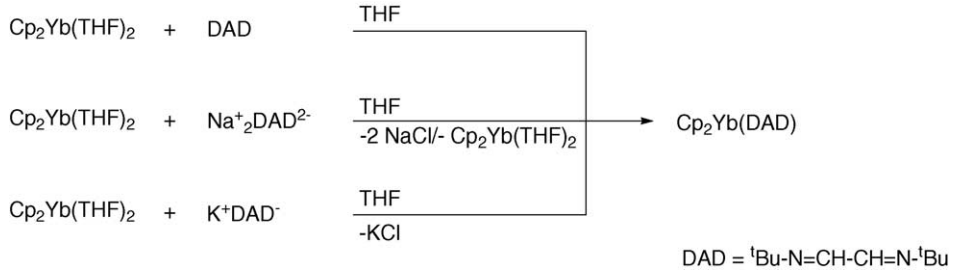

Scheme 13. Synthesis of $Cp_2Yb(DAD)$.

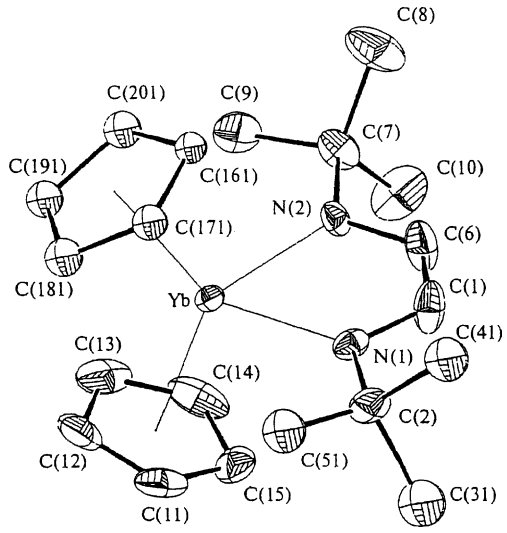

Fig. 22. Molecular structure of $Cp_2Yb(DAD)$.

molecule is coordinated.

$$Cp_3Ln + HSBT + THF \rightarrow Cp_2Ln(SBT)(THF) + CpH$$

(Cp = C_5H_5, Ln = Yb, Dy, Sm, Y, HSBT, = 2-mercapto-benzothiazole)

The crystal structural analysis shows that in $Cp_2Yb(SBT)(THF)$ and $Cp_2Dy(SBT)(THF)$ each lanthanide ion is coordinated by two η^5-bonded cyclopentadienyl groups, one oxygen atom of THF, one sulfur and one nitrogen atom from the chelating benzothiazole-2-thiolate ligand to form a distorted trigonal-bipyramidal coordinated geometry (Fig. 23).

The Yb–S distance of 2.84 Å is longer than those found in related compounds, while the Yb–N distance of 2.39 Å is relatively short compared with analogous compounds. Presumably, the rather long Ln–S and the rather short Ln–N bond distance result from the fact that the benzothiazole-2-thiolate group has a resonance structure as shown in Scheme 14 where the negative charge is partially delocalized to the N atom.

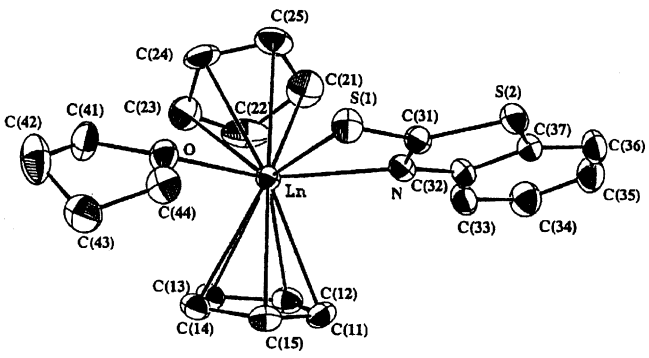

Fig. 23. Molecular structure of $Cp_2Ln(SBT)(THF)$.

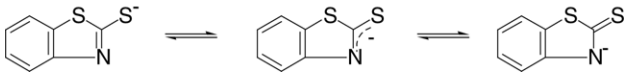

Scheme 14. Resonance structures of SBT^-.

The reaction of $Cp^*_2Sm(CH_2C_6H_5)(THF)$ with N_2O was studied by Magull and co-workers [29]. N_2O was bubbled into a solution of $Cp^*_2Sm(CH_2C_6H_5)(THF)$ in toluene leading to $[Cp^*_2Sm(C_6H_5CH_2NNO)]_2$ via an unusual insertion reaction of N_2O into the Sm–C σ-bond. Single crystal X-ray determinations revealed a dimeric structure with two samarium centers linked via an (η^1:η^2) bridge by two benzyldiazotato ligands forming a nearly planar $Sm_2N_2O_2$ ring (Fig. 24). The distorted tetrahedral coordination geometry is completed with two η^5-bonded pentamethylcyclopentadienyl ligands.

In contrast, the reaction of $[Cp^*_2Yb(CH_2C_6H_5)(THF)]$ with KSCN and 18-crown-6 shows a substitution of the benzyl group with NCS^- giving $[K(18\text{-crown-}6)Cp^*_2Yb(NCS)_2]$. The solid-state structure shows a polymeric chain structure where two Cp^*_2Yb units are connected over a [K(18-crown-6)(NCS)] bridge (Fig. 25) with tetrahedrally coordinated Yb^{III} ions.

Schumann et al. reported the first complexes of ytterbium and yttrium-containing sulfur functionalized cyclopentadienyl ligands [30]. Yttrium trichloride reacted with 2 equiv. of $Na(C_5H_4CH_2CH_2SEt)$ in THF to form $(\eta^5\text{-}C_5H_4CH_2CH_2SEt)_2YCl$ (Scheme 15). The stepwise reaction of lutetium trichloride with 1 equiv. of $Na(C_5H_4CH_2CH_2SEt)$ and 1 equiv. of $Na(C_5Me_5)$ yielded $(\eta^5\text{-}C_5Me_5)(\eta^5\text{-}C_5H_4CH_2CH_2SEt)LuCl$. Alkylation of $(\eta^5\text{-}C_5H_4CH_2CH_2SEt)_2YCl$ and $(\eta^5\text{-}C_5Me_5)(\eta^5\text{-}C_5H_4CH_2CH_2SEt)LuCl$ with MeLi in toluene gave the lanthanide alkyls $(\eta^5\text{-}C_5H_4CH_2CH_2SEt)_2YMe$ and $(\eta^5\text{-}C_5Me_5)(\eta^5\text{-}C_5H_4CH_2CH_2SEt)LuMe$, respectively.

Single-crystal X-ray determinations of $(\eta^5\text{-}C_5H_4CH_2CH_2SEt)_2YCl$ and $(\eta^5\text{-}C_5Me_5)(\eta^5\text{-}C_5H_4CH_2CH_2SEt)LuCl$ exhibited monomeric structures for both complexes (Fig. 26). The geometry around the metal center in $(\eta^5\text{-}C_5H_4CH_2CH_2SEt)_2YCl$ is a distorted bipyramid where the cyclopentadiene centers and the chlorine atom are in equatorial and the sulfur atoms are in axial position. The Y–S distances (2.96 and 2.94 Å) indicate a coordination of sulfur to ytterbium in the solid state. The solid-state structure of $(\eta^5\text{-}C_5Me_5)(\eta^5\text{-}C_5H_4CH_2CH_2SEt)LuCl$ shows a distorted tetrahedral coordination sphere with a Lu–S bond distance of 2.79 Å, revealing sulfur–lutetium coordination. The Cp_{centr}–Ln distances for both complexes are in the range of homologues complexes with values of 2.399 and 2.39 Å for $(\eta^5\text{-}C_5H_4CH_2CH_2SEt)_2YCl$ and 2.29 Å ($CpCH_2CH_2SEt$) and 2.29 Å (C_5Me_5) for $(\eta^5\text{-}C_5Me_5)(\eta^5\text{-}C_5H_4CH_2CH_2SEt)LuCl$, respectively.

Variable temperature NMR measurements showed the flexible structure of $(\eta^5\text{-}C_5H_4CH_2CH_2SEt)_2YCl$ and $(\eta^5\text{-}C_5Me_5)(\eta^5\text{-}C_5H_4CH_2CH_2SEt)LuCl$ in solution. The signals for the sulfur-containing side chain are broadened at room

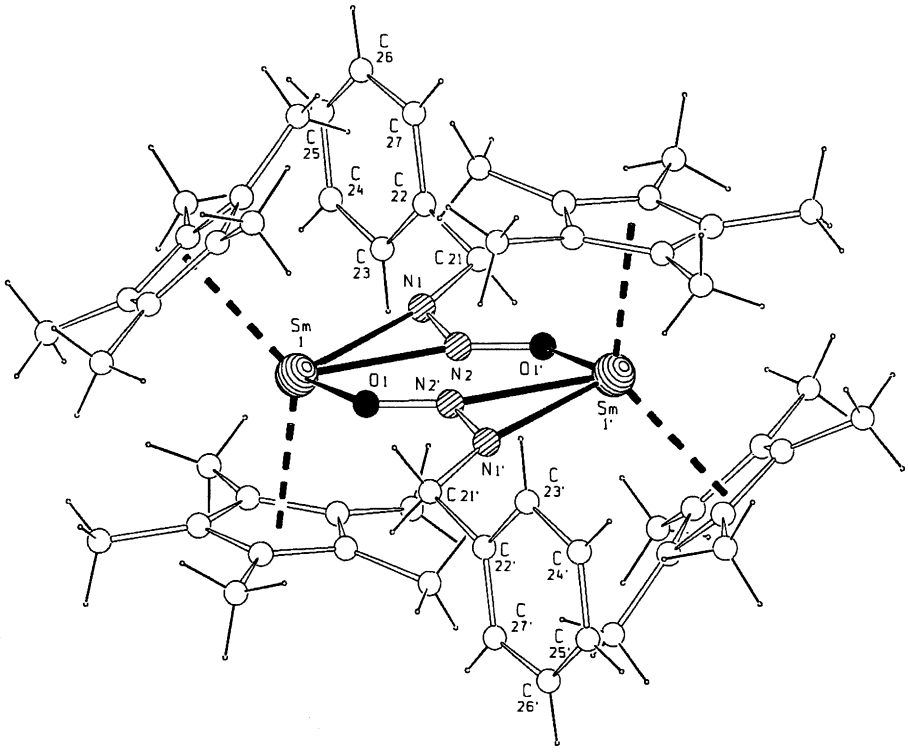

Fig. 24. Molecular structure of $[Cp^*_2SmC_6H_5CH_2NNO)]_2$.

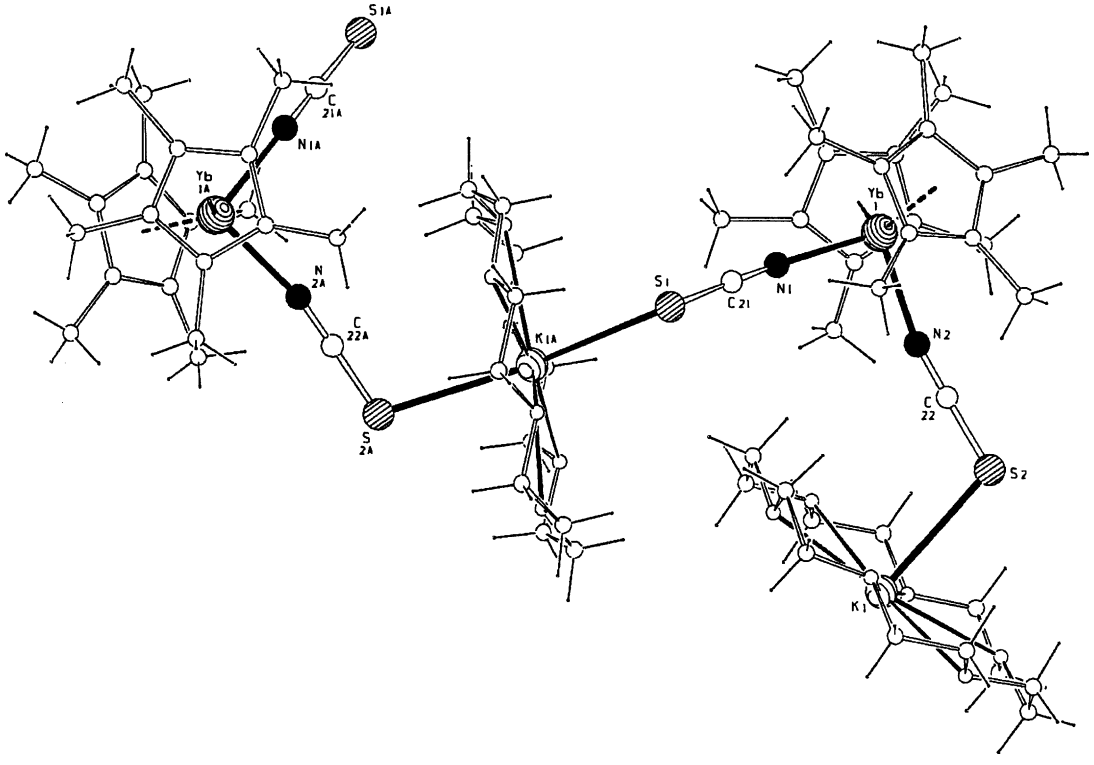

Fig. 25. Part of the molecular structure of $[K(18\text{-crown-6})Cp^*_2Yb(NCS)_2]$.

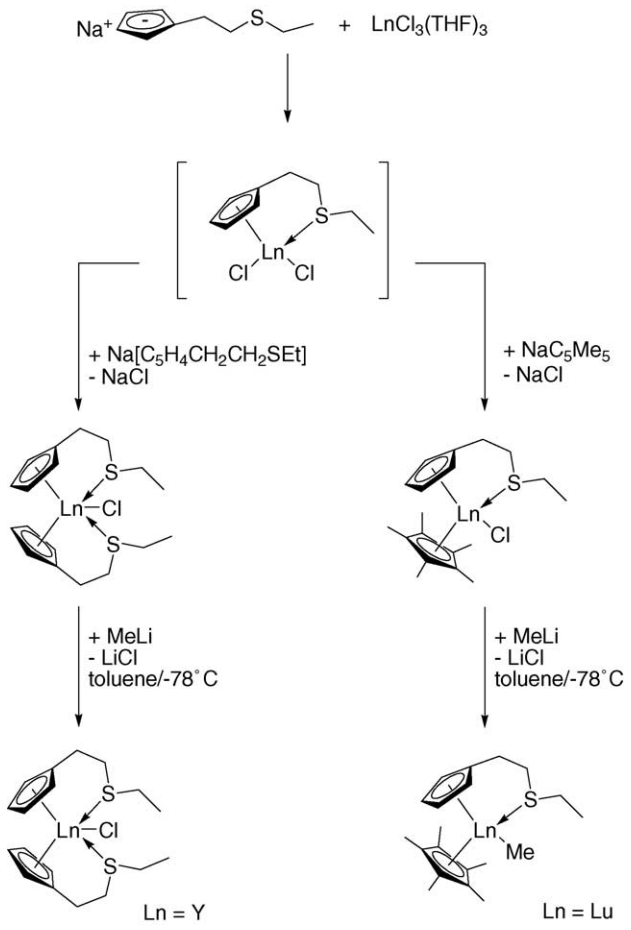

Scheme 15. Synthetic routes of the synthesis of lanthanide complexes with sulfur functionalized cyclopentadienyl complexes.

temperature in both complexes which indicates flexibility of the coordination, whereas the signals at −92 °C are sharp showing the lanthanide–sulfur coordination to be stronger and to exchange slower than the NMR time scale.

Evans et al. described the reaction of $(C_5Me_5)_3Nd$ and $(C_5Me_5)_3Sm$ with $Ph_3P{=}Se$, where the tris(pentamethylcyclopentadienyl) lanthanides function as one-electron donors [31]. The reaction of 1 equiv. of tris(pentamethylcyclopentadienyl) neodymium or tris(pentamethylcyclopentadienyl) samarium with 1 equiv. of $Ph_3P{=}Se$ leads to the Se_2^{2-}-bridged dimers $[\{(C_5Me_5)_2Nd\}_2(\mu\text{-}\eta^2{:}\eta^2\text{-}Se_2)]$ and $[\{(C_5Me_5)_2Sm\}_2(\mu\text{-}\eta^2{:}\eta^2\text{-}Se_2)]$, respectively (Scheme 16, Eq. (1)).

$(C_5Me_5)_3Ln$ complexes act like one-electron reducing agents. $Se{=}PPh_3$ is reduced to Ph_3P and $(\mu\text{-}\eta^2{:}\eta^2\text{-}Se_2)[(C_5Me_5)_2Nd]_2$. As a by-product, $(C_5Me_5)_2$ is isolated, which is in good agreement with a one-electron reduction. Single X-ray determinations reveal the dimeric structure of $(\mu\text{-}\eta^2{:}\eta^2\text{-}Se_2)[(C_5Me_5)_2Nd]_2$with a symmetric $Se–Se^{2-}$ bridge between both neodymium centers (Fig. 27). The Se–Se distance is 2.389 Å and is in good agreement to known Se–Se single bonds.

The reaction behavior of $(C_5Me_5)_3Sm$ is slightly different. An equimolar reaction of $(C_5Me_5)_3Sm$ with $SePPh_3$ leads to the homologous $Se–Se^{2-}$-bridged dimer $(\mu\text{-}\eta^2{:}\eta^2\text{-}Se_2)[(C_5Me_5)_2Sm]_2$. In contrast to $(C_5Me_5)_3Nd$, where $(\mu\text{-}\eta^2{:}\eta^2\text{-}Se_2)[(C_5Me_5)_2Nd]_2$ and unreacted $(C_5Me_5)_3Nd$ could be isolated, the reaction of 2 equiv. $(C_5Me_5)_3Sm$ with 1 equiv. of $Se{=}PPh_3$ in THF gives the Se^{2-}-bridged dimer $(\mu\text{-}Se)[(C_5Me_5)_2Sm(THF)]_2$, which is also the product of the reaction of $(C_5Me_5)_3Sm$ with $(\mu\text{-}\eta^2{:}\eta^2\text{-}Se_2)[(C_5Me_5)_2Sm]_2$ (Scheme 16, Eq. (2)). The different reaction behavior presumably is caused by the different ionic radii of Nd^{3+} and Sm^{3+}.

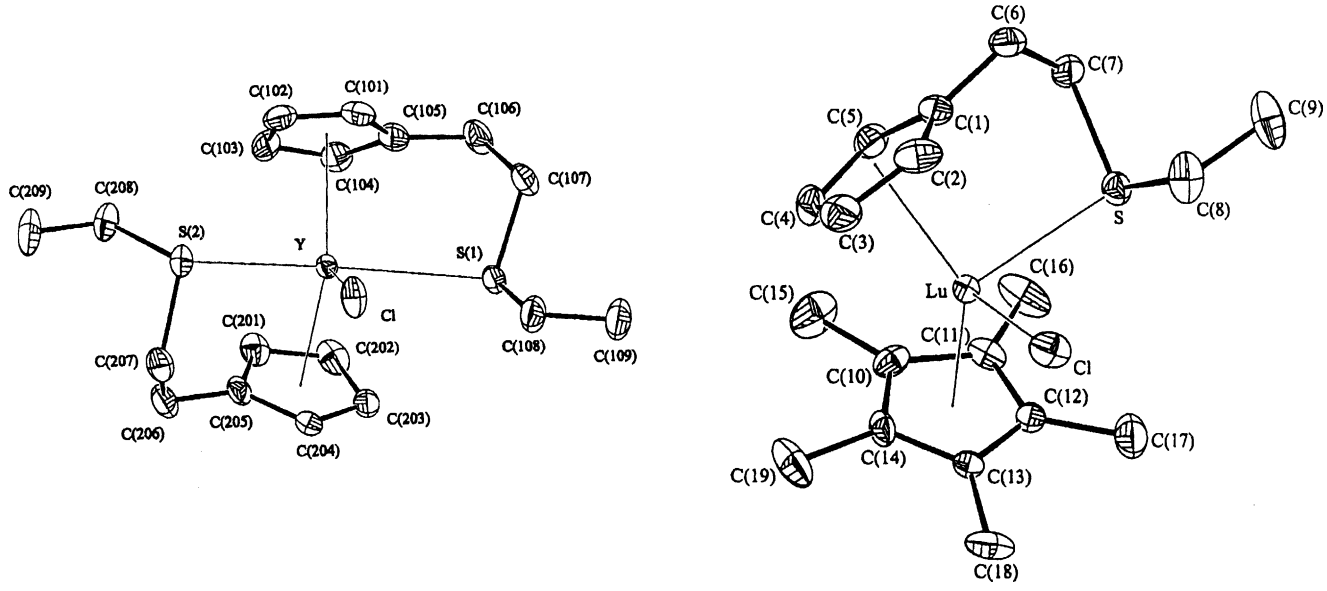

Fig. 26. Molecular structures of $(\eta^5\text{-}C_5H_4CH_2CH_2SEt)_2YCl$ and $(\eta^5\text{-}C_5Me_5)(\eta^5\text{-}C_5H_4CH_2CH_2SEt)LuCl$.

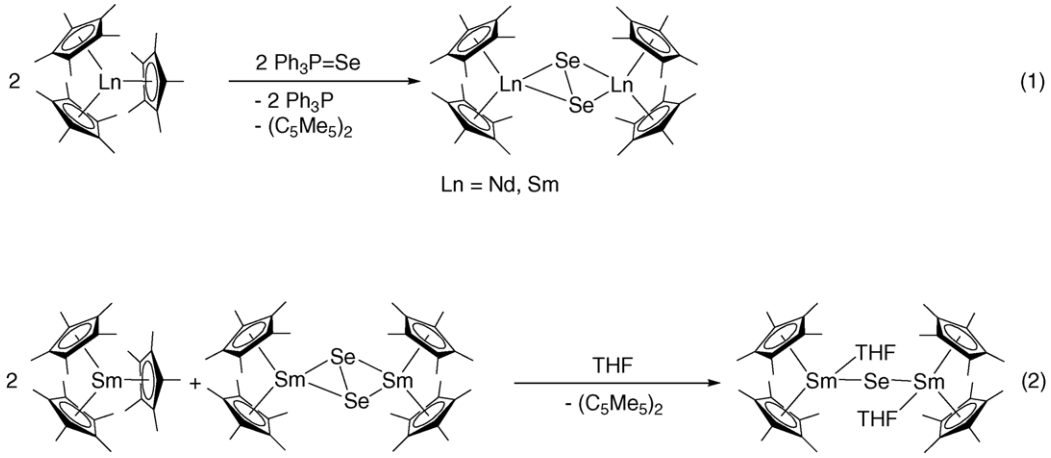

Scheme 16. Reactions of $(C_5Me_5)_3Nd$ and $(C_5Me_5)_3Sm$ with $Ph_3P{=}Se$.

Qian and co-workers reported the synthesis of $[Cp'_2Yb]_2(OC_{20}H_{20}N_2O)]$ ($Cp' = MeOCH_2CH_2C_5H_4$) from Cp'_3Yb and *trans*-(±)-2,2′-[1,2-cyclohexanediyl-bis(iminomethyl)]diphenol in THF (Scheme 17) which is in contrast to the previously described (Chapter 2.2.1) reaction of Cp'_3Sm with *trans*-(±)-2,2′-[1,2-cyclohexanediyl-bis(iminomethyl)]diphenol giving the mono(methoxyethylcyclopentadienyl)samarium complex $[\eta^5{:}\eta^1\text{-}Cp'Sm][(\mu{:}\eta\text{-}OC_{20}H_{20}N_2O)]_2[\eta^5\text{-}Cp'Sm]$ (Scheme E) [14]. In order to study the influence of the chelating ligand on the product behavior they also exchanged the methoxyethylcyclopentadienyl with tetrahydrofurfurylcyclopentadienyl in the reaction of Cp''_2DyCl with *trans*-(±)-2,2′-[1,2-cyclohexanediyl-bis(iminomethyl)]diphenol in THF yielding the C_2-symmetric dinuclear lanthanoidocene $[Cp''_2Dy]_2(OC_{20}H_{20}N_2O)]$, while a salt elimination reaction of Cp'_2DyCl ($Cp' = MeOCH_2CH_2C_5H_4$) with the disodium salt of *trans*-(±)-2,2′-[1,2-cyclohexanediyl-bis(iminomethyl)]diphenol gives the dinuclear mono(methoxyethylcyclopentadienyl) complex $([(MeOCH_2CH_2C_5H_4)Dy(OC_{20}H_{20}N_2O)]_2$ (Scheme 17). With the relatively small lanthanide center ytterbium the C_2-symmetric complex $[Cp'_2Yb]_2(OC_{20}H_{20}N_2O)]$ could be isolated, whereas the use of a larger lanthanide center (Sm) leads to the abstraction of two cyclopentadienyl ligands at each samarium. When the ligand is tetrahydrofurfurylcyclopentadiene, the C_2-symmetric dinuclear lanthanocene aryloxides can be obtained even with a relatively larger lanthanide ion (Dy in case of $[Cp''_2Dy]_2(OC_{20}H_{20}N_2O)]$).

Pernin and Ibers reported the synthesis of the imidodiphosphinochalcogenido complexes $Cp_2Y[\eta^3\text{-}N(SPPh_2)_2]$ and $Cp_2Y[\eta^3\text{-}N(SPPh_2)_2]$ ($Cp = C_5H_5$) [32]. These complexes have been synthesized in THF via a protonolysis reaction between Cp_3Y and the amines $HN(SPPh_2)_2$ and $HN(SePPh_2)_2$, respectively.

$$HN(SPPh_2)_2 + Cp_3Y \rightarrow Cp_2Y[\eta^3\text{-}N(SPPh_2)_2] + CpH$$

$$HN(SePPh_2)_2 + Cp_3Y \rightarrow Cp_2Y[\eta^3\text{-}N(SePPh_2)_2] + CpH \quad (Cp = C_5H_5)$$

In both compounds, the $[N(QPPh_2)_2]^-$ ligand (Q = S, Se) is bonded to the Y center in η^3-fashion. Additionally, the Y atom is coordinated to two cyclopentadienyl ligands, which leads to the formal coordination number of 9. Single-crystal X-ray determinations of the structures of both compounds showed the Y atom coordinated to the nitrogen atom of the $[N(QPPh_2)_2]^-$ ligand (Q = S, Se) and to both S atoms and Se atoms, respectively (Fig. 28). The molecules possess an approximate two-fold symmetry with Y–S distances of 2.93 Å and Y–Se distances of 3.05 Å.

The NMR spectra indicate that on the NMR time scale the molecules possess two-fold symmetry in solution. Furthermore, the molecules retain their Y–Q bonds in solution.

Lappert and co-workers reported that treatment of the appropriate compounds $[LaCp''_3]$, $[CeCp''_3]$, $[PrCp''_3]$ or $[NdCp''_3]$ with 2 equiv. of each [18]-crown-6 and potassium in benzene at ambient temperature affords the red or red–brown crystalline salts $[K([18]\text{-crown-6})][Ln\{Cp''\}_2(\mu\text{-}C_6H_6)]$ (Ln = La, Ce, Pr, Nd; $Cp'' = \eta^5\text{-}C_5H_3(SiMe_3)_2$-1,3) with $[K([18]\text{-crown-6})][Cp'']$ as a by-product [33] (Scheme 18).

Proton NMR spectra in benzene-d_6 show the lanthanum species to be diamagnetic, consistent with the presence of a lanthanate(III) anion. The signals of the [18] crown-6 moi-

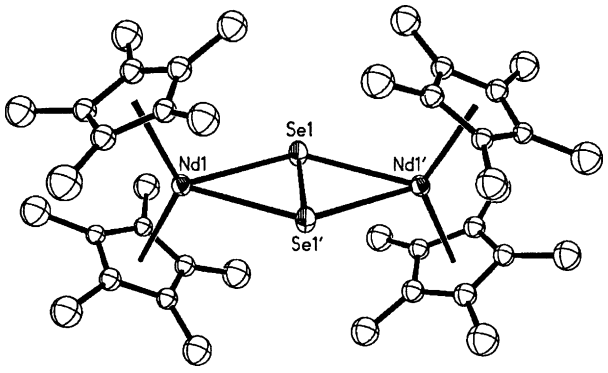

Fig. 27. Molecular structure of $(\mu\text{-}\eta^2{:}\eta^2\text{-}Se_2)[(C_5Me_5)_2Nd]_2$.

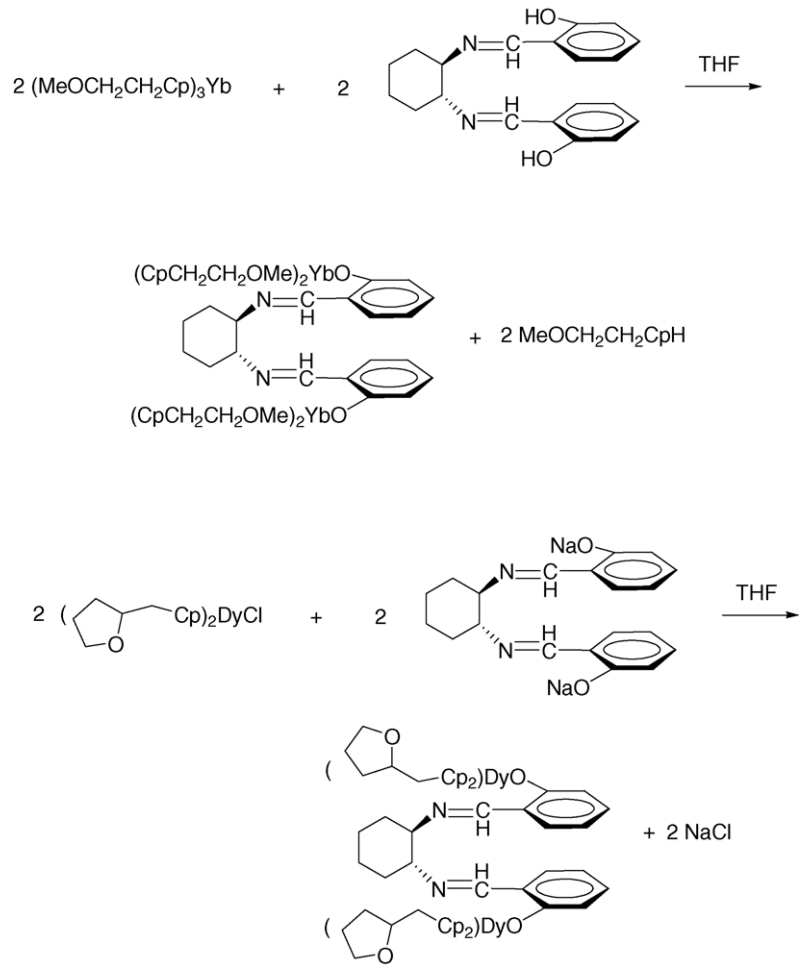

Scheme 17. Synthetic routes for the synthesis of $[Cp'_2Yb]_2(OC_{20}H_{20}N_2O)]$ ($Cp' = MeOCH_2CH_2C_5H_4$) and $[Cp''_2Dy]_2(OC_{20}H_{20}N_2O)]$ ($Cp'' = C_4H_7OCH_2C_5H_4$).

ety in the spectra of the Ce, Pr and Nd complexes are only slightly paramagnetically shifted. Hydrolysis of these lanthanide complexes yields cyclohexa-1,4-diene.

The molecular structures of the isomorphous salts $[Ln\{\eta^5\text{-}C_5H_3(SiMe_3)_2\text{-}1,3\}_2(\mu\text{-}C_6H_6)]$ (Ln = La, Ce, Nd) reveal that each consists of a tight ion pair with a C_6H_6 ligand bridging the K and Ln atoms (Fig. 29).

The potassium has close contacts to the six crown ether oxygen atoms and the centroids of the 2,3- and 5,6-carbon atoms of the C_6H_6 ligand. The latter is boat-shaped with

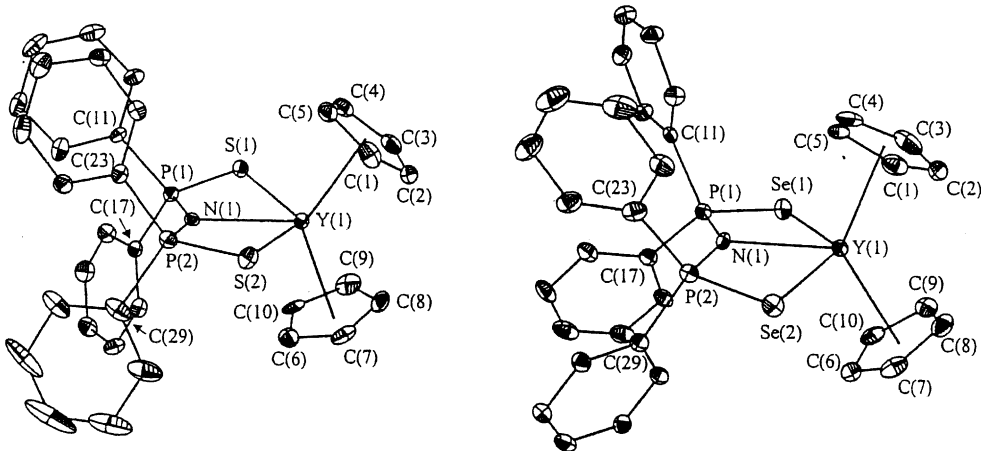

Fig. 28. Molecular structure of $Cp_2Y[\eta^3\text{-}N(SPPh_2)_2$ and $Cp_2Y[\eta^3\text{-}N(SePPh_2)_2]$.

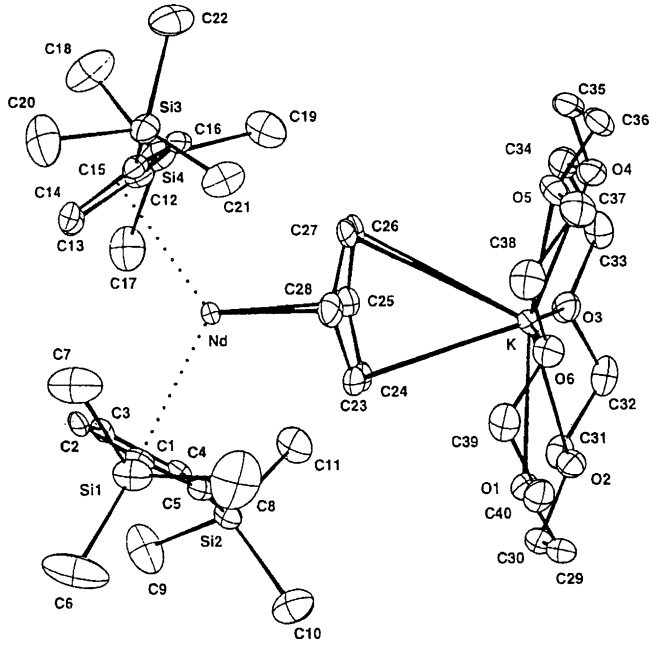

Fig. 29. Molecular structure of [K([18]-crown-6)][Nd{η^5-$C_5H_3(SiMe_3)_2$-1,3}$_2$(μ-C_6H_6)].

the shortest C–Ln distances being those to the 1- and 4-carbon atoms (2.62 Å/2.65 Å for La, 2.59 Å/2.61 Å for Ce and 2.56 Å/2.57 Å for Nd). The endocyclic bond angles at the 1- and 4-carbon atoms are narrower ($110.65 \pm 1.15^\circ$) than those at the other four ($122.4 \pm 1.2^\circ$), while the four C–C bonds to the 1- and 4-carbon atoms are longer (1.46 ± 0.02 Å) than the remaining two (1.35 ± 0.013 Å).

EPR studies of the reaction of [LaCp″$_3$] with K and [18]-crown-6 in benzene show the presence of at least four La(II) paramagnetic intermediate species prior to formation of [K([18]-crown-6)][La{η^5-$C_5H_3(SiMe_3)_2$-1,3}$_2$(μ-C_6H_6)].

Schumann et al. reported the synthesis of the lanthanidocene chloride complexes [(η^5-$C_5H_4SiMe_2R)_2Ln(\mu$-Cl)]$_2$ (R = *t*-Bu, Me; Ln = Y, Sm, Lu) from the appropriate lanthanide trichlorides and *t*-butyldimethylsilylcyclopentadienylpotassium or trimethylsilylcyclopentadienylpotassium, respectively (Scheme 19) [34]. The reactions were carried out in THF at ambient temperature. The dimeric dicyclopentadienyllanthanide chlorides react with 2 equiv. of methyllithium in diethylether to give the dimeric lanthanide methyl complexes [(η^5-$C_5H_4SiMe_2R)_2Ln(\mu$-Me)]$_2$ (R = *t*-Bu, Me; Ln = Y, Sm, Lu) which are moderately stable in atmospheric moisture. The reaction of the monochlorides [(η^5-$C_5H_4SiMe_3)_2Ln(\mu$-Cl)]$_2$ (Ln = Y, Sm, Lu) with methyllithium in a 1:4 ratio in THF afforded the monomeric lanthanidocene methyl complexes (η^5-$C_5H_4SiMe_2R)_2Ln(\mu$-Me)$_2$Li(THF)$_2$ (Ln = Y, Sm, Lu). Treatment of [(η^5-$C_5H_4SiMe_2R)_2Ln(\mu$-Me)]$_2$ (R = *t*-Bu, Me; Ln = Y, Sm, Lu) with stoichiometric amounts of H_2O in toluene yields the dimeric lanthanidocene hydroxy complexes [(η^5-$C_5H_4SiMe_2R)_2Ln(\mu$-OH)]$_2$ (R = *t*-Bu, Me; Ln = Y, Sm, Lu).

Schumann et al. showed that the decomposition reactions of the dicyclopentadienyl lanthanidocene methyl complexes [(η^5-$C_5H_4SiMe_2R)_2Ln(\mu$-Me)]$_2$ (R = *t*-Bu, Me; Ln = Y, Sm, Lu) in moist air depend on the ionic radius of the lanthanoid center and on the steric demand of the cyclopentadienyl ligand. The hydroxyl complexes [(η^5-$C_5H_4SiMe_2R)_2Ln(\mu$-OH)]$_2$ (R = *t*-Bu, Me; Ln = Y, Sm, Lu) were found to be intermediate products in the decomposition process. Single-crystal X-ray determinations of [(η^5-$C_5H_4SiMe_2{}^t$Bu)$_2$Lu(μ-Cl)]$_2$, [(η^5-$C_5H_4SiMe_3)_2$Y(μ-Me)]$_2$, [(η^5-$C_5H_4SiMe_2R)_2Lu(\mu$-OH)]$_2$ show the dimeric structure of these compounds (Fig. 30). The metal centers are coordinated by two cyclopentadienyl rings and the two bridging ligands (Cl, Me, OH) in a distorted pseudo-tetrahedral fashion. This coordination geometry closely resembles the coordination sphere of known dimeric dicyclopentadienyl lanthanidocene(III) complexes, as well as the bond distances and bond angles are in good agreement with known homologous compounds.

With Mak and co-workers yet another group examined the hydrolysis of organolanthanide compounds [35]. Partial hydrolysis of the cationic organolanthanide compounds [Cp″$_2$Sm]$_2$[B(C_6H_5)$_4$] and [Cp″$_2$Sm]$_2$[$CB_{11}H_6Br_6$] (Cp″ = $(Me_3Si)_2C_5H_3$) in toluene at $-30\,^\circ$C gave (μ-O)(μ-OH_2)[Cp″$_2$Sm]$_2$ and two distinct crystalline forms of [Cp″$_2$Sm(μ-OH)]$_2$, respectively. The two crystalline forms (form A and B) are not crystallographically interconvertible, and they are clearly distinguishable from one another. The

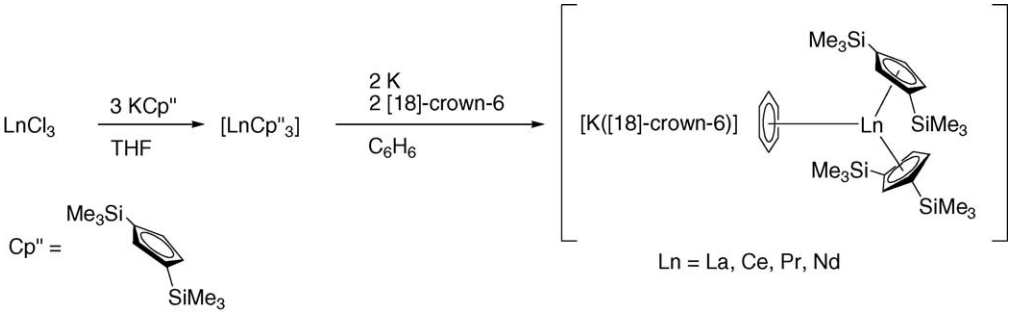

Scheme 18. [K([18]-crown-6)][Ln{η^5-$C_5H_3(SiMe_3)_2$-1,3}$_2$(μ-C_6H_6)] (Ln = La, Ce, Pr, Nd).

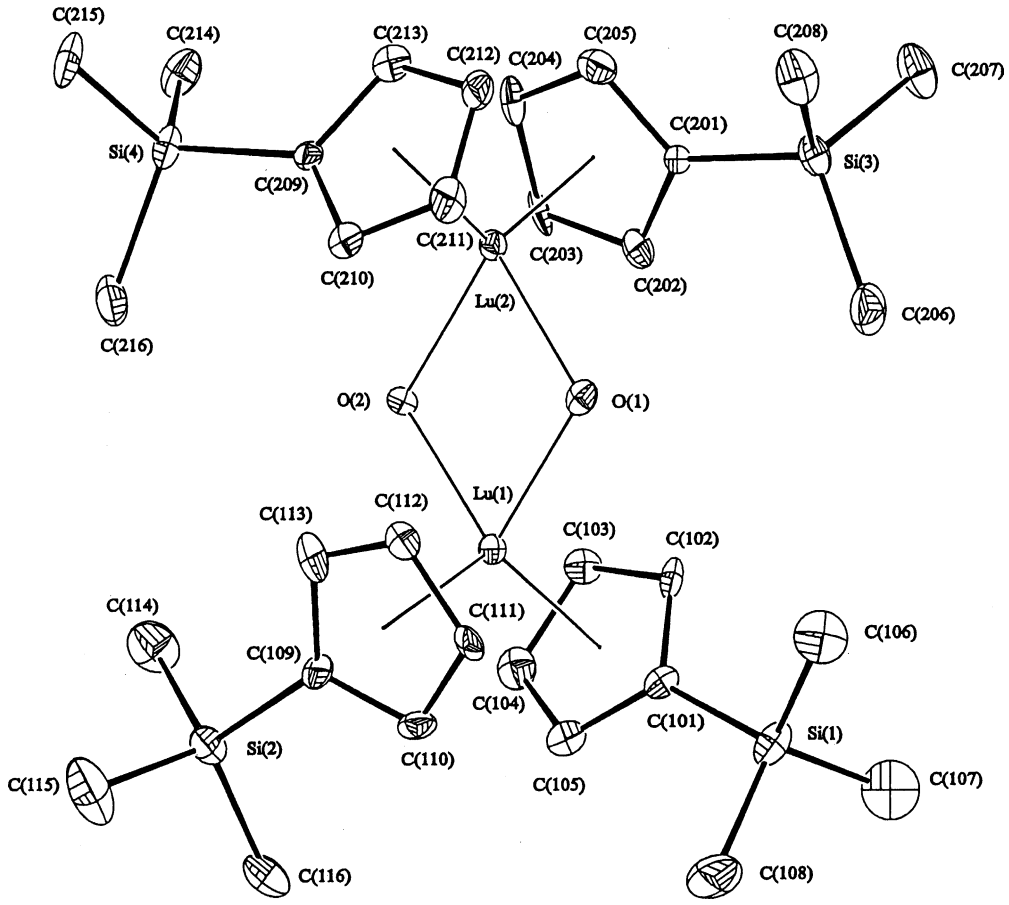

Fig. 30. Molecular structure of $[(\eta^5\text{-}C_5H_4SiMe_2R)_2Lu(\mu\text{-}OH)]_2$.

authors discuss that these observations imply that there may be a continuous process leading from organosamarium hydroxo to oxo compounds. The solid-state IR spectrum of $(\mu\text{-}O)(\mu\text{-}OH_2)[Cp''_2Sm]_2$ displays a broad band at 3300 cm^{-1} attributable to the O–H stretching frequency of the coordinated H_2O molecule, while the spectra of the two forms of $[Cp''_2Sm(\mu\text{-}OH)]_2$ exhibit one sharp band at 3668 cm^{-1} that is usually assigned to the O–H stretching mode of the Ln(OH)Ln unit.

Single-crystal X-ray determinations on $(\mu\text{-}O)(\mu\text{-}OH_2)[Cp''_2Sm]_2$ and $[Cp''_2Sm(\mu\text{-}OH)]_2$ confirmed their dimeric structure (Fig. 31). The samarium centers in $[Cp''_2Sm(\mu\text{-}OH)]_2$ are coordinated by two cyclopentadienyl rings and the OH– groups with Sm–O distances of 2.308–2.41 Å for the different forms of the molecule. $(\mu\text{-}O)(\mu\text{-}OH_2)[Cp''_2Sm]_2$ shows a dimeric structure as well with one oxygen bridge with Sm–O distances of 2.25 Å/2.32 Å and one H_2O bridge (Sm–O = 2.61 Å/2.63 Å).

Visseaux et al. examined the stability of coordinatively unsaturated dicyclopentadienyl neodymium hydrides [36]. The tris-alkylborohydride $Cp'_2NdHBEt_3$ ($Cp' = C_5H_4CH_2CH_2OCH_3$) obtained by reaction of $NaHBEt_3$ with Cp'_2NdCl (Scheme 20, Eq. (2)) is fairly stable in benzene solution whereas the hydride Cp'_2NdH formed from Cp'_2NdCl and NaH or by hydrogenolysis of Cp'_2NdR ($R = CH_2SiMe_3$ or $CH(SiMe_3)_2$ is a species of very short life, undergoing rearrangement to Cp'_3Nd (Scheme 20, Eq. (1)). The transient hydride can be trapped with ketones e.g. acetone or pivalone, leading to the alkoxides $Cp'_2NdOCHR'_2$ ($R' = Me$ or CMe_3) (Scheme 20, Eq. (4)). $Cp'_2NdOCHMe_2$ is not isolable, but was detected by its NMR spectra. In contrast, the use of the sterically hindered ketone pivalone afforded the stable alkoxide $Cp'_2NdOCH(CMe_3)_2$.

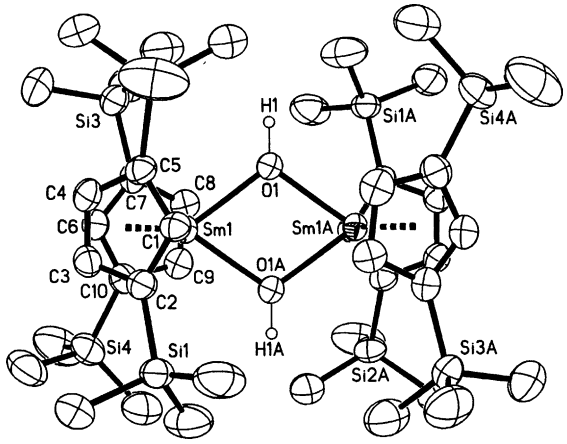

Fig. 31. Molecular structures of $(\mu\text{-}O)(\mu\text{-}OH_2)[Cp''_2Sm]_2$ and $[Cp''_2Sm(\mu\text{-}OH)]_2$ (form A).

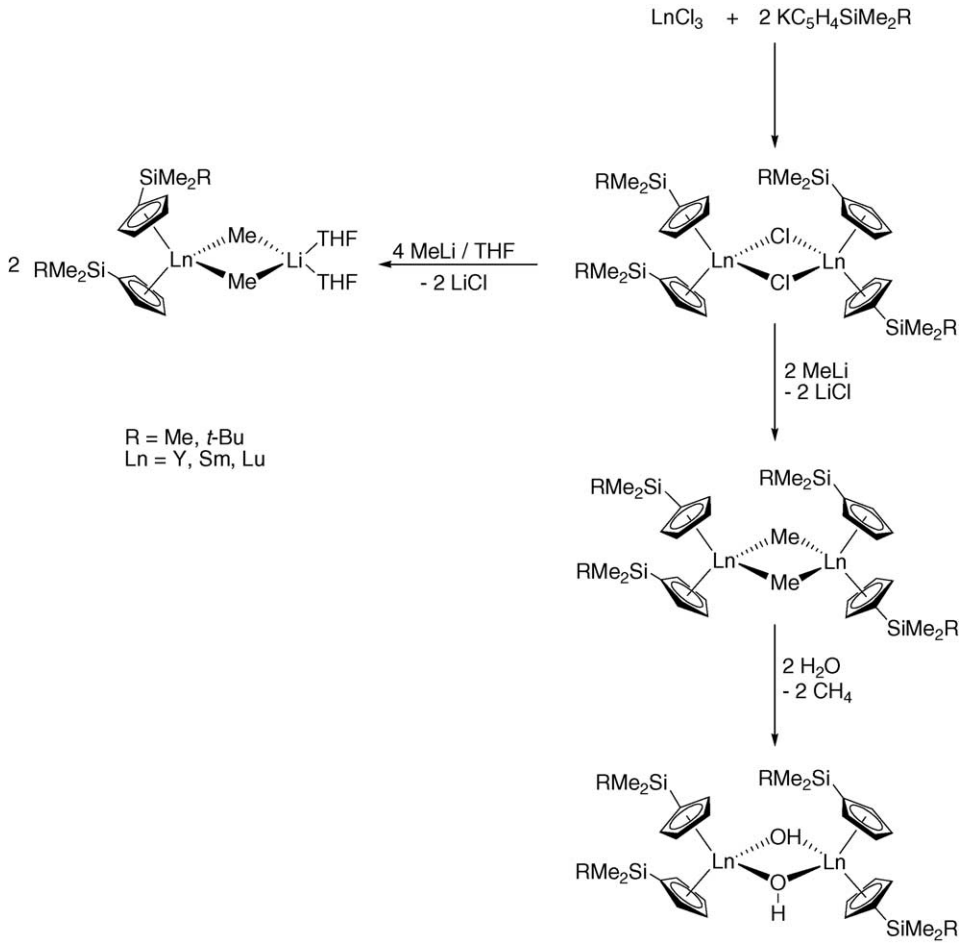

Scheme 19. Synthetic routes for the synthesis of the dicyclopentadienyl chloride, methyl and hydroxy complexes $[(\eta^5\text{-}C_5H_4SiMe_2R)_2Ln(\mu\text{-}X)]_2$ (R = *t*-Bu, Me; Ln = Y, Sm, Lu; X = Cl, Me, OH).

$Cp'_2NdOCH(CMe_3)_2$ is also produced by the reaction of pivalone with the borohydrides $Cp'_2NdHBEt_3$ and Cp'_2NdBH_4, and is also formed in the alcoholysis of Cp'_3Nd with pivalic alcohol (Scheme 20, Eq. (3)).

2.2.2.1. ansa-Cyclopentadienyl complexes. Schumann et al. published a large series of mixed substituted dicyclopentadienyldimethylsilanes and the corresponding lanthanidocene complexes [37]. They described the reaction of Me_2SiCl_2

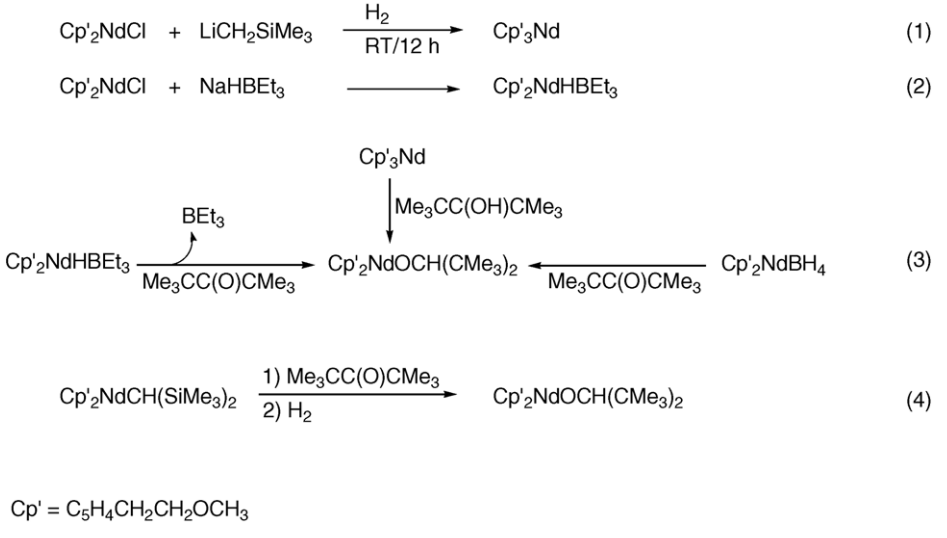

Scheme 20. Synthesis and reaction behaviour of neodymium hydrides.

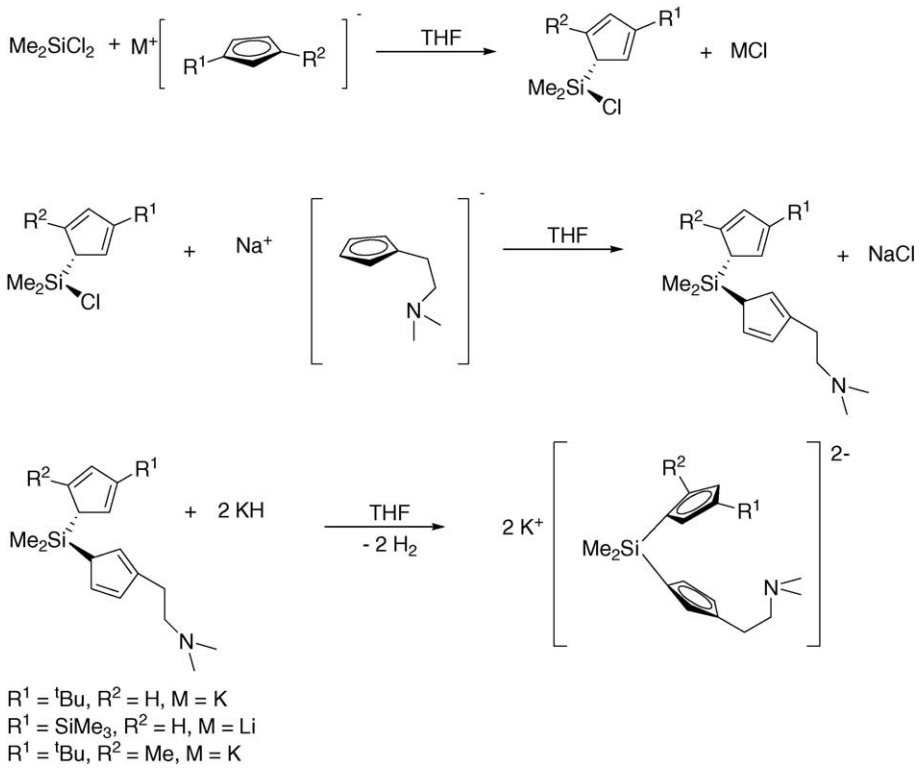

Scheme 21. Synthesis of the potassium salts of donor-functionalized cyclopentadienes.

with $K[C_5H_4{}^tBu]$, $Li[C_5H_4SiMe_3]$ or $K[C_5H_3{}^tBuMe\text{-}3]$ followed by treatment with $K[C_5H_4CH_2CH_2NMe_2]$ yielding mixed substituted dicyclopentadienyldimethylsilanes which after double deprotonation with potassium hydride afforded the dipotassium salts $K_2[Me_2Si(C_5H_3{}^tBu\text{-}3)(C_5H_3CH_2CH_2NMe_2\text{-}3)]$, $K_2[Me_2Si(C_5H_3SiMe_3\text{-}3)(C_5H_3CH_2CH_2NMe_2\text{-}3)]$ and $K_2[Me_2Si(C_5H_2{}^tBu\text{-}3\text{-}Me\text{-}5)(C_5H_3CH_2CH_2NMe_2\text{-}3)]$, respectively (Scheme 21).

The reaction of the dipotassium salts with lanthanide trichlorides in a 1:1 molar ratio gave the *ansa*-lanthanidocenes according to Scheme 21. Asymmetrical substitution of the cyclopentadiene ligands leads to the possible formation of four different isomers. However, the NMR spectra imply the presence of a racemic mixture of just one enantiomeric form. The NMR spectra in benzene show two signals for the methyl protons of the amino function, which implies the coordination of the nitrogen to the metal. Single-crystal X-ray determinations of $[Me_2Si(C_5H_2{}^tBu\text{-}3\text{-}Me\text{-}5)(C_5H_3CH_2CH_2NMe_2\text{-}3)]SmCl$ and $[Me_2Si(C_5H_2{}^tBu\text{-}3\text{-}Me\text{-}5)(C_5H_3CH_2CH_2NMe_2\text{-}3)]LuCl$ reveal their monomeric structure with pseudo-tetrahedral coordinated metal centers (Fig. 32). The metal centers are coordinated by the cyclopentadienyl ligands in an η^5-fashion, chlorine and the nitrogen atom of the dimethylamino group. The metal–Cp and metal–N distances of both complexes are in good agreement with those of related complexes.

Alkylation of some of the lanthanidocene monochlorides with $LiCH_3$, $LiCH_2SiMe_3$, and $LiCH(SiMe_3)_2$ led to the corresponding alkylmetallocenes according Scheme 22. The alkylated species $Me_2Si(C_5H_3{}^tBu\text{-}3)(C_5H_3CH_2CH_2NMe_2\text{-}3)]LnR$ (R = Me, Ln = Sm, Y; R = CH_2SiMe_3, Ln = Y), $[Me_2Si(C_5H_3SiMe_3\text{-}3)(C_5H_3CH_2CH_2NMe_2\text{-}3)]YMe$, and $[Me_2Si\ (C_5H_2{}^tBu\text{-}3\text{-}Me\text{-}5)(C_5H_3CH_2CH_2NMe_2\text{-}3)]$ LnR (R = CH_3, Ln = Lu; R = CH_2SiMe_3, Ln = Lu; R = $CH(SiMe_3)_2$, Ln = Nd, Lu) several signal sets in the NMR spectra indicating the existence of an enantiomeric mixture like in case of the homologous monochloride complexes. NMR spectroscopic determinations in pyridine suggest dissociation the dimethylamino group in strongly basic solvents.

In order to synthesize new tris(peralkylcyclopentadienyl)samarium complexes (see Chapter 2.2.3), Evans et al. allowed SmI_3 to react with $Me_2Si(C_5Me_4K)_2$ to obtain $Me_2Si(C_5Me_4)_2SmI(THF)$ [38] (Scheme 23).

A single-crystal X-ray determination showed a monomeric structure for $(C_5Me_4)_2SmI(THF)$ with normal Sm–Cp, Sm–I and Sm–O(THF) distances.

Bulychev and co-workers showed, that the *ansa*-ytterbocene complex *meso*-$(CH_3)_2Si(3\text{-}(CH_3)_3SiC_5H_3)_2YbCl(THF)$ undergoes desolvation during recrystallization from toluene to give the dimeric complex $[meso\text{-}(CH_3)_2Si[3\text{-}(CH_3)_3SiC_5H_3]_2Yb(\mu_2\text{-}Cl)]_2$ [39]. Single-crystal X-ray determinations of the dimer showed longer Yb–Cl distances (2.631 and 2.681 Å) than that in the starting monomeric sol-

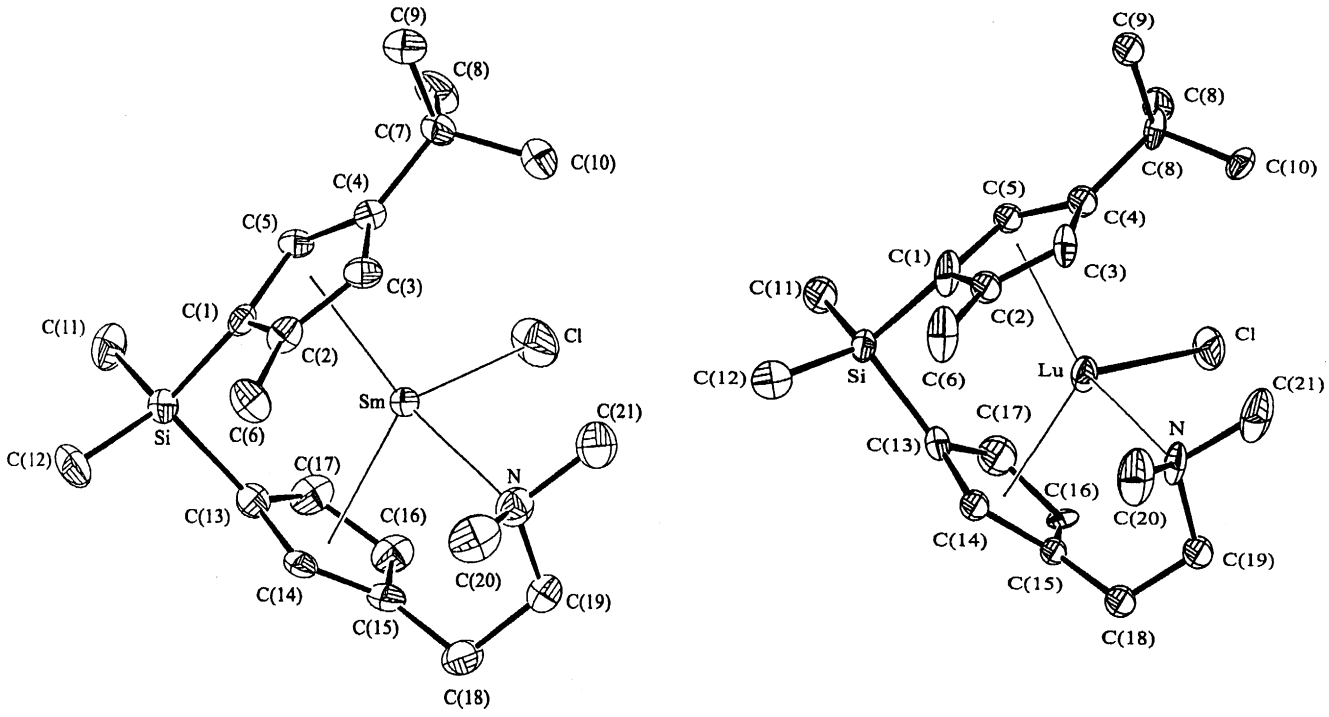

Fig. 32. Molecular structure of $[Me_2Si(C_5H_2{}^tBu\text{-}3\text{-}Me\text{-}5)(C_5H_3CH_2CH_2NMe_2\text{-}3)]SmCl$.

vated complex (2.496 Å), but they are about equal to those in other known dimeric chlorides (Fig. 33). The parameters of the metallocene fragment of the dimer are identical to those of the starting complex.

The monomeric complex *meso*-$(CH_3)_2Si(3\text{-}(CH_3)_3SiC_5H_3)_2YbCl(THF)$ reacts with $LiBH_4$ in diethyl ether, yielding the borohydride complex *meso*-$(CH_3)_2Si(3\text{-}(CH_3)_3SiC_5H_3)_2YbBH_4(THF)$ with a tridentate BH_4 group,

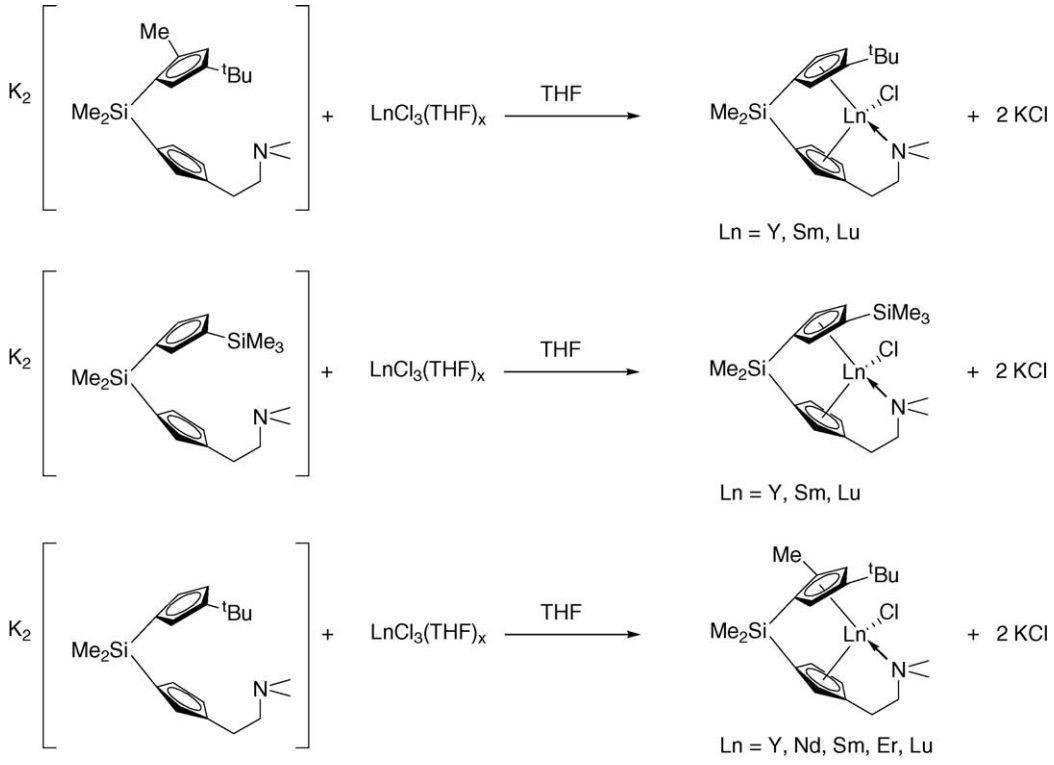

Scheme 22. Synthesis of donor-functionalized *ansa*-metallocenes of yttrium, neodymium, erbium and lutetium.

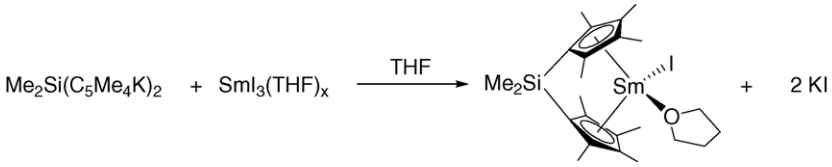

Scheme 23. Synthesis of $(SiMe_2C_5Me_4)_2SmI(THF)$.

while in similar lanthanide borohydrates the BH_4 group is often bonded in a bidentate fashion with B–H bond length typical for such compounds.

The chiral silicon-bridged lanthanidocene chlorides $[MeRSi(C_5H_4)(C_5Me_4)LnCl]_2$ (R = Et, Ph; Ln = Y, La, Sm, Lu) were made by Schumann et al. [40] according to Scheme 24 from the disodium salts $[MeRSi(C_5H_4)(C_5Me_4)]Na_2$ (R = Et, Ph) and the corresponding lanthanide trichlorides in THF.

The ^1H NMR spectra indicate the presence of monomeric THF-containing complexes of the type $MeRSi(C_5H_4)(C_5Me_4)LnCl(THF)$ as primary products which on vacuum-drying lose their THF under formation of the dimers. Single-crystal X-ray determination of $[MeEtSi(C_5H_4)(C_5Me_4)SmCl(THF)]_2$ shows the dinuclear complex (Fig. 34). One THF molecule is coordinated to each samarium. Distances and angles are roughly similar to that of known compounds of the same type.

2.2.3. Tris(cyclopentadienyl) complexes

Lappert and co-workers reported the synthesis of the new tris(cyclopentadienyl)lanthanoide(III) complexes $[LaCp''_3]$

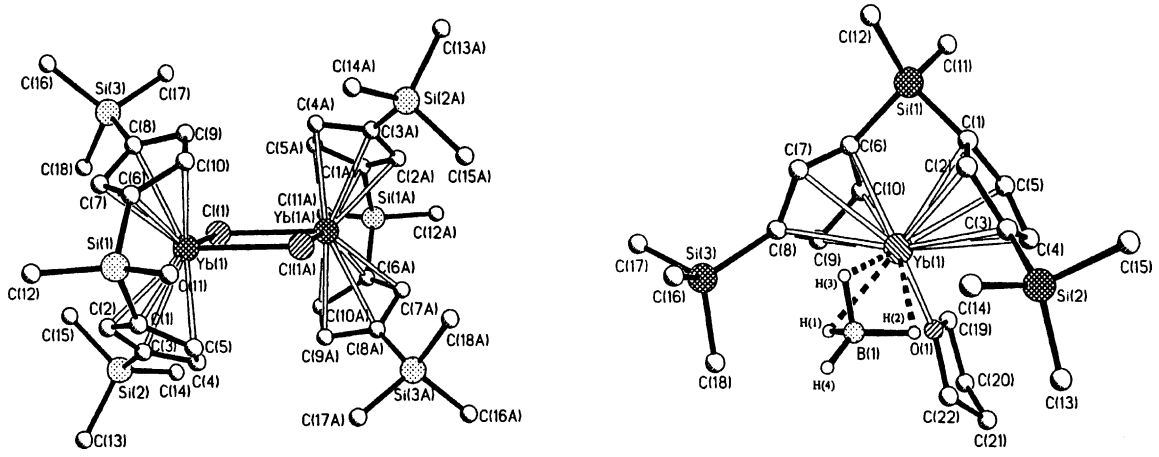

Fig. 33. Molecular structures of $[meso\text{-}(CH_3)_2Si[3\text{-}(CH_3)_3SiC_5H_3]_2Yb(\mu_2\text{-}Cl)]_2$ and $meso\text{-}(CH_3)_2Si(3\text{-}(CH_3)_3SiC_5H_3)_2YbBH_4(THF)$.

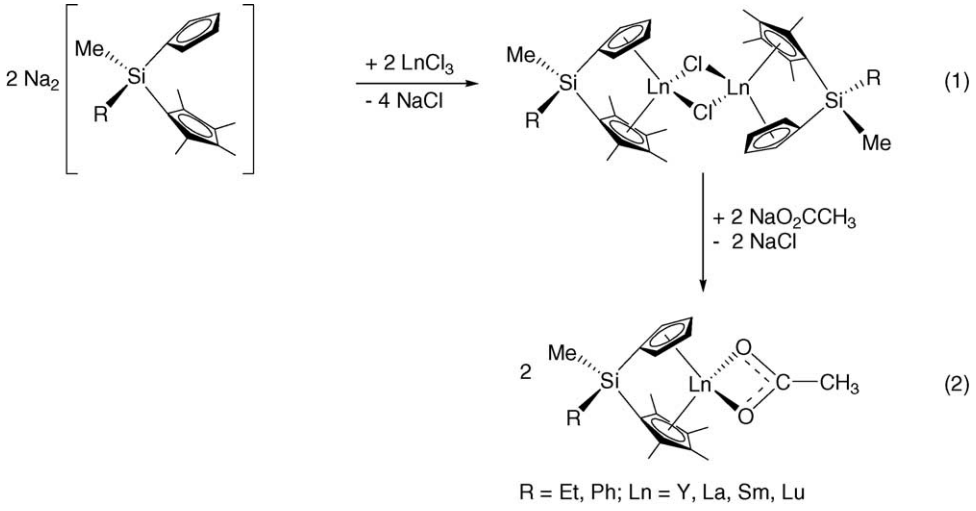

Scheme 24. Synthetic routes for the synthesis of $[MeRSi(C_5H_4)(C_5Me_4)LnCl]_2$ (R = Et, Ph; Ln = Y, La, Sm, Lu) and the corresponding monomeric acetates $[MeRSi(C_5H_4)(C_5Me_4)LnO_2CMe]$ (R = Et, Ph; Ln = Y, La, Sm, Lu).

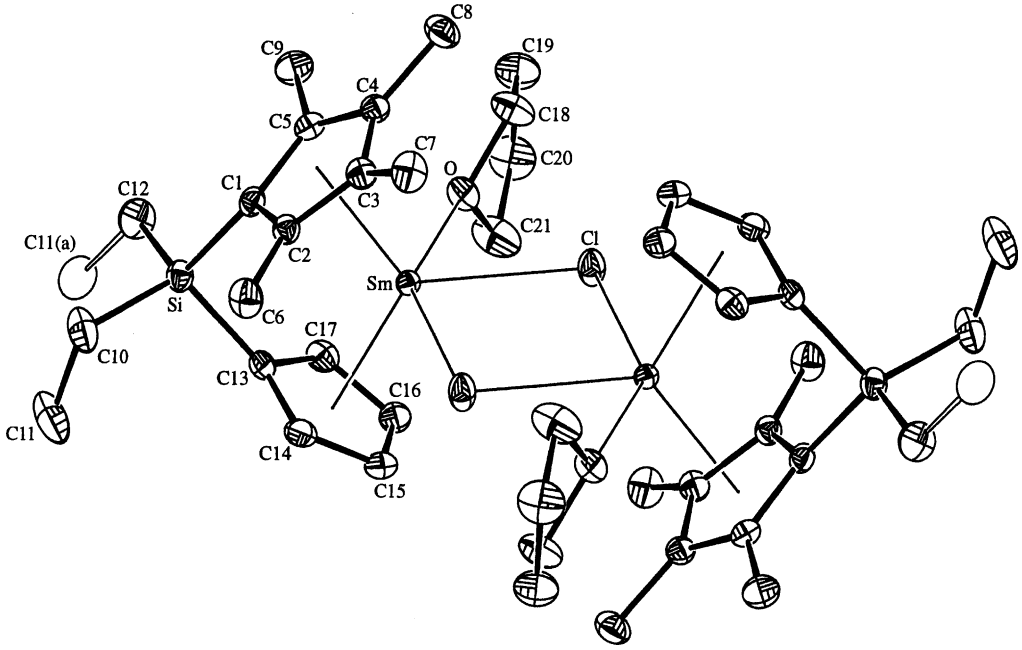

Fig. 34. Molecular structure of $[MeEtSi(C_5H_4)(C_5Me_4)SmCl(THF)]_2$.

and $[PrCp''_3]$ with $Cp'' = \eta^5$-$C_5H_3(SiMe_3)_2$-1,3 which were made from the appropriate anhydrous lanthanide(III) triflates or chlorides and 3/2 $MgCp''_2$ or 3 KCp'' in THF at ambient temperature [33]. Reactions of $[LaCp''_3]$ and $[LaCp''_3]$ have been described above (Chapter 2.2.2).

Evans et al. showed that the reaction of $Me_2Si(C_5Me_4)_2SmI(THF)$ with KC_5Me_5 in toluene yielded the base-free complex $Me_2Si(C_5Me_4)_2Sm(C_5Me_5)$, whereas the same reaction in THF produced the THF adduct $Me_2Si(C_5Me_4)_2Sm(C_5Me_5)(THF)$ [38] (Scheme 25, Eqs. (1) and (2)).

Similarly to the reaction with KC_5Me_5, treatment of $Me_2Si(C_5Me_4)_2SmI(THF)$ with KC_5Me_4R (R = Et, *n*-Pr, *i*-Pr) in toluene afforded the base free tris(cyclopentadienyl) systems (Scheme 25, Eq. (3)). Single-crystal X-ray determinations revealed a pseudo-tetrahedral coordina-

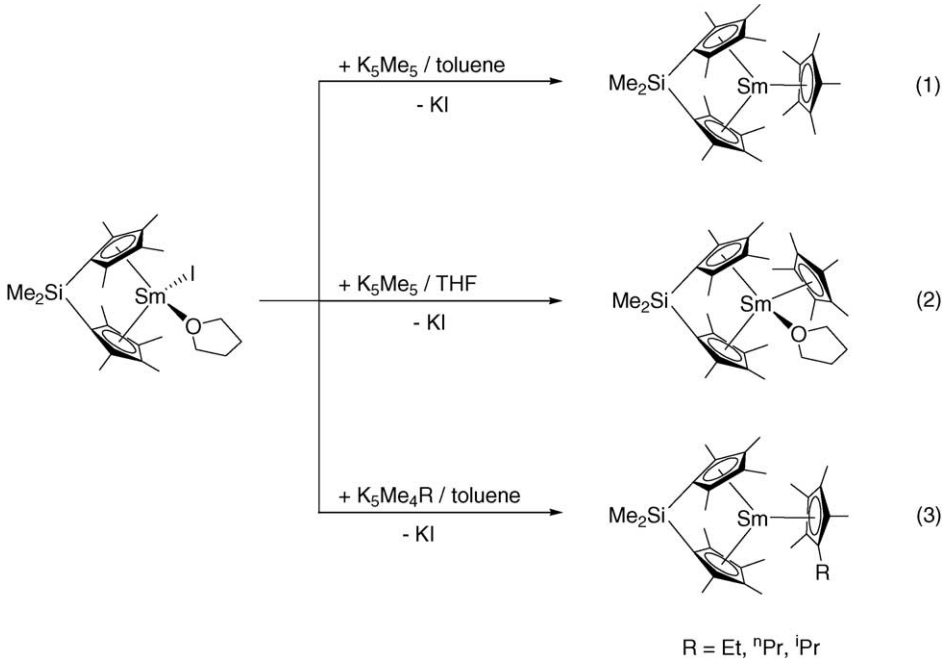

Scheme 25. Reaction of $Me_2Si(C_5Me_4)_2SmI(THF)$ with the potassium salts of various cyclopentadienyls.

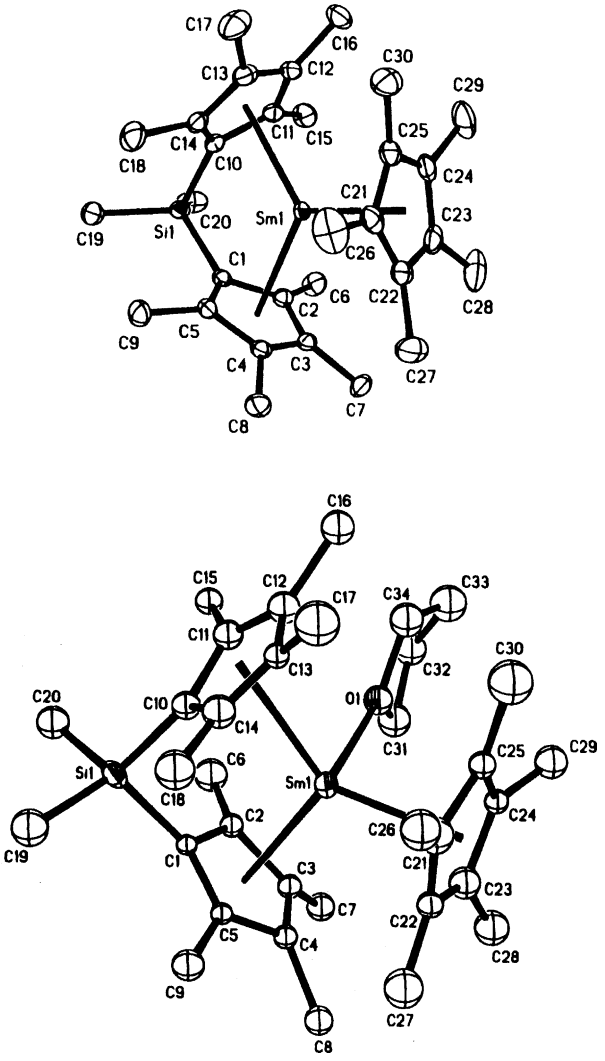

Fig. 35. Molecular structures of $Me_2Si(C_5Me_4)_2Sm(C_5Me_5)(THF)$ and $Me_2Si(C_5Me_4)_2Sm(C_5Me_5)$.

tion sphere for $Me_2Si(C_5Me_4)_2Sm(C_5Me_5)(THF)$ and a pseudo-trigonal one for $Me_2Si(C_5Me_4)_2Sm(C_5Me_5)$ and $Me_2Si(C_5Me_4)_2Sm(C_5Me_4$*n*-Pr), respectively (Fig. 35).

Bond lengths and angles are in the same range as in similar compounds. The (ring centroid)–metal(ring centroid) angles of the $Me_2Si(C_5Me_4)_2$ units in each structure range from 115.2° to 123.3° and have average Sm–C(ring) distances of 2.70–2.92 Å. The average Sm–C(C_5Me_4R) distance is 2.77 and 2.82 Å. The β-carbon of the propyl substituent in $Me_2Si(C_5Me_4)_2Sm(C_5Me_4{}^nPr)$ is orientated to the samarium at a distance of 3.36 Å. In contrast to $(C_5Me_5)_3Sm$ the complexes $Me_2Si(C_5Me_4)_2Sm(C_5Me_5)(THF)$ and $Me_2Si(C_5Me_4)_2Sm(C_5Me_4R)$ (R = Me, Et, *n*-Pr, *i*-Pr) do not show the reductive ring opening reaction of THF and consistently no polymerization of ethylene or reduction chemistry as observed for $(C_5Me_5)_3Sm$.

Lappert and co-workers described the synthesis of a series of homoleptic tris(substituted-cyclopentadienyl)lanthanide(III) complexes $[LnCp_3{}^R]$ (Ln = La, Ce, Pr, Nd, Sm, Gd, Tb, Dy, Er, Tm, Yb) $[Cp_3{}^R = C_5H_4(CH(SiMe_3)_2)]$ [41]. The complexes were synthesized from the appropriate lanthanide trichlorides or TmI_3 in the case of thulium with 3 equiv. of KCp^R in THF. Single-crystal X-ray determinations show the isostructural complexes of $NdCp_3{}^R$ and $TmCp_3{}^R$ to be monomeric with bond lengths and angles in the expected areas (Fig. 36). No short M-C agnostic interactions were observed. As potential starting materials for organoneodymium(II) complexes, $NdCp_3{}^t$ and $NdCp_3{}^{tt}$ as well as $CeCp_3{}^{tt}$ were synthesized ($Cp^t = C_5H_4(SiMe_2{}^tBu)$, $Cp^{tt} = C_5H_3(SiMe_2{}^tBu)_2$-1,3) from the related lanthanide trichlorides and 3 equiv. of $NaCp_3{}^t$ or $KCp_3{}^{tt}$, respectively. $NdCp_3{}^t$, $NdCp_3{}^{tt}$ and $CeCp_3{}^{tt}$ are monomeric with η^5-bonded cyclopentadienyl ligands. All complexes are highly soluble in hydrocarbons owing to the bulky substituents.

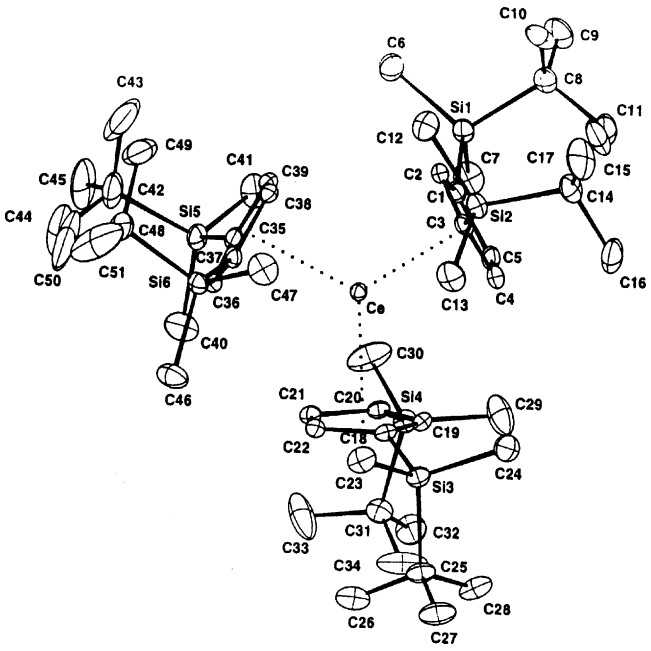

Fig. 36. Molecular structure of $Ce[C_5H_3(SiMe_2{}^tBu)_2$-1,3$]_3$.

The X-ray structure determination of single crystals of $CeCp_3{}^{tt}$ (Fig. 36) revealed an approximate C_3 symmetry with Ce–C(centroid) distances of 2.55°.

A series of tris(cyclopentadienyl)lanthanoid(III) sulfoxide adducts as well as their tris (indenyl) analogues (see Chapter 2.4) were synthesized by Fischer and co-workers [42]. These complexes were investigated using variable temperature NMR and circular dichroism. This new class of adducts was prepared by the reaction of the THF adducts of the tris(cyclopentadienyl)lanthanides with the sulfoxides MTSO (OS(Me)4-MeC_6H_4) or DPSO ($OSPh_2$) in toluene (Table 1).

In Fig. 37, molecular structures of two representative examples of the MTSO and DPSO adducts are compared. As expected for the strongly oxophilic Ln^{3+} ions, the sulfoxide ligand is coordinated exclusively through its oxygen atom.

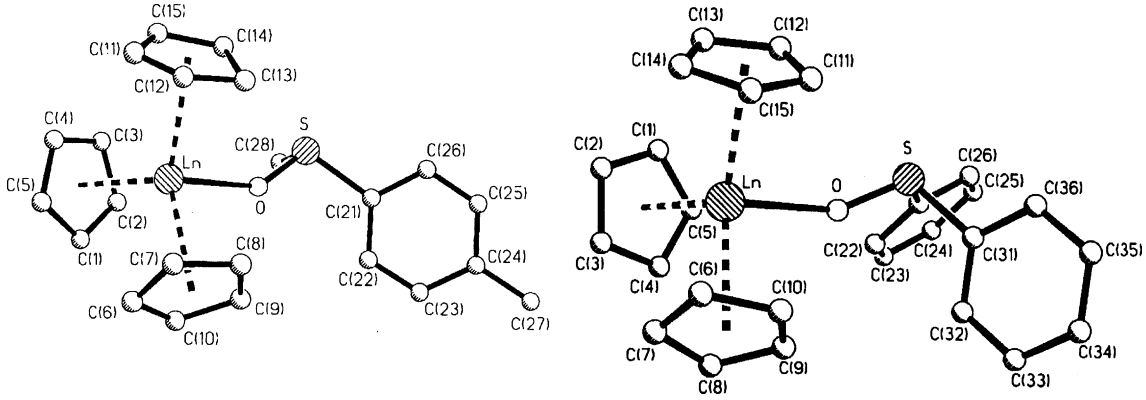

Fig. 37. Molecular structures of $[LnCp_3(OS(Me)/4\text{-}MeC_6H_4)]$ (Ln = La, Pr, Nd) and $[LnCp_3(OSPh_2)]$ (Ln = La, Pr).

Table 1
List of known $[LnCp_3(OSR/R')]$ complexes (R/R′ = Me/4-MeC_6H_4 or Ph/Ph), with (*R*)-(+)-MTSO

MTSO	La	Pr	Nd	Sm	Yb
DPSO	La	Pr	Nd		

Ln–O distances are shorter by about 10 pm than in the corresponding THF adducts.

2.3. Arene complexes

Metal-π-arene interactions were reported by Niemeyer and Hauber for the solid-state structures of two Lewis-donor-free aryl-bis(cyclopentadienyl)lanthanides [43]. Ar′Yb$(C_5H_4Me)_2$ and Ar′Sm$(C_5H_5)_2$ (Ar′ = 2,6-$Mes_2C_6H_3$) have been obtained by the reaction of LiAr′ with Yb$(C_5H_4Me)_3$ or Sm$(C_5H_5)_3$ in toluene. Single-crystal X-ray determinations reveal η^5-coordination of the cyclopentadienyl ligands to the metal centers in both cases and η^1-coordination to the *ipso*-carbon atom of the aryl groups (Fig. 38). Additional π-arene contacts to one mesityl group give rise to a different pyramidalization of the metal centers, which depends on the size of the central lanthanide ion.

The influence of intramolecular lanthanide-π-arene interactions on the structural architecture of homoleptic aryl-

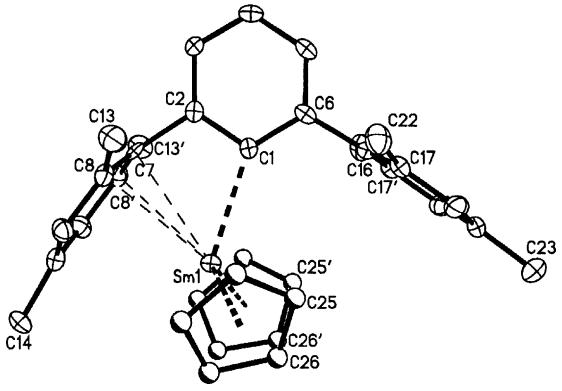

Fig. 38. Molecular structure of Ar′Sm$(C_5H_5)_2$ (Ar′ = 2,6-$Mes_2C_6H_3$).

oxolanthanide complexes was studied by Deacon et al. [44]. The homoleptic binuclear aryloxolanthanide(II) complexes $[Eu_2(Odpp)(\mu\text{-}Odpp)_3]$, $[Yb_2(Odpp)_2(\mu\text{-}Odpp)_2]$ and $[Yb_3(Odpp)_7]$ ($^-$Odpp = 2,6-diphenylphenolate) have been prepared by direct reactions of ytterbium or europium metal with 2,6-diphenylphenol in the presence of mercury at elevated temperatures in sealed tubes (Scheme 26).

X-ray diffraction studies of $[Eu_2(Odpp)_4]$ and $[Yb_2(Odpp)_4]$ reveal different binuclear structures (Fig. 39). In the europium complex three aryloxide oxygens bridge two Eu ions, with a terminal Odpp and three η^1-π-bonded substituent phenyl groups also being attached to one europium, and three η^2-π-bonded phenyl groups to the other. By contrast, both Yb atoms of $[Yb_2(Odpp)_4]$ have one terminal and two bridging Odpp ligands in a pyramidal arrangement and the coordination sphere is completed by π-interactions of pendant phenyl groups (one η^4- and one η^3- to one Yb, and an η^6- and an η^1-Ph group to the other). The structure of $[Yb_3(Odpp)_7]$ comprises an unprecedented $[Yb(II)_2(Odpp)_3]^+$ cation and a $[Yb(III)(Odpp)_4]^-$ anion.

Arene complexes with boratabenzene derivatives as π-bonded arene ligands were synthesized by Herberich et al. [45]. The bis(boratabenzene)scandium complexes $ScCl(C_5H_5BMe)_2]_2$ $ScCl(3,5\text{-}Me_2C_5H_3BNMe_2)_2]_2$ and $ScCl(3,5\text{-}Me_2C_5H_3BN(SiMe_3)_2)_2$ are synthesized from the solvent free lithium boratabenzenes and $ScCl_3$ in toluene (Scheme 27).

$$2ScCl_3 + 4LiL \rightarrow [ScClL_2]_2 + 4LiCl$$
$$(L = C_5H_5BMe \text{ or } 3,5\text{-}Me_2C_5H_3BNMe_2) \quad (12)$$

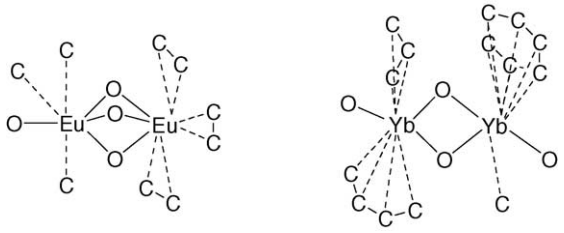

Scheme 26. Simplified representation of the coordination sphere around the metal centers in $[Eu_2(Odpp)_4]$ and $[Yb_2(Odpp)_4]$.

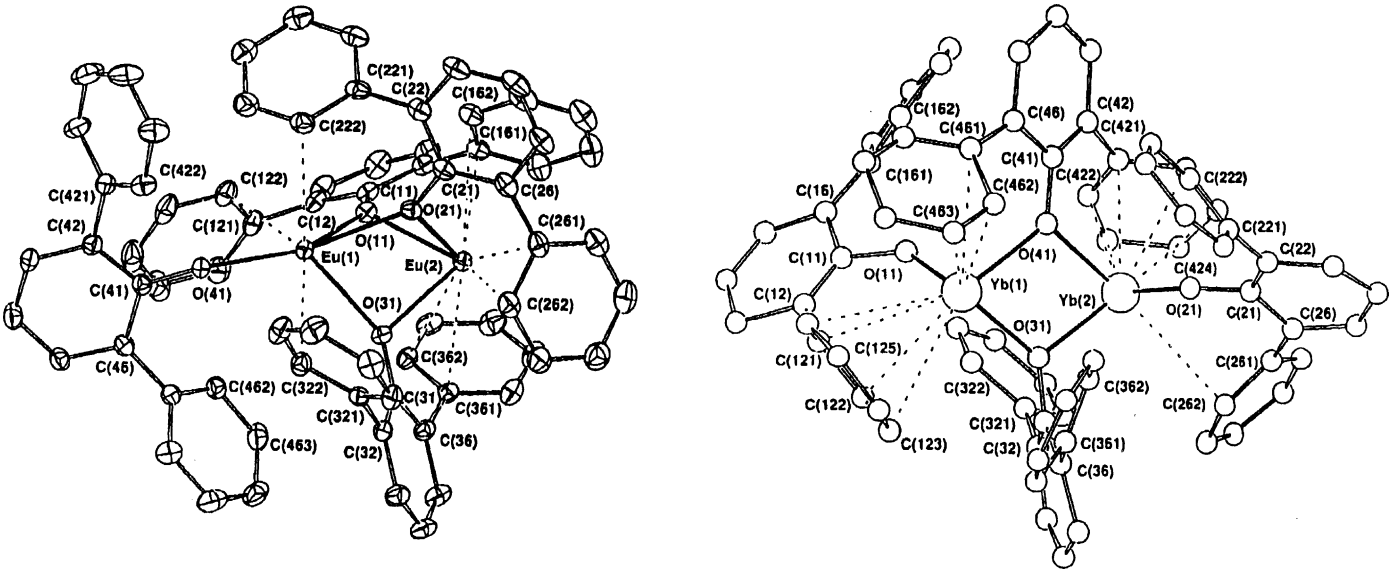

Fig. 39. Molecular structures of $[Eu_2(Odpp)_4]$ and $[Yb_2(Odpp)_4]$.

$$ScCl_3 + 2LiL \rightarrow ScClL_2 + 2LiCl \quad (L = 3,5\text{-}Me_2C_5H_3BN(SiMe_3)_2) \qquad (13)$$

Single-crystal X-ray determinations of all three complexes were performed. Complex $[ScCl(C_5H_5BMe)_2]_2$ possesses a doubly chloro-bridged dinuclear structure with four facially coordinated boratabenzene ligands (Fig. 40). The structure of $ScCl(3,5\text{-}Me_2C_5H_3BNMe_2)_2]_2$ differs in that each scandium atom binds to one boratabenzene in an unprecedented N-B-C-2 coordination mode and facially to the second boratabenzene ligand. In solution $ScCl[3,5\text{-}Me_2C_5H_3BNMe_2)_2]_2$ is fluxional, displaying only one type of boratabenzene ligand. $ScCl[3,5\text{-}Me_2C_5H_3BN(SiMe_3)_2]_2$ is mononuclear, because of the bulkiness of the boratabenzene.

2.4. Indenyl complexes

The first examples of racemic bis(2-dimethylaminoethylindenyl) divalent unsolvated organolanthanide complexes were presented by Qian et al. [46]. $(Me_2NCH_2CH_2C_9H_6)_2Sm$ and $(Me_2NCH_2CH_2C_9H_6)_2Yb$ were synthesized according to Scheme 28 by the reaction of $K(Me_2NCH_2CH_2C_9H_6)$ with LnI_2 (Ln = Sm, Yb) in THF at room temperature.

The molecular structure of the ytterbium complex as determined by single-crystal X-ray diffraction revealed the intermolecular coordination of both dimethylaminoethyl groups with Yb–N distances of 2.58 and 2.608 Å (Fig. 41). Only one possible diasteroemeric conformation with *trans*-arrangement of both indenyl rings and coordinated side arms is present.

Schumann et al. synthesized a series of donor-functionalized *ansa*-cyclopentadienyl-indenyl and *ansa*-bis(indenyl) complexes of yttrium, samarium, thulium, and lutetium [47]. The stepwise reaction of Me_2SiCl_2 with $K[C_5H_3{}^tBuMe\text{-}3]$ or $Li[C_9H_7]$ followed by the reaction with $K[C_9H_6CH_2CH_2NMe_2\text{-}1]$ and subsequent deprotonation with KH or BuLi, yielded the two dimethylsilyl-bridged complexes $K_2[(C_5H_2{}^tBu\text{-}3\text{-}Me\text{-}5)SiMe_2(1\text{-}C_9H_5CH_2CH_2NMe_2\text{-}3)]$ and $Li_2[(1\text{-}C_9H_6)SiMe_2(1\text{-}C_9H_5CH_2CH_2NMe_2\text{-}3)]$, respectively.

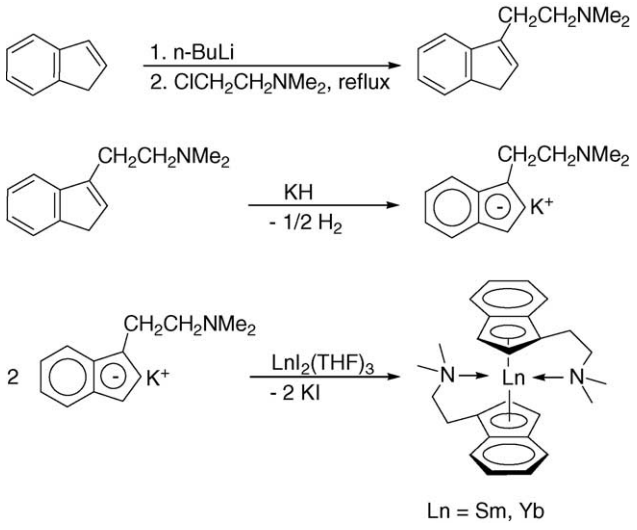

Scheme 28. Synthesis of $(Me_2NCH_2CH_2C_9H_6)_2Sm$ and $(Me_2NCH_2CH_2C_9H_6)_2Yb$.

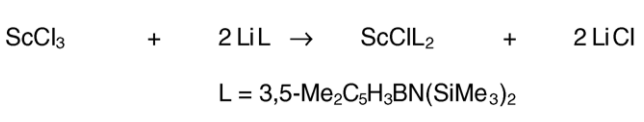

Scheme 27. Synthesis of various boratabenzene complexes.

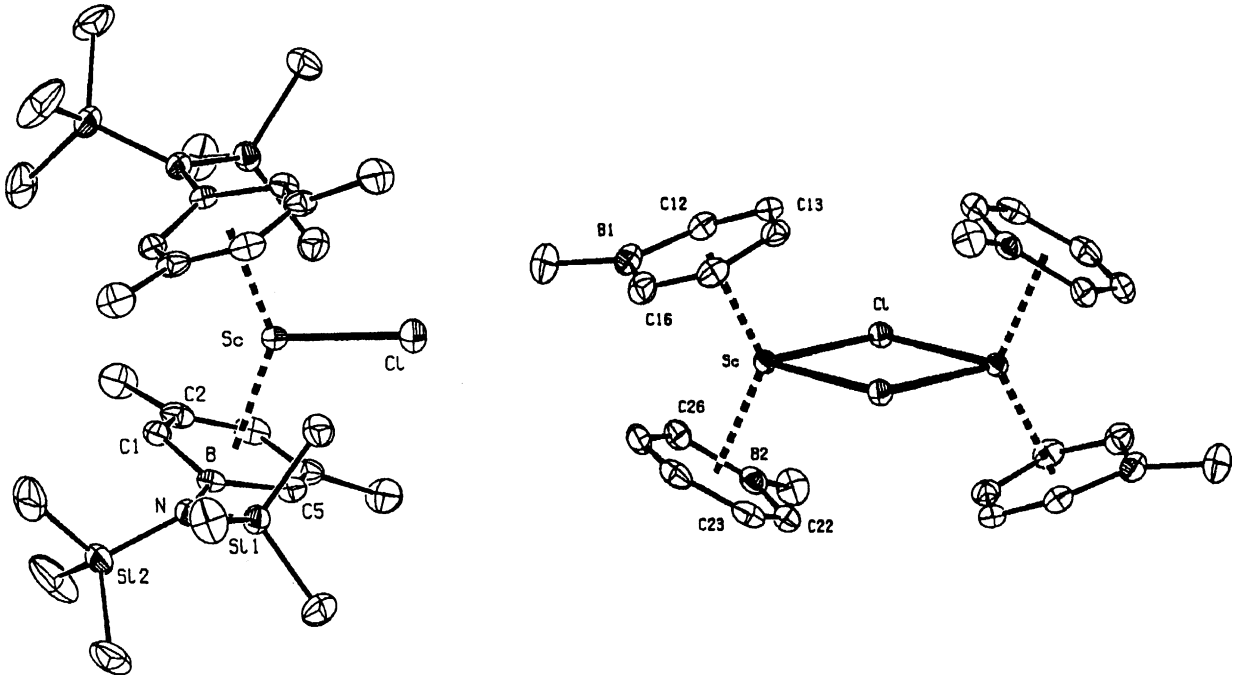

Fig. 40. Molecular structures of $[ScCl(C_5H_5BMe)_2]_2$ and $ScCl(3,5\text{-}Me_2C_5H_3BN(SiMe_3)_2)_2$.

The reaction of the lithium precursor with $LuCl_3$ according to Scheme 29 (Eq. (1)) afforded $[(1\text{-}C_9H_6)SiMe_2(1\text{-}C_9H_5CH_2CH_2NMe_2\text{-}3)]LuCl$. Treatment of $K_2[(C_5H_2{}^tBu\text{-}3\text{-}Me\text{-}5)SiMe_2(1\text{-}C_9H_5CH_2CH_2NMe_2\text{-}3)]$ with the THF adducts of YCl_3, $SmCl_3$ and $LuCl_3$, or the DME adduct of TmI_3 gave the mixed *ansa*-metallocenes $[(C_5H_2{}^tBu\text{-}3\text{-}Me\text{-}5)SiMe_2(1\text{-}C_9H_5CH_2CH_2NMe_2\text{-}3)]LnX$ (X = Cl, Ln = Y, Sm, Lu; X = I, Ln = Tm) (Scheme 29, Eq. (2)). ^1H NMR spectra of all complexes in polar solvents (instead of the thulium one) at room temperature show the magnetic non-equivalence of the protons of the dimethylamino group and hence prove the existence of a strong N → M coordination even in polar solvents like pyridine. 2D-NMR spectroscopic determinations led to the assumption that only one set of enantiomers exists in solution.

Single-crystal X-ray determinations of $[(C_5H_2{}^tBu\text{-}3\text{-}Me\text{-}5)SiMe_2(1\text{-}C_9H_5CH_2CH_2NMe_2\text{-}3)]LnX$ (X = Cl, Ln = Lu) and (X = I, Ln = Tm) show the monomeric complexes with

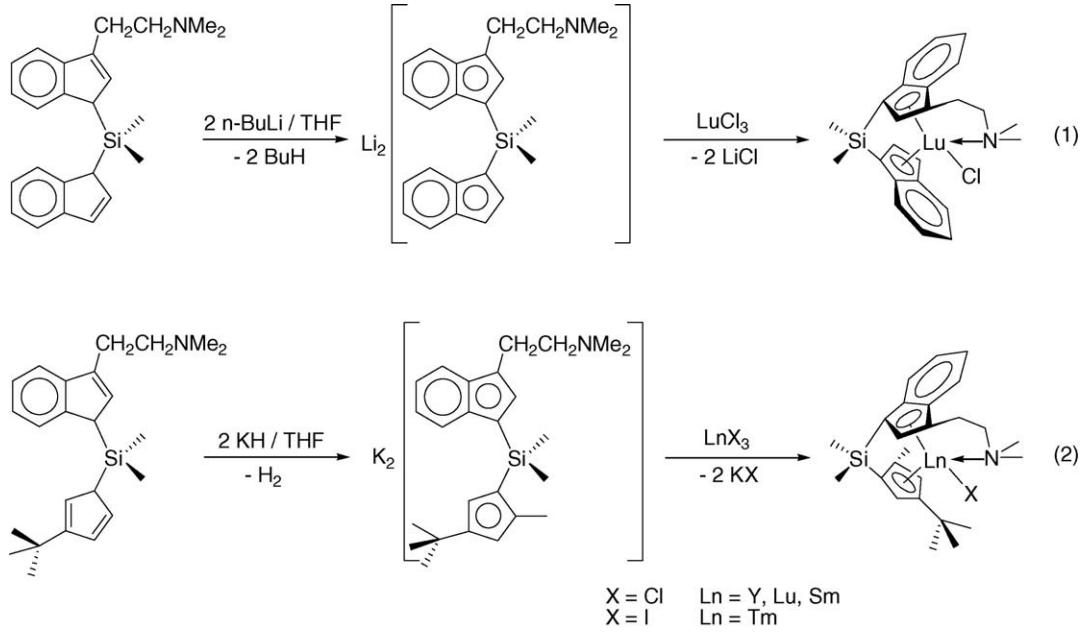

Scheme 29. Synthesis of mixed donor-functionalized indenyl complexes of Y, Sm, Tm and Lu.

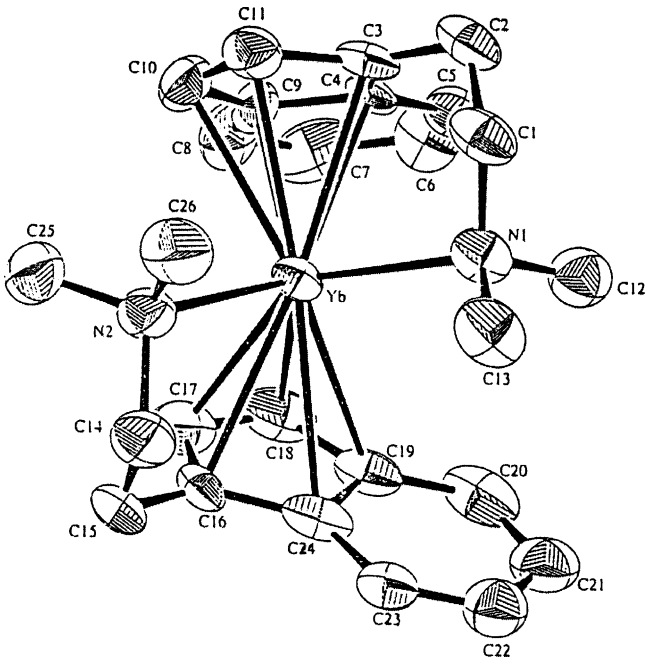

Fig. 41. Molecular structure of $(Me_2NCH_2CH_2C_9H_6)_2Yb$.

short Ln–N bonds (2.45 Å for Lu, 2.50/2.47 Å for Tm) (Fig. 42).

In addition to the halide atom, both the cyclopentadienyl and the indenyl part of the *ansa*-ligand are η^5-coordinated to the lanthanide atom with nearly equal bond distances (Lu–Cp(centr.) 2.32 Å, Lu–Ind(centr.) 2.33 Å; Tm–Cp(centr.) 2.34 Å, Tm–Ind(centr.) 2.34 Å).

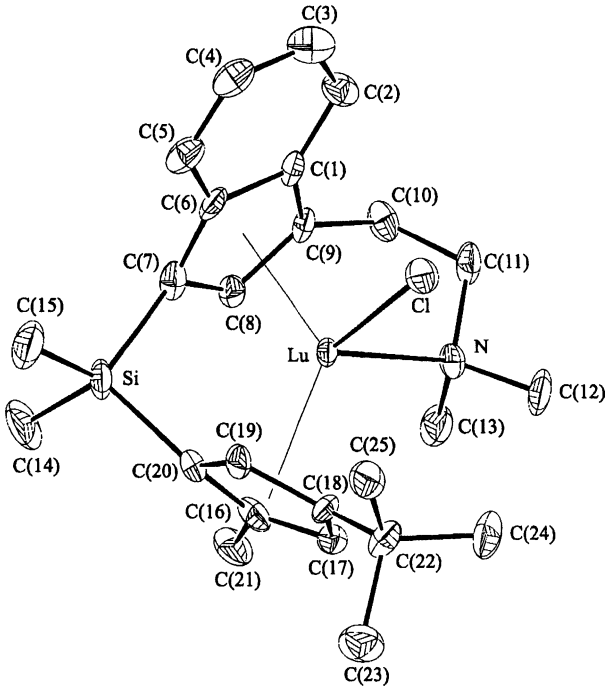

Fig. 42. Molecular structure of $[(C_5H_2{}^tBu\text{-}3\text{-}Me\text{-}5)SiMe_2(1\text{-}C_9H_5CH_2CH_2NMe_2\text{-}3)]LuCl$.

The synthesis and structure of *meso*-[ethylene-bis(η^5-indenyl)]ytterbium(III) bis(trimethylsilyl)amide and the syntheses of *rac*- and *meso*-[ethylenebis(η^5-indenyl) ytterbium(III)chloride][$LiCl(Et_2O)_2$] and *rac*- and *meso*-[ethylenebis(η^5-indenyl)lutetium(III)chloride][$LiCl(Et_2O)_2$] were reported by Broene and co-workers [48]. The complexes are synthesized by metathesis of dilithiated 1,2-bis(indenylethane) with either $YbCl_3$ or $LuCl_3$ in THF followed by solvent exchange with diethyl ether to give the *rac/meso* mixture of [ethylenebis(η^5-indenyl)Ln(III)chloride][$LiCl(Et_2O)_2$] (Ln = Yb, Lu) (Scheme 30).

In the Yb case, the major diastereomer formed is *meso*, while in the lutetium reaction, the *rac* diastereomer is the predominant species. The amide complex *meso*-[ethylene-bis(η^5-indenyl)]ytterbium(III)-bis(trimethylsilyl)amide was synthesized by the reaction of *meso*-[ethylene-bis(η^5-indenyl)ytterbium(III) chloride][$LiCl(Et_2O)_2$] with Na[$N(SiMe_3)_2$] in diethyl ether. Single-crystal X-ray determinations revealed a small centroid–Yb–centroid angle of 122.0° caused by the constraining effect of the ethyl bridge (Fig. 43).

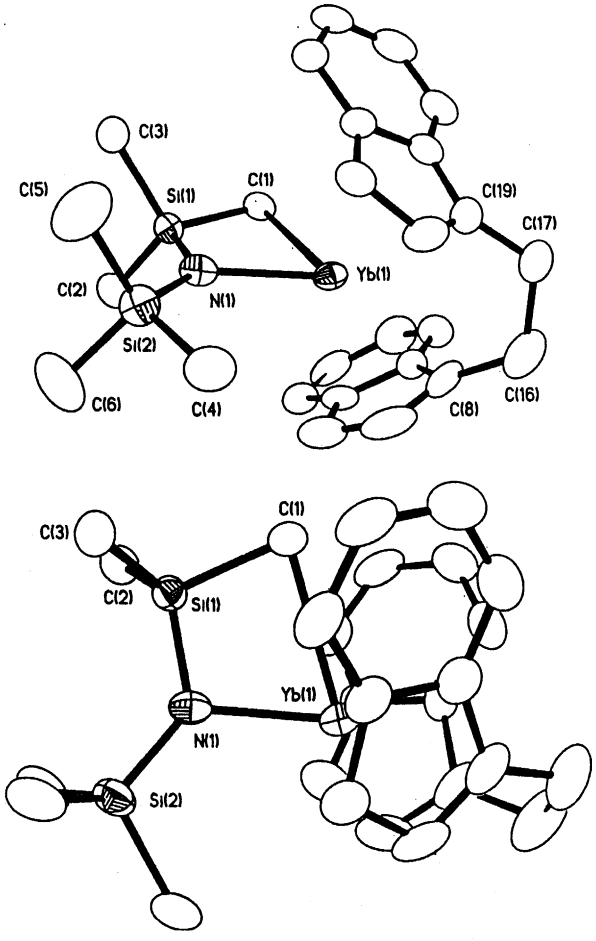

Fig. 43. Molecular structure of *meso*-[ethylene-bis(η^5-indenyl)]ytterbium(III)-bis(trimethylsilyl)amide.

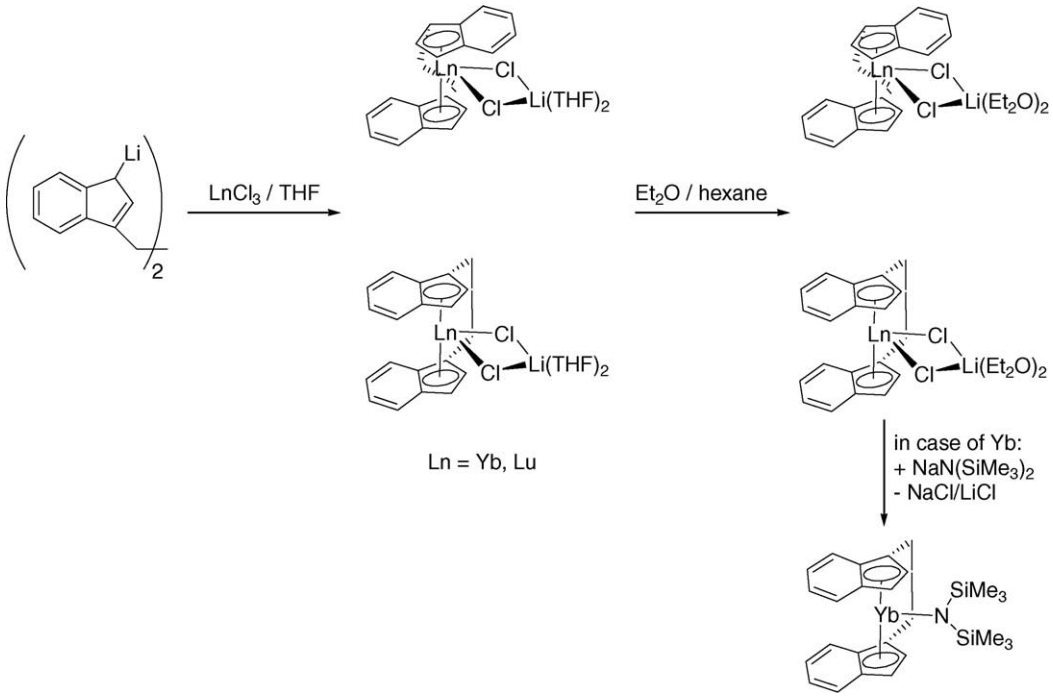

Scheme 30. Synthesis of ethylene-bridged bis(indenyl) complexes of Yb and Lu.

The amide derivative *meso*-[ethylene-bis(η^5-indenyl)] ytterbium(III) bis(trimethylsilyl)amide catalyzes the hydroamination of primary olefins in excellent yields.

Bulychev and co-workers reported the formation of different Yb(II) indenyl complexes [49]. Metallation of 2,2-bis(1′-indene)propane by sodium hydride and subsequent reaction of the sodium derivative with $YbCl_3$ yielded $(C_9H_7)_2Yb(DME)$ besides a benzofulvene by-product (Scheme 31).

Single-crystal X-ray data show a rather unusual orientation of the indenyl ligands with their benzene rings directed towards the oxygen atoms of the coordinated DME. The centroid–Yb distances (2.43 Å) and the centroid–Yb–centroid angle (129.4°) are in the anticipated ranges (Fig. 44).

Two more Yb(II) indenyl complexes were synthesized by the reaction between $(CH_2)_2(1\text{-Ind}')_2Li_2$ and $YbCl_3$ in diethyl ether and subsequent reduction of the product with sodium metal in THF yielding *rac*-$(CH_2)_2(1\text{-Ind}')_2Yb(THF)_2$ where Ind′ = C_9H_6 and 4,7-$(CH_3)_2C_9H_4$. Solid-state structural data of both complexes are basically identical to each other with values in the expected areas.

Qian and et al. reported the synthesis of *ansa*-metallocene alkyl complexes of yttrium and lutetium with an ether-bridged indenyl ligand [50]. The reaction of the corresponding monochlorides with $LiCH_2SiMe_3$ in THF afforded the pure *rac ansa*-lanthanocene alkyl complexes [$O(CH_2CH_2\text{-}C_9H_6$]$LnCH_2SiMe_3$ (Ln = Y, Lu) (Scheme 32).

The authors claim that only the *rac* diastereomer was formed owing to the non-bonded interactions between the six-membered fragment of the indenyl moiety and the alkyl group.

In analogy to the tris(cyclopentadienyl)lanthanide(III) sulfoxide adducts, Fischer and co-workers synthesized tris(indenyl)lanthanide(III) sulfoxide adducts, too [42]. These complexes were investigated using single crystal X-ray analysis, variable temperature NMR and circular dichroism. The 1:1 adducts have been prepared in toluene from the homologous THF adducts and MTSO (OS(Me)4-MeC_6H_4) and DPSO ($OSPh_2$), respectively, yielding the complexes [$Ln(C_9H_7)_3$(OS(Me)/4-MeC_6H_4)] and [$Ln(C_9H_7)_3(OSPh_2)$] (Table 2).

While solid [$Ln(C_9H_7)_3$MTSO] (Ln = La, Pr) contains exclusively oxygen-bonded sulfoxide and three η^5-coordinated

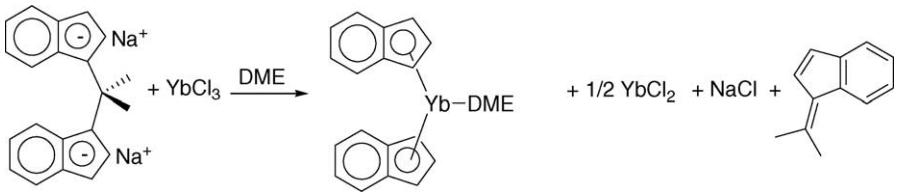

Scheme 31. Formation of the Yb(II) complex $(C_9H_7)_2Yb(DME)$.

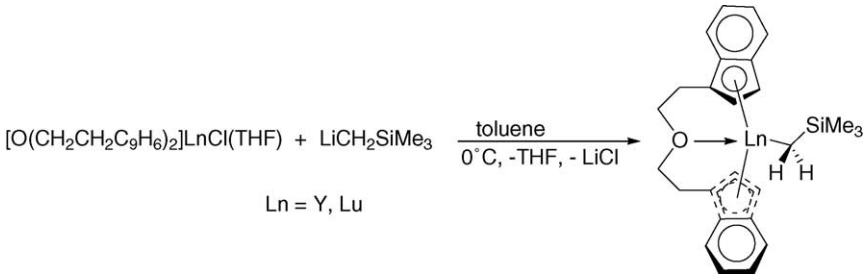

Scheme 32. Synthesis of $[O(CH_2CH_2C_9H_6]LnCH_2SiMe_3$ (Ln = Y, Lu).

Table 2
List of known $[Ln(C_9H_7)_3(OSR/R')]$ complexes (R/R′ = Me/4-MeC_6H_4 or Ph/Ph), with (*R*)-(+)-MTSO and (*S*)-(−)-MTSO, respectively

MTSO	La	Pr	Nd	Sm
DPSO	La	Pr	Nd	

indenyl ligands in a chiral arrangement around the metal ion, the C_9H_7 ligands of the paramagnetic molecules in solution (Ln = Pr, Nd, Sm) are involved in rapid η^5-η^1-fluxionality (Fig. 45). Both variable temperature ^{1}H NMR and f–f circular dichroism spectroscopy indicate that a second chirogenic center is generated that lies closer to the metal ion than the chiral sulfur atom of the MTSO ligand. Surprisingly, the NMR spectra of solutions of mixtures of $[Ln(C_9H_7)_3MTSO]$ with (*R*)-(+)-MTSO and (*S*)-(−)-MTSO, or/and with two different metals reveal rapid inter-molecular sulfoxide exchange. On the other hand, mutual MTSO/THF exchange seems to be inhibited, which suggests that the facile sulfoxide exchange follows a special mechanistic pathway, which is discussed in the article.

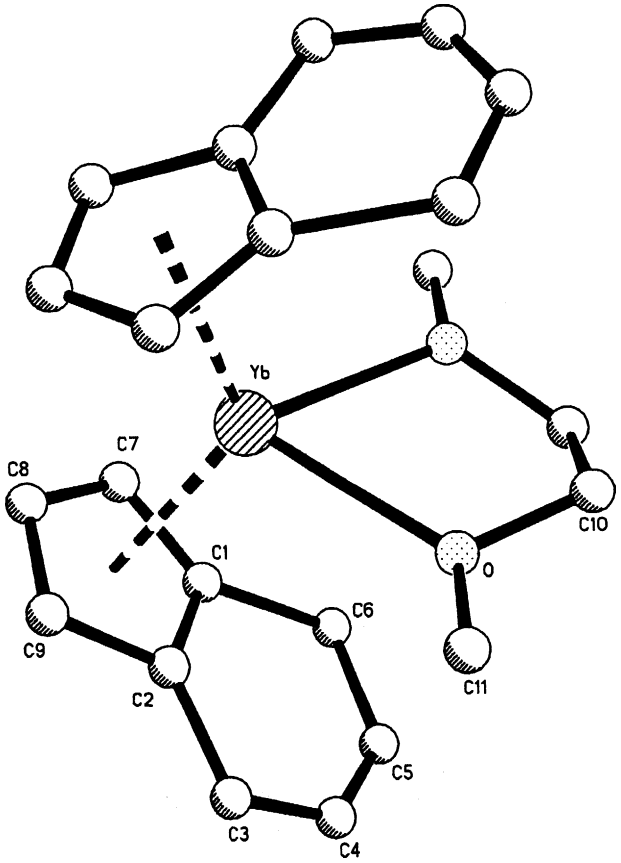

Fig. 44. Molecular structures of $(C_9H_7)_2Yb(DME)$.

2.5. Fluorenyl complexes

Qian et al. reported the synthesis of diphenylmethylene-bridged fluorenyl cyclopentadienyl lanthanocene complexes with C_S symmetry [51]. The reaction of lanthanide chlorides $LnCl_3$ with the dilithium salt of $(C_{13}H_9)CPh_2(C_5H_5)$ in THF at ambient temperature led to the formation of the 'ate' complexes $[Li(THF)_4][LnCl_2\{(C_{13}H_8)CPh_2(C_5H_4)\}]$ (Ln = Lu, Y) (Scheme 33).

Treatment of $Ln(BH_4)_3(THF)_3$ with 3 equiv. of $Li_2(C_{13}H_8)CPh_2(C_5H_4)$ in THF solution gave the anionic complexes $[Li(THF)_4][Ln(BH_4)_2\{(C_{13}H_8)CPh_2(C_5H_4)\}]$ (Ln = La, Nd). Single-crystal X-ray determinations of $[Li(THF)_4][Ln(BH_4)_2\{(C_{13}H_8)CPh_2(C_5H_4)\}]$ (Ln = La, Nd) and $[Li(THF)_4][LuCl_2\{(C_{13}H_8)CPh_2(C_5H_4)\}]$ revealed the existence of discrete cation/anion pairs (Fig. 46).

The Ln–C (Cp ring) distances in these complexes are within the range expected for *ansa*-lanthanocenes. The Ln–C (fluorenyl ring) distances show differences of up to 0.3 Å probably owing to the inclined rigid planar fluorenyl ligation.

A novel C_S-symmetric fluorenyl *ansa*-yttrocene, *ansa*-$Me_2Si(\eta^3\text{-Flu})(\eta^5\text{-Cp}')YCl_2Li(OEt_2)_2$ (Flu = $C_{13}H_8$, Cp′ = C_5Me_4) has been prepared by a salt metathesis reaction from YCl_3 and the dilithium salt of the ligand $Me_2Si(FluH)(Cp'H)$ by Do and co-workers [52] (Scheme 34). The X-ray structure of the complex revealed unusual η^3-fluorenyl coordination to the Y^{3+} ion (Fig. 47). Treatment of *ansa*-$Me_2Si(\eta^3\text{-Flu})(\eta^5\text{-Cp}')YCl_2Li(OEt_2)_2$ with $Na(SiMe_3)_2$ afforded the corresponding bis(trimethylsilyl)amide derivative *ansa*-$Me_2Si(\eta^3\text{-Flu})(\eta^5\text{-Cp}')YN(SiMe_3)_2$.

In the bis(trimethylsilyl)amide complex, the Y–Flu bonding is partially slipped towards η^3. Furthermore, the authors are discussing a π-dative bond nature of the Y–N bond and an additional interaction between the Y center and one methyl group of the $N(SiMe_3)_2$ fragment. The amide complex was found to be active in the polymerization of methyl methacrylate.

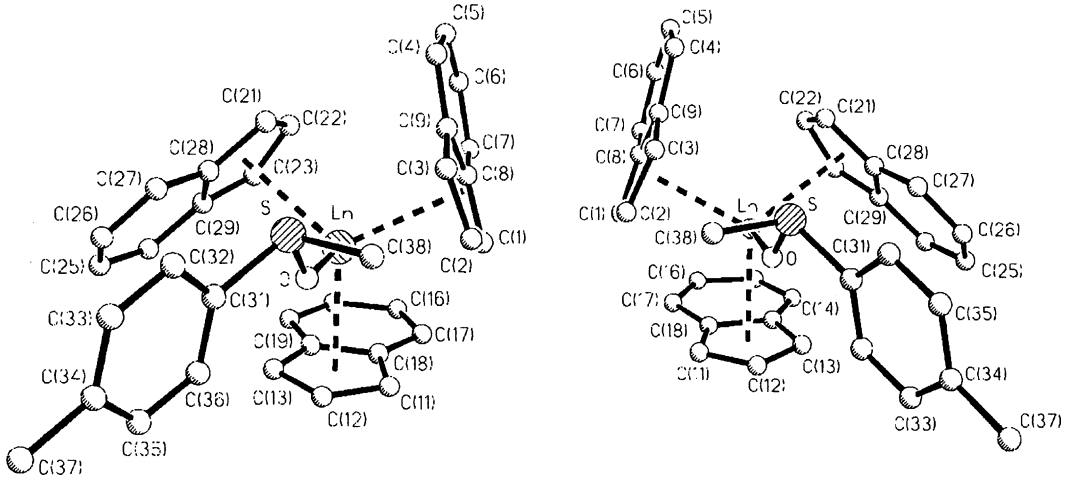

Fig. 45. Molecular structures of $[Ln(C_9H_7)_3(OS(Me)/4\text{-}MeC_6H_4)]$ (Ln = La, Pr) (a) (*R*)-(+)-MTSO and (b) (*S*)-(−)-MTSO as the coordinating sulfoxide.

2.6. Clusters

A series of organolanthanide indenyl clusters are reported by Xie and co-workers [53,54]. Treatment of $Me_2Si(C_9H_7)(C_2B_{10}H_{11})$ with 4 equiv. of $NaNH_2$ in THF, followed by reaction with 1 equiv. of $LnCl_3$ at room temperature, afforded $[\{(\eta^5\text{-}\mu^2\text{-}C_9H_6SiMe_2NH)Ln\}_2(\mu^3\text{-}Cl)(THF)]_2(\mu^4\text{-}NH)^{\bullet}(THF)_n$ ($n = 1$, Ln = Gd, Er; $n = 0$, Ln = Dy), which represents the first examples of organometallic clusters containing a central μ^4-imido group, as well as indenyl ligands. The solid-state structure of the Er complex revealed a butterfly arrangement of four metals which are connected by four doubly bridging μ^2-$NHSiMe_2$(indenyl) units over the edges, by two triply bridging μ^3-Cl atoms spanning three Er atoms in each case, and by a quadruply bridging μ^4-NH group located on the crystallographic two-fold axis (Fig. 48a).

Another type of tetranuclear cluster, $[\{(\eta^5\text{-}C_9H_6SiMe_2)_2N\}(\mu^2\text{-}NH_2)Ln_2(THF)_2]_2(\mu^3\text{-}Cl)_2(\mu^2\text{-}Cl)_2^{\bullet}THF$ (Ln = Gd, Y), was obtained when the above reactions were carried out at reflux temperature. The solid-state structure of $[\{(\eta^5\text{-}C_9H_6SiMe_2)_2N\}(\mu^2\text{-}NH_2)Gd_2(THF)_2]_2(\mu^3\text{-}Cl)_2(\mu^2\text{-}Cl)_2^{\bullet}THF$ derived from single X-ray analysis revealed that the cluster consists of a distorted-tetrahedral arrangement of four Gd atoms from two $[\{(\eta^5\text{-}C_9H_6SiMe_2)_2N\}(\mu^2\text{-}NH_2)Gd_2(THF_2]^{2+}$ units that are connected by two doubly bridging μ^2-Cl atoms spanning two Gd atoms in each case. Each metal is both η^5-bonded to one indenyl group and σ-bonded to one oxygen atom, one nitrogen atom and three chloro

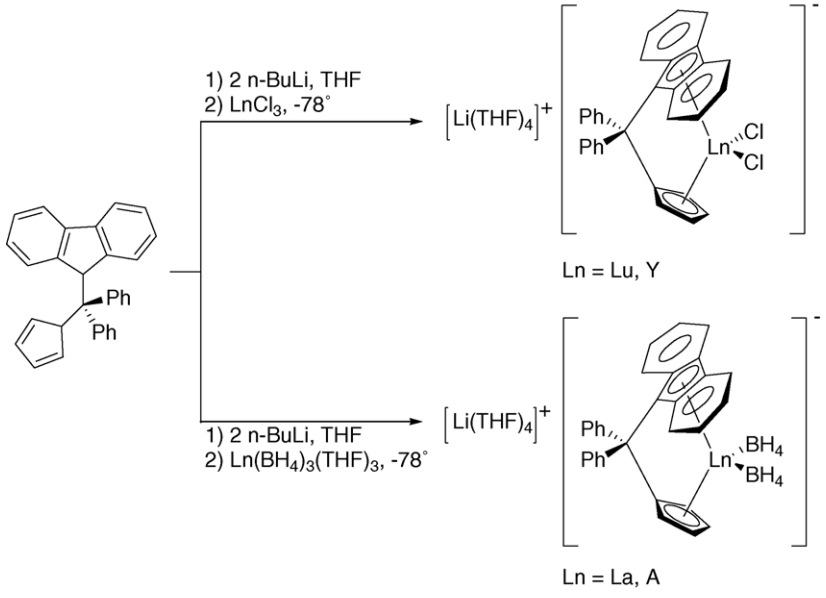

Scheme 33. Synthetic pathways to $[Li(THF)_4][LnCl_2\{(C_{13}H_8)CPh_2(C_5H_4)\}]$ (Ln = Lu, Y) and $[Li(THF)_4][Ln(BH_4)_2\{(C_{13}H_8)CPh_2(C_5H_4)\}]$ (Ln = La, Nd).

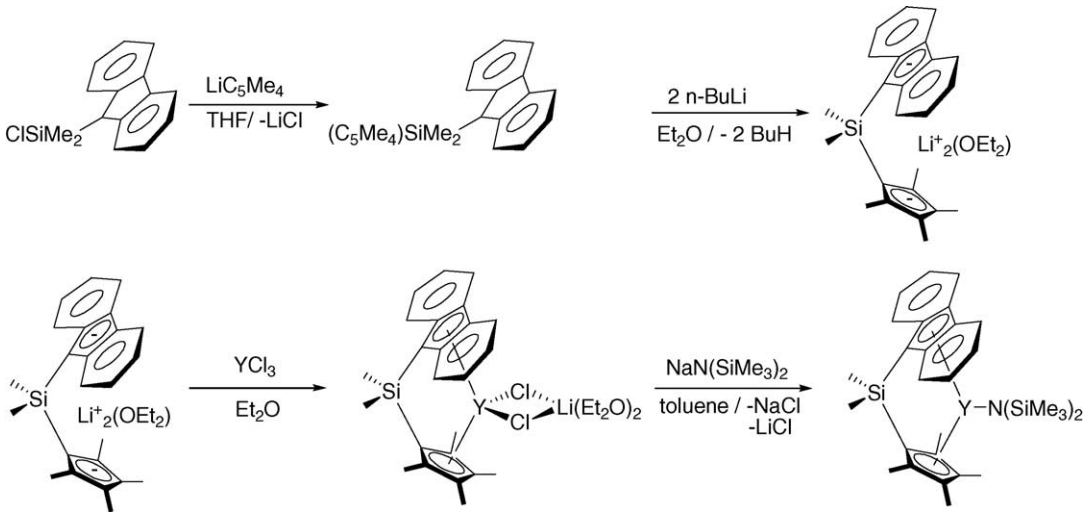

Scheme 34. Synthesis of *ansa*-$Me_2Si(\eta^3\text{-Flu})(\eta^5\text{-Cp}')YCl_2Li(OEt_2)_2$ and *ansa*-$Me_2Si(\eta^3\text{-Flu})(\eta^5\text{-Cp}')YN(SiMe_3)_2$ (Flu = $C_{13}H_8$, Cp′ = C_5Me_4).

ligands. Treatment of $Me_2Si(C_9H_7)(C_2B_{10}H_{11})$ with 8 equiv. of $NaNH_2$ in THF, followed by reaction with 1 equiv. of $LnCl_3$ at room temperature, gave the trinuclear clusters $[([\eta^5\text{-}C_9H_6SiMe_2)_2N][\mu^2\text{-},\mu^2\text{-}Me_2Si(NH)_2](\eta^5\text{-}\mu^2\text{-}C_9H_6SiMe_2NH)(\mu^2\text{-}Cl)_2Ln_3(THF)_3$ (Ln = Gd, Er). These results indicate that $NaNH_2$ serves as both base and nucleophile in the reactions. The *o*-carborane can be recovered by sublimation under vacuum.

Jin et al. reported the reaction of the half-sandwich *tert*-butylcyclopentadienyl ($Cp^t = \eta^5\text{-}Bu^tC_5H_4$) neodymium complex $[Cp^tNdCl_2(THF)_2]_2$ with Na_2Se_5 giving the organoneodymium polyselenide complex $[Na(THF)_6][Cp^t{}_6Nd_6Se_{13}]$, which has been characterized by X-ray crystallography [55].

$$3[Cp^tNdCl_2(THF)_2]_2 + 6Na_2Se_5 \rightarrow [Na(THF)_6][Cp^t{}_6Nd_6Se_{13}]$$

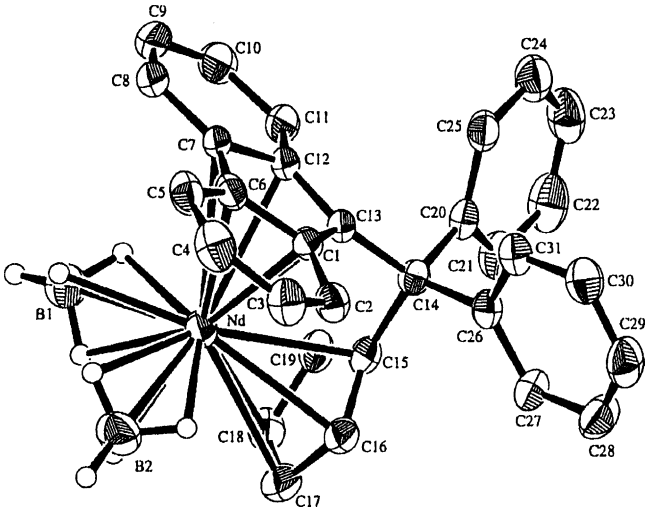

Fig. 46. Molecular structure of the $[Nd(BH_4)_2\{(C_{13}H_8)CPh_2(C_5H_4)\}]^-$ anion.

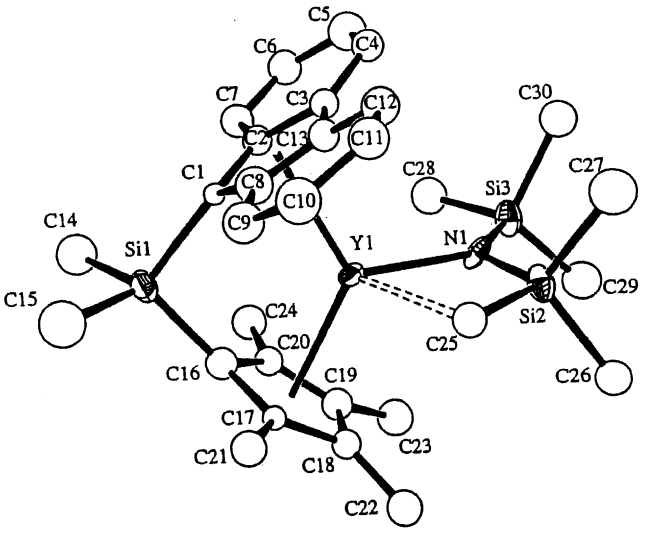

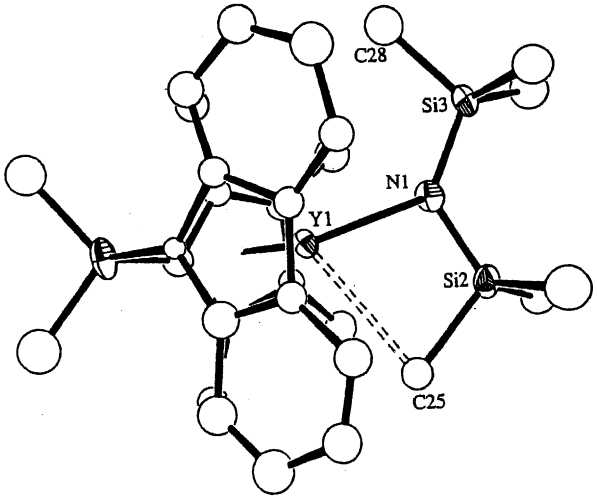

Fig. 47. Molecular structure of *ansa*-$Me_2Si(\eta^3\text{-Flu})(\eta^5\text{-Cp}')YN(SiMe_3)_2$ (Flu = $C_{13}H_8$, Cp′ = C_5Me_4).

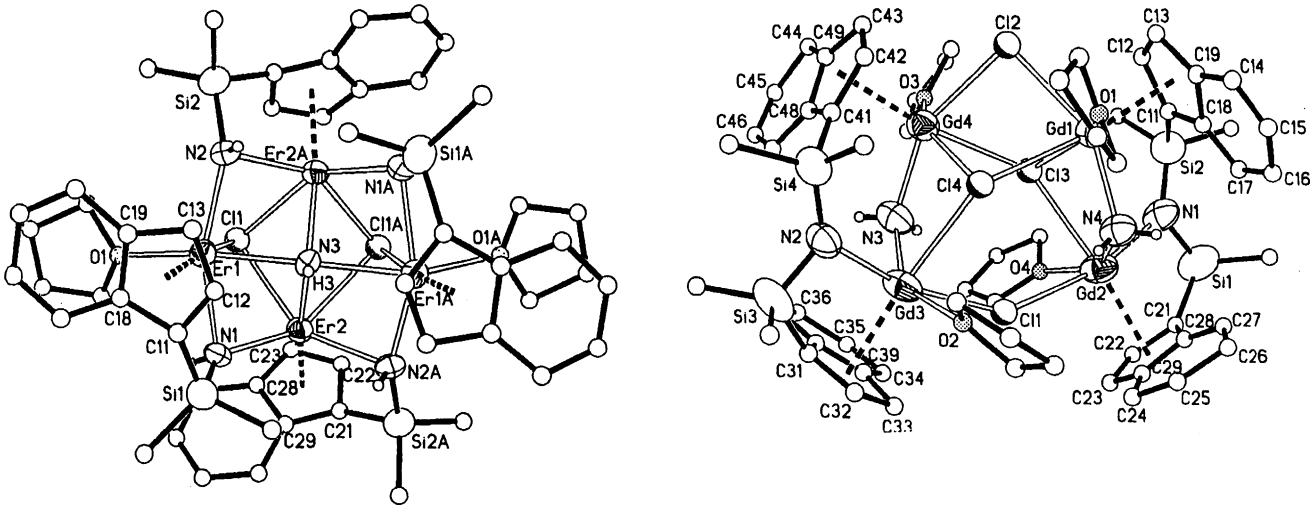

Fig. 48. Molecular structures of (a) $[\{(\eta^5\text{-}\mu^2\text{-}C_9H_6SiMe_2NH)Er\}_2(\mu^3\text{-}Cl)(THF)]_2(\mu^4\text{-}NH)^{\bullet}(THF)$ and (b) $[\{(\eta^5\text{-}C_9H_6SiMe_2)_2N\}(\mu^2\text{-}NH_2)Gd_2(THF)_2]_2(\mu^3\text{-}Cl)_2(\mu^2\text{-}Cl)_2{}^{\bullet}THF$.

Fig. 49 shows the solid-state structure of the anion in $[Na(THF)_6][Cp^t{}_6Nd_6Se_{13}]$ where each Nd atom is coordinated with six Se atoms. The distances between Nd and the Se atoms are between 2.888 and 3.214 Å, whereas the Se atoms can be divided into three types: a central Se atom which is coordinated to six Nd atoms; six pairs of bridging Se_2 units in which one Se atom is coordinated to three Nd atoms; and the other one is connected with only two Nd atoms.

2.7. Complexes with cyclooctatetraenyl ligands

Triple decked bent metallocenes of europium and ytterbium were reported by Evans et al. [56]. $YbI_2(THF)_2$ reacts with KC_5Me_5 and $K_2C_8H_8$ in THF to form $[(C_5Me_5)Yb(THF)]_2(\mu\text{-}\eta^8\text{:}\eta^8\text{-}C_8H_8)$, which can be desolvated at 30 °C and 10^{-7} Torr to afford the solvent-free complex $[(C_5Me_5)Yb]_2(\mu\text{-}\eta^8\text{:}\eta^8\text{-}C_8H_8)$. The molecular structure shows two divalent $[(C_5Me_5)Yb]^+$ moieties bridged by a $(C_8H_8)^{2-}$ unit with 159° and 161° (C_5Me_5 ring centroid)–Yb–(C_8H_8 ring centroid) angles (Fig. 50). $[(C_5Me_5)Eu(THF)_2]_2(\mu\text{-}\eta^8\text{:}\eta^8\text{-}C_8H_8)$ can be desolvated analogously at 55 °C and 10^{-7} Torr to afford $[(C_5Me_5)Eu]_2(\mu\text{-}\eta^8\text{:}\eta^8\text{-}C_8H_8)$, which shows ($C_5Me_5$ ring centroid)–Yb–(C_8H_8 ring centroid) angles of 149.3° and 148.9°. $[(C_5Me_5)Yb]_2(\mu\text{-}\eta^8\text{:}\eta^8\text{-}C_8H_8)$ reacts with 1,3,5,7-cyclooctatetraene to form $(C_5Me_5)Yb(C_8H_8)$.

Evans et al. also reported the synthesis of the divalent lanthanide COT complexes $[\{[Zr_2(OiPr)_9]Ln\}_2(C_8H_8)]$ (Ln = Yb, Sm) from $[\{[Zr_2(OiPr)_9]LnI\}_2]$ and $K_2C_8H_8$ (Scheme 35 Eq. (1)) [21]. The monoanionic $[Zr_2(OiPr)_9]^-$ unit is used as a cyclopentadienyl analogue.

X-ray diffraction studies show the bimetallic Ln(II) complexes with the Sm centers coordinated to the bridging COT ligand in an η^8-fashion (Fig. 51).

$[\{[Zr_2(OiPr)_9]Sm\}_2(C_8H_8)]$ reacts with 1,3,5,7-C_8H_8 to form the hexane-soluble Sm(III) complex $[[Zr_2(OiPr)_9]Sm(C_8H_8)]$, in a manner analogous to the reduction of C_8H_8 by $[(C_5Me_5)Sm(C_8H_8)]$. The molecular structure (Fig. 51) shows the monomeric complex with one η^8-coordinated COT ligand and the monoanionic $[Zr_2(OiPr)_9]^-$ unit attached to the Sm in a tetradentate fashion.

2.8. Organolanthanide complexes in organic synthesis

Molander and Dowdy presented a facile intramolecular hydroamination process catalyzed by $[Cp^{TMS}{}_2NdMe]_2$ ($Cp^{TMS} = C_5H_4[SiMe_3]$) [57]. The lanthanide-catalyzed hydroamination enables a rapid access to 10,11-dihydro-5*H*-dibenzo[*a*,*d*]cyclohepten-5,10-imines (Scheme 36).

McDonald and Marks reported a series of organolanthanide complexes of the general type $Cp^*{}_2LnCH(SiMe_3)_2$

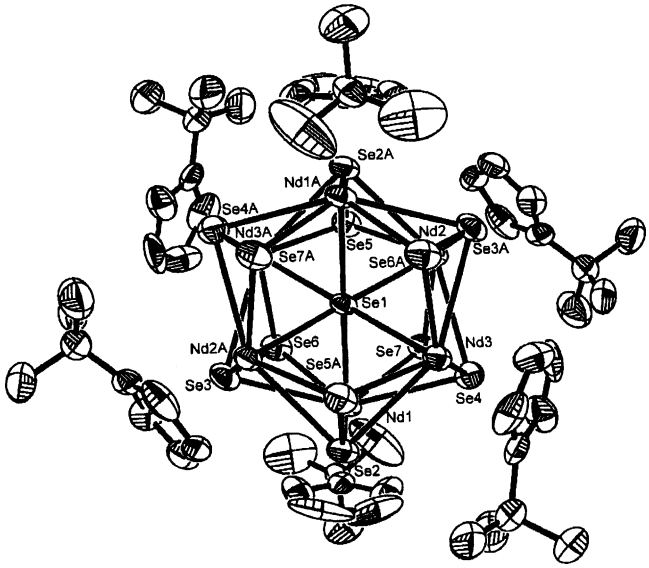

Fig. 49. Molecular structure of the anion of $[Na(THF)_6][Cp^t{}_6Nd_6Se_{13}]$.

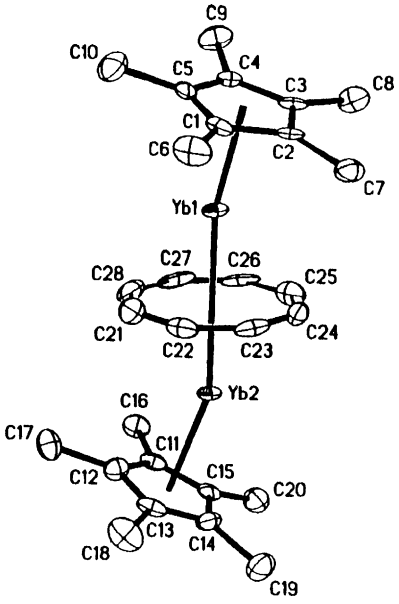

Fig. 50. Molecular structure of $[(C_5Me_5)Yb]_2(\mu\text{-}\eta^8\text{:}\eta^8\text{-}C_8H_8)$.

($Cp^* = \eta^5\text{-}C_5Me_5$; Ln = La, Sm, Y, Lu; TMS = $SiMe_3$) to be effective as precatalysts for the rapid, regioselective, and highly diastereoselective intramolecular hydroamination/cyclization (ICH) of aminoallenes [58]. The hydroamination of aminoallenes with the general formula $RCH{=}C{=}CH(CH_2)_nCHR'NH_2$ yields the corresponding heterocycles $RCH{=}CHCHNHCH(R')(CH_2)_{n-1}CH_2$ (R = CH_3, *n*-C_3H_7, *n*-C_5H_{11}; R′ = H, CH_3, *n*-C_4H_9, $CH_2{=}CHCH_2CH_2$; *n* = 2,3). The mono- and disubstituted pyrrolidines and piperidines produced bear an α-alkenyl functionality available for further synthetic manipulation. Table 3 shows two examples of the hydroamination products.

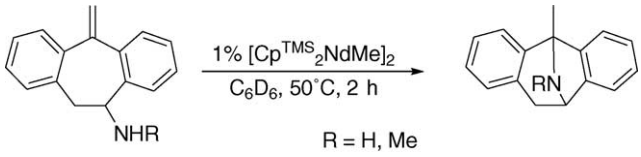

Scheme 36.

Kinetic and mechanistic data parallel organolanthanide-mediated intramolecular aminoalkene and aminoalkyne hydroamination/cyclizations, implying turnover-limiting allene insertion into the Ln–N bond followed by rapid protonolysis of the resulting Ln–C bond (Scheme 37).

Diastereoselective hydroamination/cyclization reactions found their application in the total synthesis of the pyrrolidine alkaloid (+)-197B and pyrrolizidine alkaloid (+)-xenovenine reported by McDonald, Marks and co-workers [59]. The organolanthanide precatalysts $Cp^*_2LnCH(SiMe_3)_2$ and

$$[\{[Zr_2(OiPr)_9]LnI\}_2] + K_2C_8H_8 \rightarrow [\{[Zr_2(OiPr)_9]Ln\}_2(C_8H_8)] + 2\,KI \quad (1)$$

Ln = Yb, Sm

$$[\{[Zr_2(OiPr)_9]Sm\}_2(C_8H_8)] + C_8H_8 \rightarrow 2\,[[Zr_2(OiPr)_9]Sm(C_8H_8)] \quad (2)$$

Scheme 35.

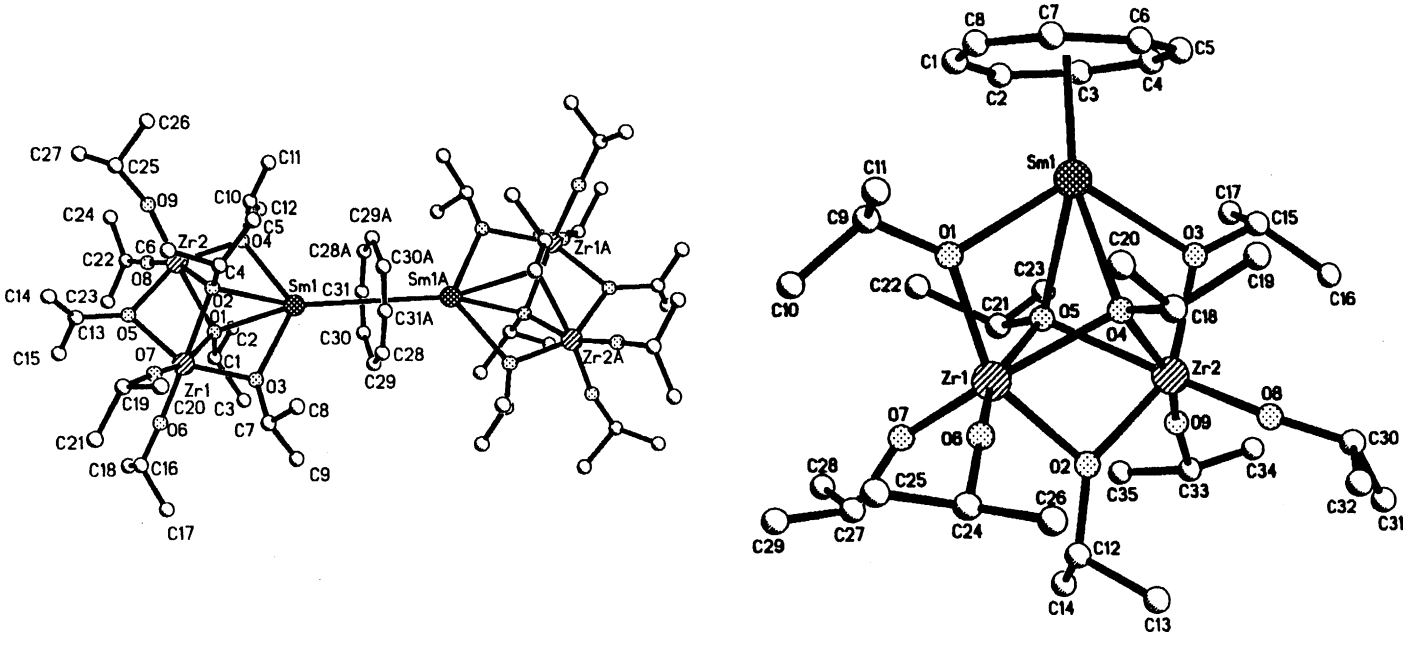

Fig. 51. Molecular structures of $[\{[Zr_2(OiPr)_9]Sm\}_2(C_8H_8)]$ and $[[Zr_2(OiPr)_9]Sm(C_8H_8)]$.

Table 3

Substrate	Product	Precatalyst
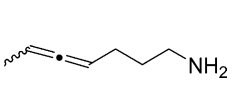	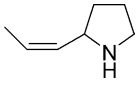	(a) $Cp^*_2YCH(SiMe_3)_2$ (b) $Cp^*_2SmCH(SiMe_3)_2$
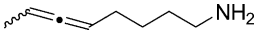	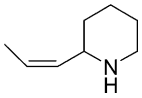	(a) $Cp^*_2YCH(SiMe_3)_2$ (b) $Cp^*_2SmCH(SiMe_3)_2$

$Me_2SiCp''(tBuN)Ln(SiMe_3)_2$ ($Cp^* = \eta^5$-C_5Me_5; $Cp'' = \eta^5$-Me_4C_5; Ln = La, Nd, Sm) catalyze the regio- and stereoselective cyclohydroamination of the aminoallenes (5S,8S)-5-amino-trideca-8,9-diene and the aminoallene (5S)-5-amino-pentadeca-1,8,9-triene, which are the key steps of the total synthesis of the above mentioned molecules.

Marks and co-workers reported the organolanthanides $[Me_2Si(C_5Me_4)(^tBuN)]LnN(SiMe_3)_2$ (Ln = Nd, Lu, Sm) and $[Me_2Si(C_5Me_4)(^tBuN)]LnCH(SiMe_3)_2$ (Ln = Yb, Lu) (see Chapter 2.2.1 for the synthesis) to be significantly more active as precatalysts for the aminoalkene hydroamination/cyclization than the corresponding bis(cyclopentadienyl) complexes $(C_5Me_5)_2LnN(SiMe_3)_2$ and $(C_5Me_5)_2LnCH(SiMe_3)_2$ [22].

Schumann et al. described the dimeric lanthanide methyl complexes $[(\eta^5$-$C_5H_4SiMe_2R)_2Ln(\mu$-$Me)]_2$ (R = *t*-Bu, Me; Ln = Y, Sm, Lu) (Chapter 2.2.2) to be effective precatalysts for the hydrosilylation of a series of alkenes and alkynes using phenylsilane as the hydrosilylation agent [34].

Cyclization/silylation reactions of nitrogen-containing enynes catalyzed by the complexes $Cp^*_2LnMe(THF)$ (Ln = Y, Lu) were investigated by Molander and Corrette [60]. Using standard conditions, the $Cp^*_2YMe(THF)$ complex suffers from poor reactivity at room temperature with nitrogen positioned in α position to the alkyne. This can be overcome by either slow catalyst addition or by using $Cp^*_2LuMe(THF)$ as the catalyst, which contains the smaller Lu(III) ion. The use of $Cp^*_2LuMe(THF)$ allowed them to prepare various nitrogen-containing ring systems in excellent yields with good to excellent diastereoselectivities at room temperature. The results of these studies highlight the ability to tune the reactivity of an organolanthanide complex by changing the metal center. Tables 4 and 5 show examples of the catalytic reactions performed.

Ishii and co-workers published the possibility of catalyzing the acetylcyanation of aldehydes with acetonecyanohydrin and isopropenylacetate by $Cp^*_2Sm(THF)$ (Scheme 38) [61].

2.9. Organolanthanides as polymerization catalysts

Dormond and co-workers published the polymerization of styrene (catalyst/styrene ratio = 1:1000) using anionic or neutral allylic samarium or neodymium species as catalysts, without addition of any co-catalysts [62]. Random syndiotactic-rich material was obtained from anionic tetra(allyl)lanthanides, whereas the neutral

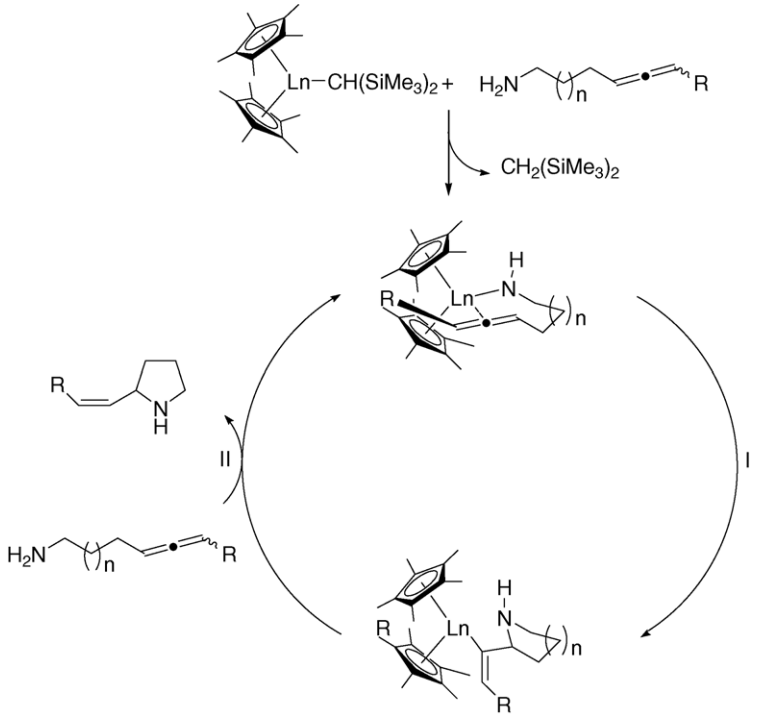

Scheme 37. Proposed catalytic cycle for the intramolecular hydroamination/cyclization of aminoallenes.

Table 4
Cyclization/silylation of enynes to afford five-membered nitrogen heterocycles

Substrate	Product	Precatalyst	Conditions	Isolated yield (%)
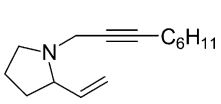	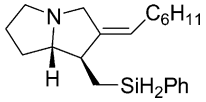	$Cp^*_2YMe(THF)$	r.t., 24 h	43
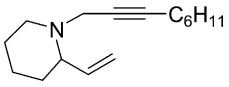	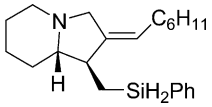	$Cp^*_2YMe(THF)$	50 °C, 24 h	82
		$Cp^*_2LuMe(THF)$	r.t., 6 h	92
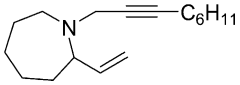	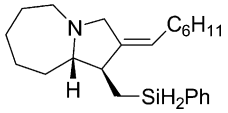	$Cp^*_2YMe(THF)$	50 °C, 48 h	82
		$Cp^*_2YMe(THF)$	r.t., 44 h	64
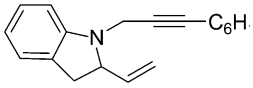	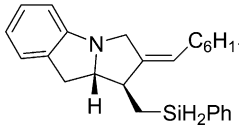	$Cp^*_2YMe(THF)$	90 °C, 24 h	34
		$Cp^*_2LuMe(THF)$	r.t., 5 d	43

tris(allyl)lanthanides or anionic *ansa*-bis(cyclopentadienyl) bis(allyl)lanthanides afforded isotactic-rich polystyrene.

Barbier-Baudry et al. showed, that the bisallyl-*ansa*-lanthanide complexes $(Me_2CC_5H_4)_2Ln(allyl)_2Li(DME)$ (Ln = Sm, Nd) act as single component catalysts of diene polymerization [63]. The polymerization of an equimolar mixture of isoprene and 1-hexene led to a co-polymer (1-hexene/isoprene = 1:10) essentially formed of 1,4-*trans*-polyisoprene blocks separated by only one inserted hexyl group. The tetra(allyl)lanthanide complexes $[Li(dioxane)_{1.5}][Ln(allyl)_4]$ (Ln = Sm, Nd) showed no hexene insertion under the same polymerization conditions and formed a mixture of *cis*- and *trans*-polyisoprene.

Hou, Wakatsuki and co-workers reported a stereospecific polymerization of 1,3-butadiene with samarocene-based catalysts [64]. The lanthanide-based single-site catalyst system $(C_5Me_5)_2Sm(THF)_2$ with MMAO (modified methylaluminoxane-containing isobutylaluminoxane) as a co-catalyst (1:200) induces rapid polymerization of butadiene at 50 °C in toluene, with the conversion of 2500 equiv. of butadiene reaching to 65% in 5 min (TON: 20000 butadiene/Sm-mol/h). The resulting polybutadiene possesses a very high 1,4-*cis*-microstructure (98.8%), high molecular weight (M_n = 400900), and narrow MWD (M_w/M_n = 1.82). This shows that this catalytic system can effect both high 1,4-*cis* selectivity and "living" control on the molecular weight of the polymer products.

Marks and co-workers reported efficient and selective silanolytic ($PhSiH_3$, *n*-$BuSiH_3$, $C_6H_5CH_2SiH_3$) chain transfer in organolanthanide-catalyzed ethylene polymerization and ethylene co-polymerization with several α-olefins [65]. The result is a series of silyl-capped polyolefins. In $[(Me_5C_5)_2LnH]_2$ (Ln = Y, La, Sm, Lu) and $[Me_2Si(Me_4C_5)_2LnH]_2$-mediated ethylene homopolymerization and ethylene co-polymerization, both primary arylsilanes ($PhSiH_3$) and alkylsilanes (*n*-$BuSiH_3$, $C_6H_5CH_2SiH_3$) function as efficient chain-transfer agents.

Table 5
Cyclization/silylation of enynes with $Cp^*_2YMe(THF)$ to afford six-membered nitrogen heterocycles

Substrate	Product	Silane	Isolated yield (%)
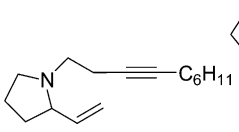	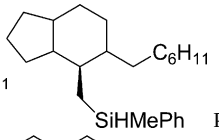	$PhMeSiH_2$	100
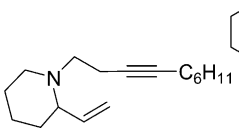	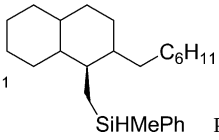	$PhMeSiH_2$	94

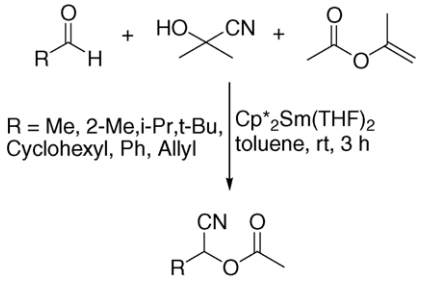

Scheme 38.

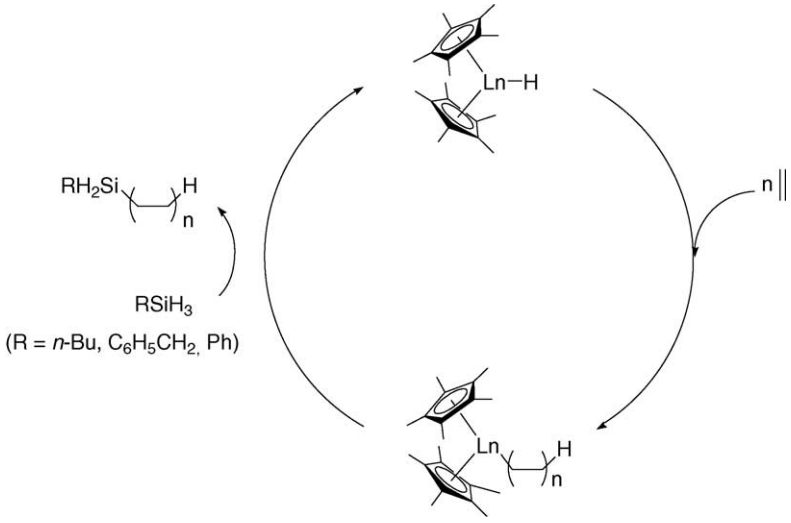

Scheme 39. Proposed catalytic cycle for silyl-capped polyolefins mediated by organolanthanide catalysts.

In the case of ethylene polymerization mediated by $[(Me_5C_5)_2SmH]_2$, the mechanism of chain transfer is supported by the observation that the number-average molecular weight (M_n) of the capped polyethylenes formed at constant concentrations of catalyst, $PhSiH_3$, and ethylene is inversely proportional to the concentration of $PhSiH_3$ (Scheme 39). The authors also found the use of silane-activated $Me_2Si(Me_4C_5)_2LnCH(SiMe_3)_2$ precatalysts to be efficient in producing silyl-endcapped ethylene/1-hexene and ethylene/styrene co-polymers.

Ring-opening polymerization of lactones using SmX_2 (X = I, Br, C_5H_5) catalysts was reported by Agarwal et al. [66]. Successful room temperature ring-opening polymerization of ε-caprolactone and δ-valerolactone has been carried out using the SmX_2 catalysts. SmI_2 in the presence of metallic Sm was found to have enhanced reactivity at room temperature in ring-opening polymerization processes as compared to pure SmI_2. $SmBr_2$ and $Sm(C_5H_5)_2$ showed increased reactivity compared with the Sm/SmI_2 system owing to their higher reductive power. The catalyst concentration and time of polymerization showed a remarkable effect on number-average molecular weight (M_n). A decrease in M_n on increasing reaction time and decreasing catalyst concentration was observed.

Among detailed studies of other samarium(II) aryloxide complexes, Wakatsuki and co-workers showed $[(C_5Me_5)Sm(\mu\text{-}OC_6H_2{}^tBu_2\text{-}2,6\text{-}Me\text{-}4)]_2$ to exhibit an extremely high activity for the ring-opening polymerization of ε-caprolactone and δ-valerolactone [67].

Yasuda et al. reported the synthesis and studies of the physical properties of optically active poly(estercarbonate)s, which where synthesized by co-polymerization of substituted trimethylenecarbonate with ε-caprolactone using organolanthanides among others as catalysts [68]. The homopolymerization of optically active (*R*)-1-methyltrimethylenecarbonate (1-MTC = 1-methyltrimethylenecarbonate) was performed in toluene solution using various types of initiators including $(C_5Me_5)_2Sm(THF)_2$ and $(C_5Me_5)_2SmMe(THF)$. While all other catalysts for the ring opening polymerization required relatively high temperatures (60–100 °C), the samarium complexes initiated polymerization processes at room temperature and below. $(C_5Me_5)_2Sm(THF)_2$ and $(C_5Me_5)_2SmMe(THF)$ brought about higher yields and lower polydispersities when the ring-opening polymerization was carried out at 0 °C. $(C_5Me_5)_2Sm(THF)_2$ and $(C_5Me_5)_2SmMe(THF)$ were also used in the homopolymerization of (*R*,*R*)-1,3-dimethyltrimethylenecarbonate giving polymers in high yields. $(C_5Me_5)_2Sm(THF)_2$ was also used as an initiator for the co-polymerization of (*R*,*R*)-, (*S*,*S*)- or *rac*-1,3-dimethyltrimethylene carbonate with ε-caprolactone. All polymers exhibited high molecular weights, low polydispersities, and high polymer yields. Biodegradation processes of the synthesized polymers were performed in detail.

Hessen and co-workers showed the catalytic formation of thienyl-capped polyethylene [69]. $[(C_5Me_5)_2La(C_4H_3S)]_2$ was found to be able to combine ethylene polymerization and C–H activation of thiophene to result in catalytic formation of polyethylene with 2-thienyl end-groups (Scheme 40).

2.10. Theoretical calculations

Ethylene insertion into the Sm–C bond of $H_2SiCp_2SmCH_3$, a model reaction of an olefin poly-

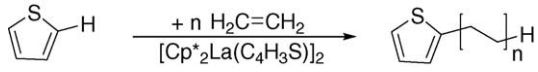

Scheme 40.

merization propagation step, has been studied by Koga using ab initio molecular orbital methods [70]. The low electronegativity of the samarium atom makes the Sm–C bond ionic, the methyl group having a charge of −0.75. The reaction passes through a loose ethylene complex with a binding energy of 15 kcal/mol and then a tight four-centered transition state with an agnostic interaction between the Sm atom and one of the methyl CH bonds. A small activation energy of 14 kcal/mol is required to pass through this transition state, indicating that this is an easy reaction. Compared with reactions involving group 4 cationic silylene-bridged metallocenes the activation energy is higher, and the reaction is less exothermic.

Kulkarni and Koga investigated also the samarium(III)-catalyzed olefin hydroboration reaction using ab initio methods [71]. The stationary structures on the model reaction path considering ethylene as alkene, Cp_2SmH as an active catalyst, and $HB(OH)_2$ as model borane were obtained at the RHF and MP2 levels, and the MP4SDQ energy calculations were carried out at the MP2 structure. In the reaction, ethylene initially coordinates to the active catalyst to form a π-complex. Then, ethylene insertion into the Sm–H bond takes place leading to stable $Cp_2SmC_2H_5$ after passing through the barrier of 4.2 kcal/mol. In the following step, the model borane adds to $Cp_2SmC_2H_5$ to form a borane complex, which thereafter passes through the smaller barrier of 1.1 kcal/mol giving rise to a product complex. In the final step, the dissociation of the hydroborated product, $C_2H_5B(OH)_2$, takes place with a large endothermicity of 40.4 kcal/mol.

3. Actinides

3.1. Actinide complexes without supporting cyclopentadienyl and cyclopentadienyl-like ligands

3.1.1. Alkyl, alkenyl and CO complexes

Scott and co-workers reported the surprisingly fast reaction of $[U(NN'_3)I]$ $[NN'_3 = N(CH_2CH_2NSiMe_2Bu^t)_3]$ with Groups 1 and 2 metal alkyls giving, via metallation of a methylsilyl group, the metallacycle $[U(bit\text{-}NN'_3)]$ (Scheme 41) [72]. The analogous $[Th(bit\text{-}NN'_3)]$ was prepared using the same procedure from $[Th(NN'_3)Cl]$ or through reduction of $[Th(NN'_3)I]$ with a potassium film. A similar reaction of $[U(NN'_3)I]$ with potassium in toluene results in formation of the dimeric U(III) complex $\{[K(\eta^6\text{-}C_6H_5Me)][[U(bit\text{-}NN'_3)]\}_2$.

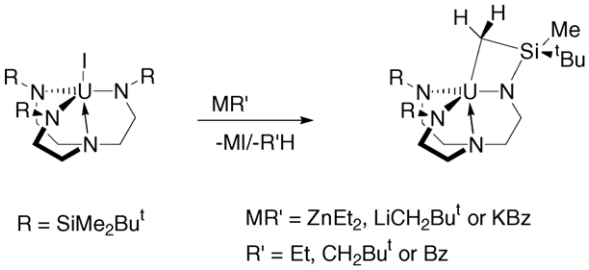

Scheme 41.

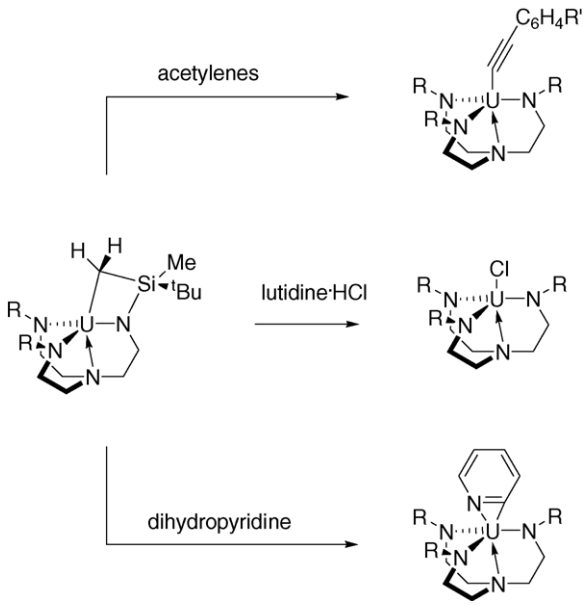

Scheme 42.

Oxidation of $[U(bit\text{-}NN'_3)]$ with air or other oxygen sources led to formation of an oxo-bridged dimer with intermolecular by metalated methylsilyl groups. Reaction of H-acidic compounds HX like lutidine•HCl, diethylamine, or *t*-butanol gave the $[U(NN'_3)X]$ complexes under reprotonation of the previously metalated methylsilylgroup. β-Hydropyridines and monosubstituted alkynes react in a similar manner to give η^2-dehydropyridyl complexes and η^1-alkynyls, respectively (Scheme 42).

Andrews and co-workers published studies of the reaction of thorium atoms with CO [73]. The reaction of laser-ablated thorium atoms with carbon monoxide in excess neon gave the first thorium carbonyl complex, ThCO, which rearranges photochemically to CThO (Scheme 43).

3.1.2. Metallacarborane complexes

Xie et al. reported the synthesis of $\{[K_2(THF)_5][(\eta^7\text{-}C_2B_{10}H_{12})(\eta^7\text{-}C_2B_{10}H_{12})U]\}_2$, which contains a metallacarborane with a novel $(\eta^7\text{-}C_2B_{10}H_{12})^{4-}$ ligand (Scheme 44) [74].

Single-crystal X-ray determinations revealed a centrosymmetrical dimer with a bent sandwich structure. Fig. 52 shows an η^6-coordination of the uranium ion to the *nido*-$C_2B_{10}H_{12}{}^{2-}$ ligand and a η^7-bonding to the *arachno* type

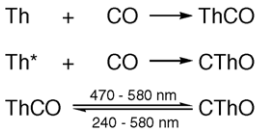

Scheme 43.

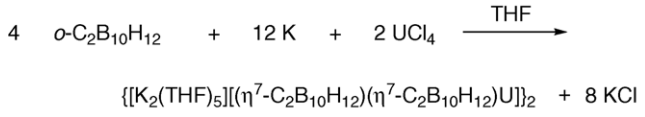

Scheme 44.

$C_2B_{10}H_{12}^{4-}$ ligand. Furthermore, a coordination of two B–H bonds of the C_2B_5 layer of the *arachno*-$C_2B_{10}H_{12}^{4-}$ is observable.

The most interesting feature of the structure is the boat conformation of the C_2B_5 layer described above with short U–C distances of 2.41 and 2.44 Å (Fig. 52) lying in the range of U–C–σ-bonds.

3.2. Cyclopentadienyl complexes

3.2.1. Bis(cyclopentadienyl) complexes

Burns and co-workers reported studies on the catalytic reduction of azides and hydrazines involving high valent organouranium complexes [75]. $(C_5Me_5)_2U(=NAd)_2$ (Ad = 1-adamantyl) reacts with hydrogen under a hydrogen atmosphere to give the corresponding reduced bis(amide) complex $(C_5Me_5)_2U(NHAd)_2$ (Scheme 45). The reaction proceeded cleanly with a rate of hydrogenation of $t_{1/2} = 4$ h. When AdN_3 was added to a solution of the bis(amide) complex, the bis(imido) compound $(C_5Me_5)_2U(=NAd)_2$ was regenerated. Heating of $(C_5Me_5)_2U(NHAd)_2$ to 55 °C in THF with AdN_3 under an atmosphere of hydrogen led to catalytic hydrogenation of AdN_3 to $AdNH_2$.

When $(C_5Me_5)_2U(=NPh)_2$ was treated with an excess of *N*,*N*′-diphenylhydrazine in the absence of hydrogen, the substrate was entirely consumed, and aniline and azobenzene were formed in a 2:1 ratio (Scheme 46). The disproportionation indicated that the *N*,*N*′-diphenylhydrazine acted upon the uranium complexes as both oxidant and reductant.

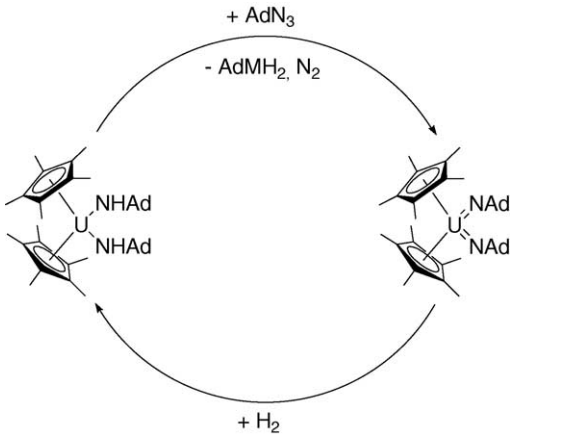

Scheme 45.

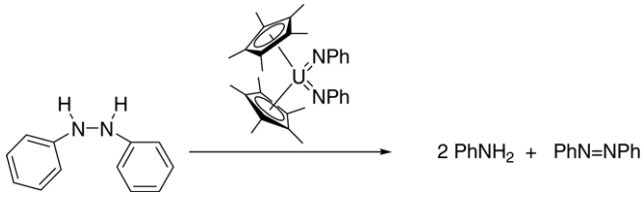

Scheme 46.

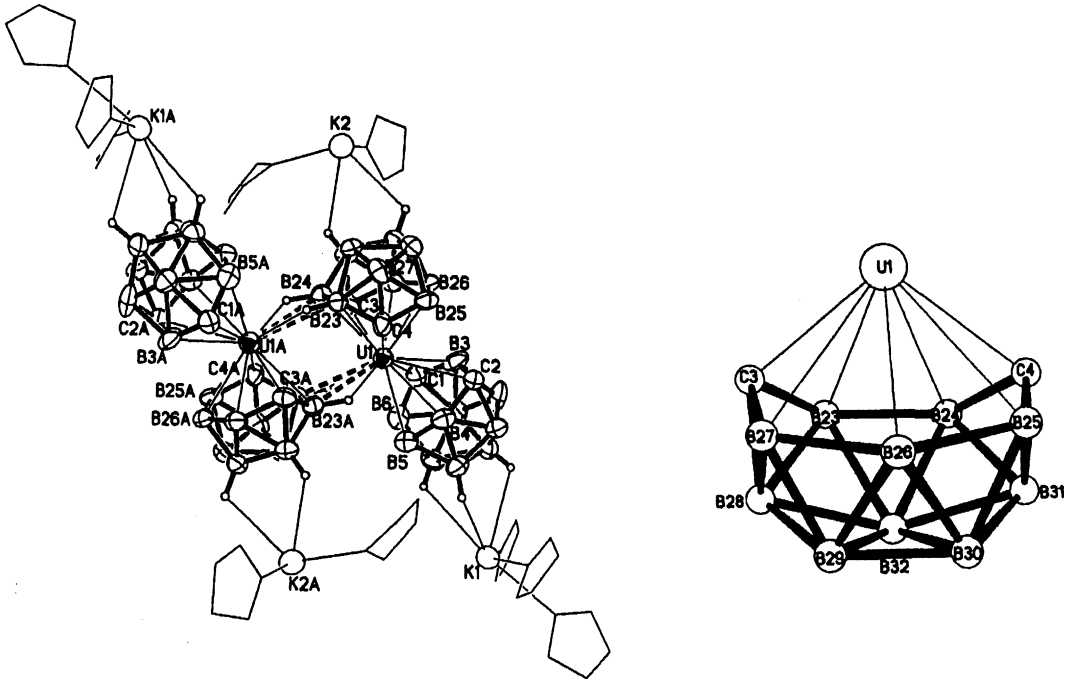

Fig. 52. Molecular structure of $\{[K_2(THF)_5][(\eta^6\text{-}C_2B_{10}H_{12})(\eta^7\text{-}C_2B_{10}H_{12})U]\}_2$ and the interaction between the uranium ion and the $(\eta^7\text{-}C_2B_{10}H_{12})^{4-}$ ligand.

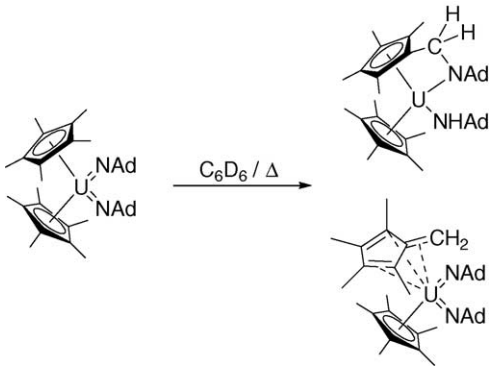

Scheme 47. Formation of the intramolecular ring bite uranium complex.

Burns and co-workers observed a C–H bond with the above described bis(imido) uranium complex [76]. Thermolysis of $(C_5Me_5)_2U(=NAd)_2$, in benzene or hexane resulted in the intramolecular C–H bond activation of a methyl group on a pentamethylcyclopentadienyl ligand across the imido functional groups. The activation product is a reduced U(IV) metallocene bis(amide) complex with an N-bonded methylene unit derived from the methyl group attached to one amide group. Scheme 47 shows the formation of the ring bite uranium complex with the two possible structures that are consistent with the ^{1}H NMR data.

Single-crystal X-ray structure determinations revealed a constrained geometry of the bifunctional amido-cyclopentadienide ligand, that leads to the distortions in the metallocene geometry. The N-bonded methylene derived from a C_5Me_5 methyl group is pulled out of the plane of the C_5 ring toward the metal center by 0.52 Å (Fig. 53).

Burns and co-workers also reported the solid-state structure of chloro(*p*-chloroanilido-*N*)bis(η^5-pentamethylcyclopentadienyl)uranium(IV) (Fig. 54) [77].

The synthesis of $[Na(18\text{-crown-6})][U(C_5Me_5)_2(S^tBu)(S)]$, which is the first *f*-element compound containing a metal–sulfur double bond, was reported by Ephritikhine and co-workers [78]. The C–S bond cleavage of a thiolate ligand of $[U(C_5Me_5)_2(S^tBu)_2]$ was induced by treatment with Na(Hg), and $[Na(18\text{-crown-6})][U(C_5Me_5)_2(S^tBu)(S)]$ was isolated after addition of 18-crown-6. Single-crystal X-ray determinations exhibited the unsupported U–S–Na linkage of the molecular complex with a U–S bond distance of 2.462 Å (Fig. 55).

Ephritikhine and co-workers reported the synthesis of bis(pentamethylcyclopentadienyl) uranium(IV) thiolate compounds and their reactions with CO_2 and CS_2 [79]. The bis(thiolato) complexes $[U(C_5Me_5)_2(SR)_2]$ (R = Me, ^{i}Pr, ^{t}Bu, Ph) were synthesized by treatment of $[U(C_5Me_5)_2Cl_2]$ with NaSR in toluene or THF. Their reactions with CO_2 and CS_2 gave the insertion derivatives $[U(C_5Me_5)_2(SR)(E_2CSR)]$ (E = O and R = ^{t}Bu; E = S and R = Me, ^{i}Pr or ^{t}Bu) and $[U(C_5Me_5)_2(E_2CSR)_2]$ (E = O and R = ^{t}Bu; E = S and R = Me or ^{t}Bu) (Scheme 48). Treatment of $[U(C_5Me_5)_2(S^tBu)(S_2CS^tBu)]$ with CO_2 gave the mixed

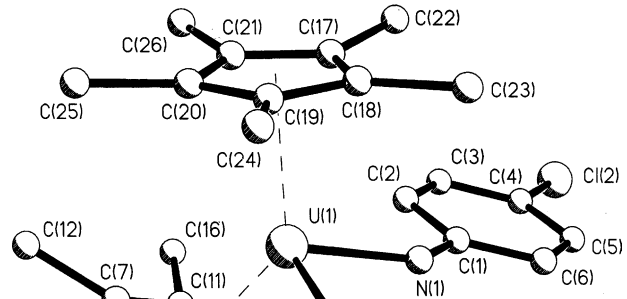

Fig. 54. Molecular structure of chloro(*p*-chloroanilido-*N*)bis(η^5-pentamethylcyclopentadienyl)uranium(IV).

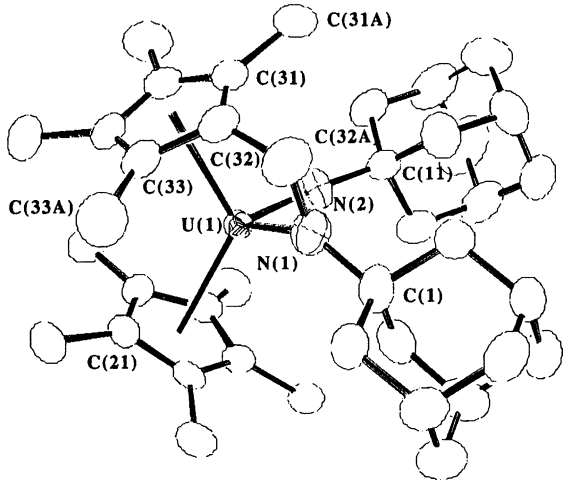

Fig. 53. Molecular structure of $(C_5Me_5)(C_5Me_4CH_2NAd)U(NHAd)$.

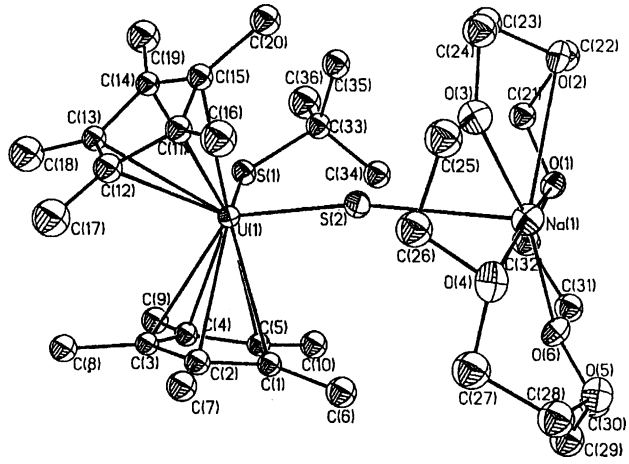

Fig. 55. Molecular structure of $[Na(18\text{-crown-6})][U(C_5Me_5)_2(S^tBu)(S)]$.

insertion complex $[U(C_5Me_5)_2(O_2CS^tBu)(S_2CS^tBu)]$. Thermolysis of the insertion compounds led to the reverse elimination reaction of CO_2 and CS_2. Reduction of $U(C_5Me_5)_2(O_2CS^tBu)_2]$ with Na(Hg) afforded the corresponding anionic U(III) complex. Single-crystal X-ray structure determinations of $[U(C_5Me_5)_2(S^tBu)(S_2CS^tBu)]$ revealed a classical bent sandwich structure (Fig. 56). The U, C(21), C(25), S(1), S(2) and S(4) atoms are coplanar, and this plane is almost perpendicular to that defined by U and the two centroids of the pentamethylcyclopentadienyl rings.

The reaction of $[U(C_5Me_5)_2Me_2]$ with $HPPh_2$ was also studied by Cendrowski-Guillaume and Ephritikhine leading to the first uranium diphenylphosphide compounds [80]. They found the reaction of $[U(C_5Me_5)_2Me_2]$ with $HPPh_2$ to be the best route to the uranium(IV) diphenylphosphide compounds $[U(C_5Me_5)_2(PPh_2)(Me)]$ and $[U(C_5Me_5)_2(PPh_2)_2]$. Thermolysis of $[U(C_5Me_5)_2(PPh_2)(Me)]$ afforded the *ortho*-metallated complex $[U(C_5Me_5)_2(PPh\{o\text{-}C_6H_4\})]$ after 24 h in refluxing toluene. Reduction of $[U(C_5Me_5)_2(PPh_2)_2]$ with KH gave the first U(III) phosphide $K[U(C_5Me_5)_2(PPh_2)_2]$.

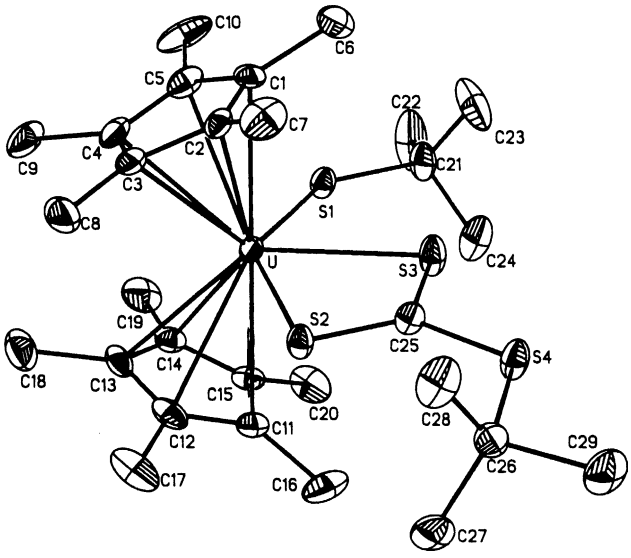

Fig. 56. Molecular structure of $[U(C_5Me_5)_2(S^tBu)(S_2CS^tBu)]$.

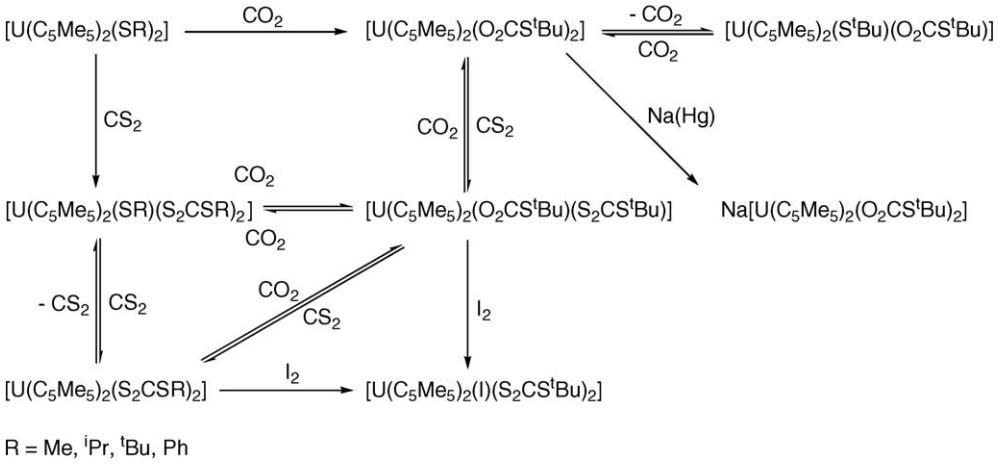

Scheme 48. Formation and reactions of the CO_2 and CS_2 insertion compounds.

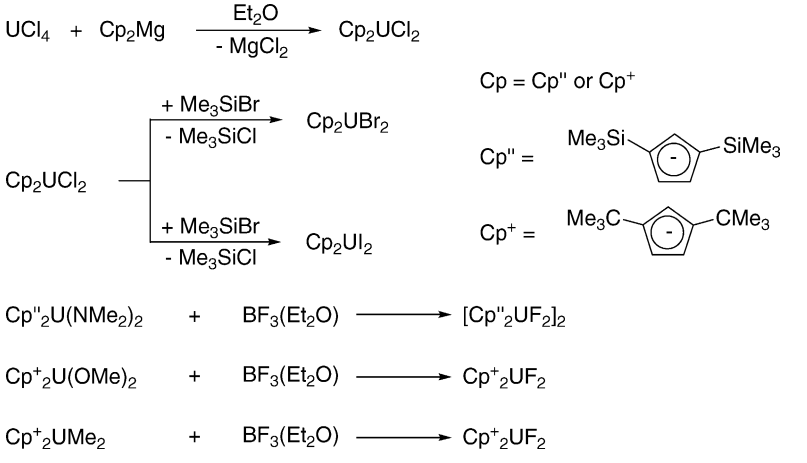

Scheme 49. Synthesis of substituted bis(cyclopentadienyl) uranium halides.

Andersen and co-workers presented detailed studies on substituted bis(cyclopentadienyl) complexes of U(IV) and U(III) [81–83]. Besides common analytical methods they used variable temperature NMR determinations and EXAFS studies to characterize the monomeric and dimeric complexes as well as their dynamic behavior. High-yield preparations of the uranium metallocenes $[1,3\text{-}(Me_3Si)_2C_5H_3]_2UCl_2$ ($Cp'' = 1,3\text{-}(Me_3Si)_2C_5H_3$) and $[1,3\text{-}(Me_3C)_2C_5H_3]_2UCl_2$ ($Cp^+ = 1,3\text{-}(Me_3C)_2C_5H_3$) have been developed from the reactions of UCl_4 with the corresponding magnesocenes Cp''_2Mg and $Cp^+{}_2Mg$ in diethyl ether [81]. The chloride ligands were exchanged with either Me_3SiBr or Me_3SiI to give the uranium metallocene bromides Cp''_2UBr_2 and $Cp^+{}_2UBr_2$ or iodides Cp''_2UI_2 and $Cp^+{}_2UI_2$ (Scheme 49).

The corresponding fluorides $(Cp''_2UF_2)_2$ and $Cp^+{}_2UF_2$ were prepared by the reaction of $BF_3{}^{\bullet}OEt_2$ with $Cp''_2U(NMe_2)_2$, $Cp^+{}_2U(OMe)_2$ or $Cp^+{}_2UMe_2$. Crystal structure determinations show monomeric structures for Cp''_2UCl_2, $Cp^+{}_2UCl_2$, Cp''_2UMe_2, $Cp^+{}_2UF_2$ and a dimeric one for $(Cp''_2UF_2)_2$ (Fig. 57). The idealized symmetry of the monomers Cp''_2UX_2 and $Cp^+{}_2UCl_2$ was found to be C_{2v} when X = F, Cl or Br and C_2 when X is I or Me; in the dimer, the idealized symmetry is C_i. The preferences can be rationalized by intramolecular and intermolecular steric effects. The solution ring conformation and intramolecular exchange process have been studied by variable-temperature ^1H NMR spectroscopy which suggests that a monomer–dimer equilibrium is present in solution in the difluoride complexes $(Cp''_2UF_2)_2$ and $Cp^+{}_2UF_2$.

Studies of the solution structure and the behavior of dimeric uranium(III) metallocene halides were performed on the complexes $[Cp''_2UX]_2$ and $[Cp^+{}_2UX]_2$ were X is F, Cl, Br or I [82]. The synthesis of these complexes was performed using reactions of the above described corresponding bis(cyclopentadienyl)uranium(IV) halides with *tert*-butyllithium. The variable-temperature ^1H NMR behavior of the uranium(III) dimers $[Cp''_2UX]_2$ and $[Cp^+{}_2UX]_2$ was examined in a range of −90 to 100 °C. At low temperature, the number of inequivalent CMe_3 or $SiMe_3$ groups implies that the solution structure is the same as the solid structure in all of these complexes. The barriers of ring rotation in the Cp″ series are strongly dependent upon the U–X distances, but all of the barriers of ring rotation in the Cp^+ series are the same. The trends in ring rotation barriers were explained by the different conformation of the Cp ligands in the dimers. In addition to the homo-halide dimers, the variable-temperature NMR behavior of the hetero-halide dimers $Cp_4U_2(\mu\text{-}X)(\mu\text{-}Y)$, where Cp is Cp″ or Cp^+ and X and Y are halides where $X \neq Y$, was examined. Above room temperature, the halide atoms exchange sites rapidly on the NMR time scale.

The structure of substituted-cyclopentadienyl uranium(III) dimers and related uranium metallocenes were deduced by EXAFS, and the crystal structures of $[Cp''_2UF]_2$ and $[Cp^+{}_2UO]_2$ were reported [83]. Both complexes have

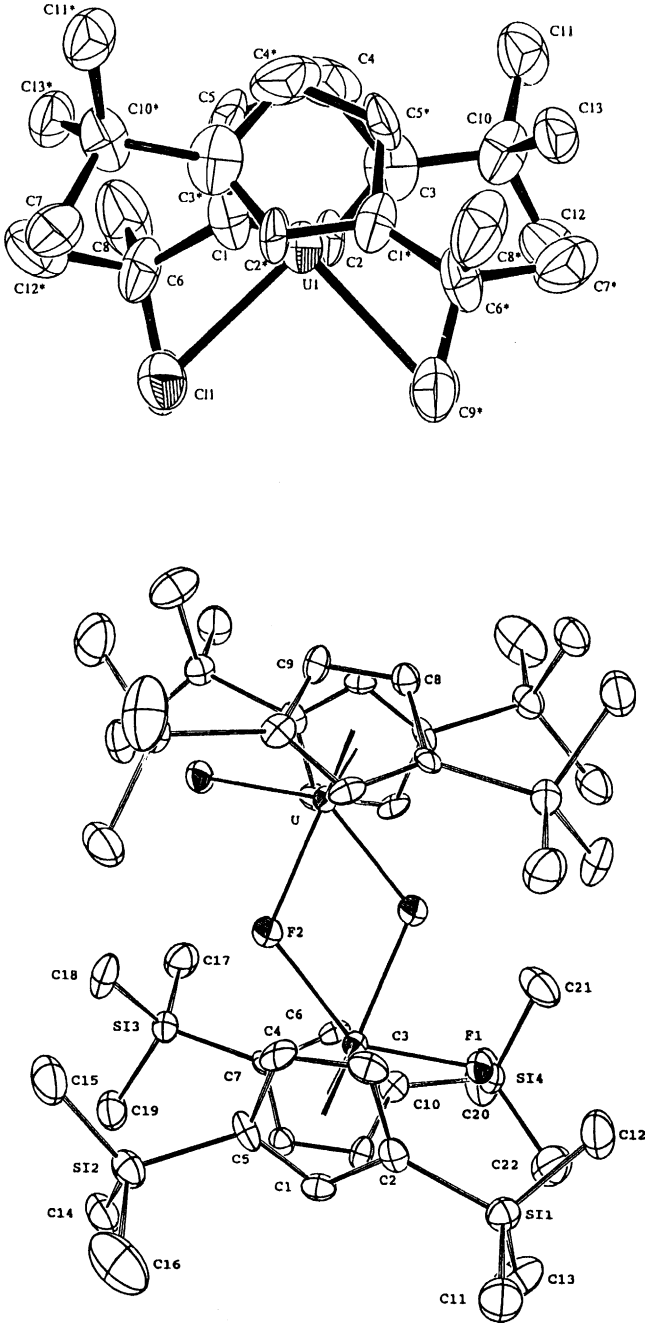

Fig. 57. Molecular structures of $Cp^+{}_2UCl_2$ and $(Cp''_2UF_2)_2$.

idealized C_{2h} symmetry, and their U···U distances are 3.85 and 3.39 Å, respectively (Fig. 58). The X-ray spectra of several uranium metallocene complexes and the numerical results from fitting the EXAFS spectra were reported. For $[Cp^+{}_2UF]_2$, the U···U distance was found by EXAFS to be similar to that in $[Cp''_2UF]_2$, implying that $[Cp^+{}_2UF]_2$ is dimeric. A structural model is advanced that correlates the U···U distances with the orientation of the cyclopentadienyl rings; the orientation depends on a subtle combination of steric repulsions between ligands on adjacent metal centers.

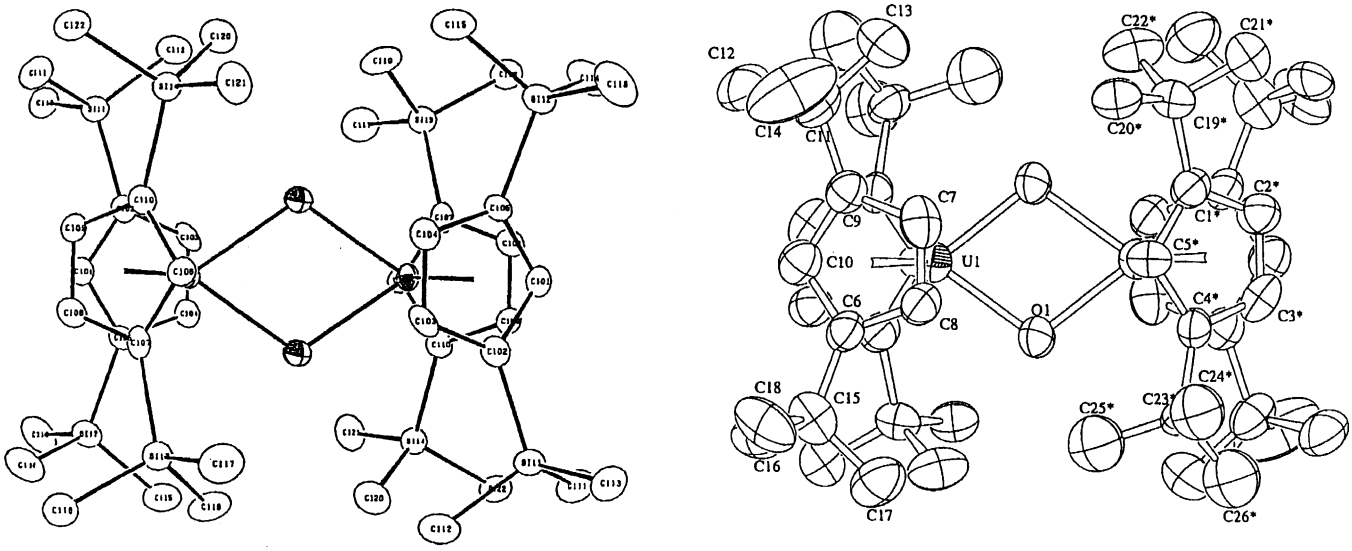

Fig. 58. Crystal structures of $[Cp''_2UF]_2$ and $[Cp^+_2UO]_2$.

3.2.1.1. ansa-Cyclopentadienyl complexes. Complexes of U(IV) containing the chelating bis(cyclopentadienyl) ligand sets $[Me_2Si(C_5Me_4)_2]^{2-}$ and $[Me_2Si(C_5Me_4)(C_5H_4)]^{2-}$ have been prepared by Burns and co-workers to examine their utility in generating organoamido complexes of uranium [84].

The chloride complexes $\{[Me_2Si(C_5Me_4)_2]UCl_2(LiCl)_2(Et_2O)_4\}$ and $\{[Me_2Si(C_5Me_4)(C_5H_4)]UCl_2(LiCl)_2(Et_2O)_4\}$ were generated by reaction of UCl_4 with the corresponding bis(cyclopentadienyl) dilithio salt in diethyl ether and tetrahydrofuran, respectively (Scheme 50). The dilithio complexes were alkylated by Grignard reagents. $[Me_2Si(C_5Me_4)_2]UMe_2$ and the benzyl derivatives employing both ligand sets have been prepared. $[Me_2Si(C_5Me_4)(C_5H_4)]UMe_2$ was not isolable because it appears to be thermally unstable. The alkyl complexes $[Me_2Si(C_5Me_4)_2]UR_2$ (R = Me, Bz) were protonated by *N,N′*-diphenylhydrazine yielding the expected U(VI) complex $[Me_2Si(C_5Me_4)_2]U(NC_6H_5)_2$. Reaction of $[Me_2Si(C_5Me_4)(C_5H_4)]UBz_2$ with *N,N′*-diphenylhydrazine gave the U(VI) monoimido dimer $\{[Me_2Si(C_5Me_4)(C_5H_4)]U(NC_6H_5)]\}_2$. The molecular structure of this complex revealed a the dimeric structure with asymmetric organoimido bridging ligands (Fig. 59).

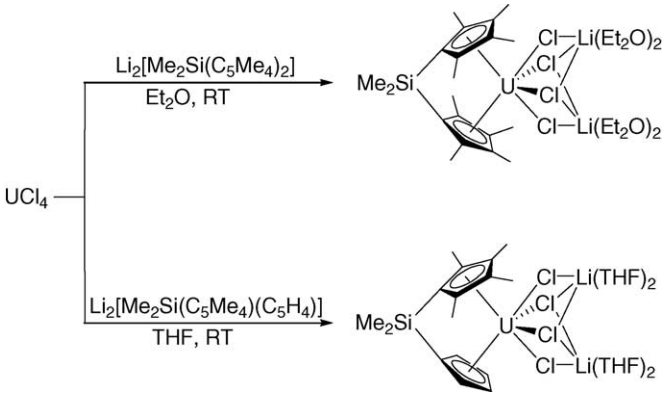

Scheme 50. Synthesis of the *ansa*-bis(cyclopentadienyl) uranium complexes $\{[Me_2Si(C_5Me_4)_2]UCl_2(LiCl)_2(Et_2O)_4\}$ and $\{[Me_2Si(C_5Me_4)(C_5H_4)]UCl_2(LiCl)_2(Et_2O)_4\}$.

3.2.2. Tris(cyclopentadienyl) complexes

Andersen, Carmona and co-workers reported studies on carbon monoxide and isocyanide complexes of trivalent uranium metallocenes [85]. Organic isocyanide complexes of trivalent uranium metallocenes of type $[Cp'_3U(CNR)]$, where $Cp' = C_5H_5$, MeC_5H_4, $Me_3CC_5H_4$, and $Me_3SiC_5H_4$ and R = Et; $Cp' = 1,3\text{-}(Me_3Si)_2C_5H_3$ and R = *t*-Bu; $Cp' = Me_4C_5H$ and R = 4-(MeO)C_6H_4 and 2,6-$Me_2C_6H_3$, were prepared (Scheme 51).

The new metallocenes $[\{1,3\text{-}(Me_3Si)_2C_5H_3\}_3U]$ and $[(C_5Me_4H)_3U]$ were prepared by synthetic routes that involve the reduction of the appropriate tetravalent uranium metallocene precursors with potassium metal and $NaC_{10}H_8$,

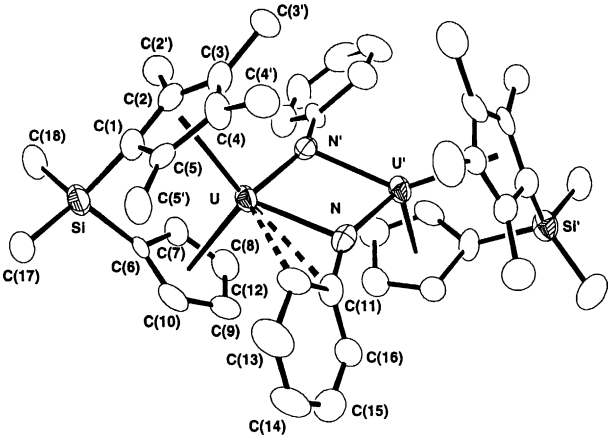

Fig. 59. Molecular structure of $\{[Me_2Si(C_5Me_4)(C_5H_4)]U(NC_6H_5)]\}_2$.

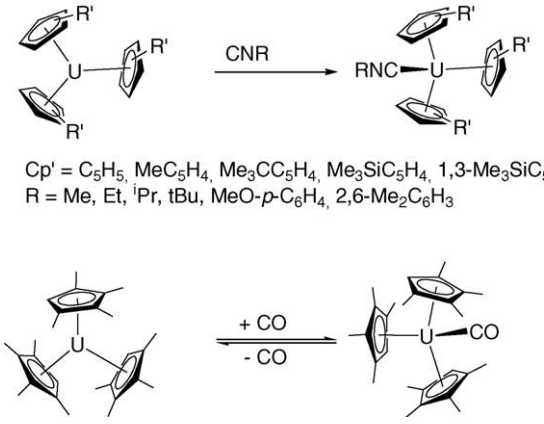

Scheme 51. Formation of the carbon monoxide and isocyanide complexes of trivalent uranium metallocene complexes.

respectively (Scheme 52). Fig. 60 shows the molecular structure of $[(C_5Me_4H)_3U]$ revealing a perfectly trigonal structure with a threefold axis (all Cp′(centroid)–U–Cp′(centroid) angles equal to 120°).

When $Cp' = MeC_5H_4$ and $R = 2,6\text{-}Me_2C_6H_3$, both 1:1 and 1:2 adducts were obtained. The IR spectra of the complexes showed that $\tilde{\nu}_{CN}$ increases slightly for the alkyl isocyanide complexes and decreases slightly for the aryl isocyanide complexes relative to $\tilde{\nu}_{CN}$ for the free ligands. The uranium metallocenes form carbon monoxide adducts in which $\tilde{\nu}_{CO}$ moves to lower wavenumbers upon coordination by 155–266 cm^{-1} (Scheme 52). In only one case a carbon monoxide adduct, $[(C_5Me_4H)_3U(CO)]$, could be isolated in crystalline form. A single-crystal X-ray determination of $[(C_5Me_4H)_3U(CO)]$ revealed a monomeric structure with a U-C(CO) bond length of 2.383 Å with an almost linear U–C–O bond angle (175.2°). The $\tilde{\nu}_{CO}$ stretching frequencies are in the order $1,3\text{-}(Me_3Si)_2C_5H_3 > Me_3SiC_5H_4 > Me_3CC_5H_4 > C_5Me_4H$. $[(C_5Me_4H)_3U]$ was shown to be the best π donor in this series of metallocenes. Solution ^1H NMR spectra showed that the adducts are fluxional, and in case of $[(C_5Me_4H)_3U(L)]$, where L = CO or 4-$(MeO)C_6H_4NC$, two fluxional processes were observed: dissociation of L at

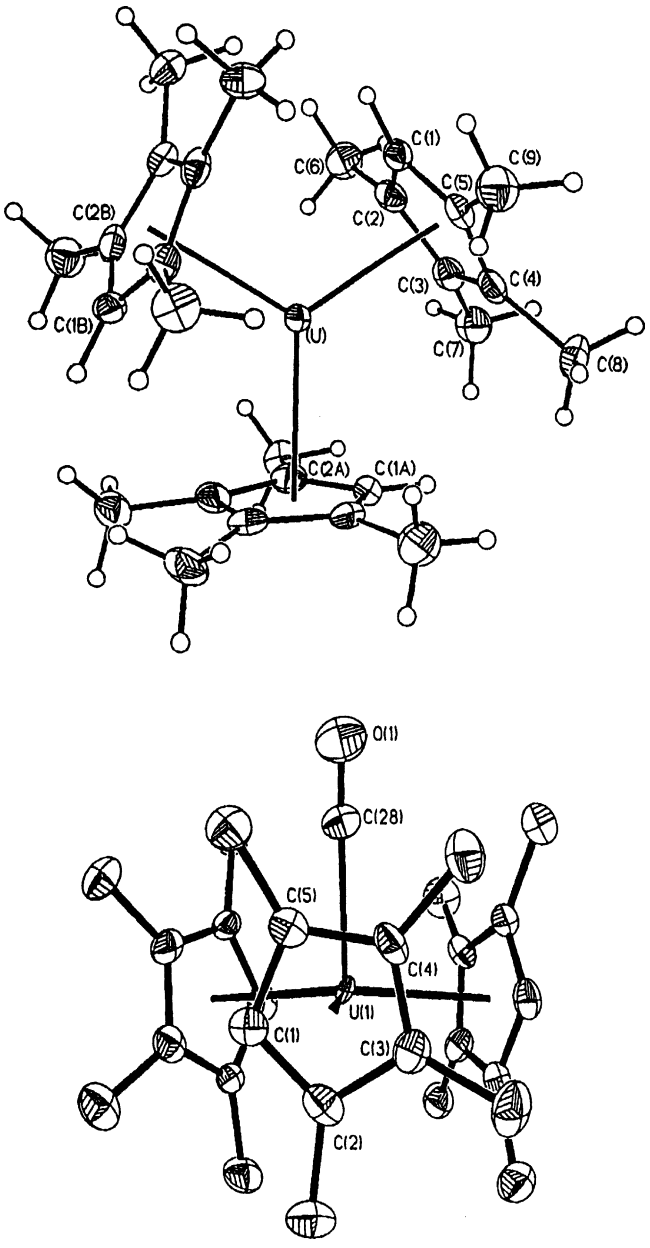

Fig. 60. Molecular structures of $[(C_5Me_4H)_3U]$ and $[(C_5Me_4H)_3U(CO)]$.

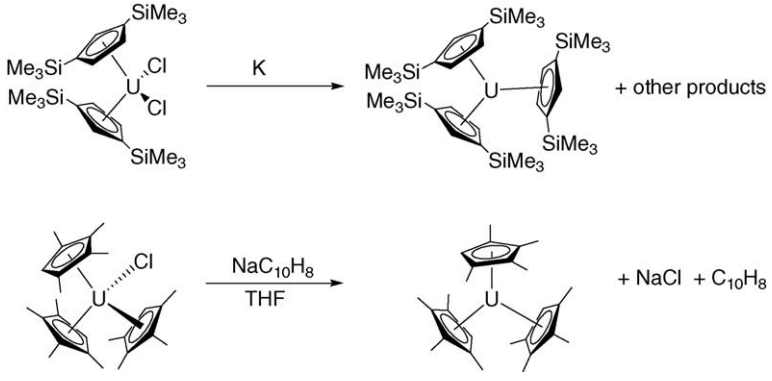

Scheme 52. Synthesis of $[\{1,3\text{-}(Me_3Si)_2C_5H_3\}_3U]$ and $[(C_5Me_4H)_3U]$.

relatively high temperature and cessation of ring rotation at low temperature.

All experimental studies reported in this work are consistent with the view that the uranium metallocenes are better π donors than their cerium analogues, and the π-donating ability is dependent upon the ring substituents.

3.3. Organoactinide complexes in organic synthesis

Eisen and co-workers showed that organoactinide complexes of the type $Cp^*_2AnMe_2$ (An = Th, U) are efficient catalysts for the hydrosilylation of terminal alkynes [86]. The chemoselectivity and regiospecificity of the reactions were found to be strongly dependent on the nature of the catalyst, the nature of the alkyne, the silane substituents, the ratio between the silane and the alkyne, the solvent, and the reaction temperature. The hydrosilylation reaction of the terminal alkynes with $PhSiH_3$ at room temperature produced the *trans*-vinylsilane as the major product along with the silylalkyne and the corresponding alkene (Scheme 53).

At higher temperatures (50–80 °C), besides the products obtained at room temperature, the *cis*-vinylsilane and the double-hydrosilylated alkene, in which the two silicon moieties are connected with the same carbon atom, were obtained. The catalytic hydrosilylation of $(Me_3Si)CCH$ and $PhSiH_3$ with $Cp^*_2ThMe_2$ was found to proceed only at higher temperature, although no *cis*-vinylsilane or double-hydrosilylated products were observed. Mechanistic studies on the hydrosilylation of ^{i}PrCCH and $PhSiH_3$ in the presence of $Cp^*_2ThMe_2$ showed that the first step in the catalytic cycle is the insertion of an alkyne into a thorium–H bond. The key organoactinide intermediates for the *cis*-vinylsilane and the double-hydrosilylation products were the $Cp^*_2An(CCR)(C(PhSiH_2) = CHR)$ (An = Th, U) complexes. These complexes were trapped (for R = ^{i}Pr) and characterized by spectroscopic methods.

Eisen and co-workers also found the cationic actinide complex $[(Et_2N)_3U][BPh_4]$ to be an active catalytic precursor for the selective dimerization of terminal alkynes [87]. The regioselectivity in this reaction was mainly toward the geminal dimer, but for bulky alkyne substituents the unexpected *cis* dimer was also obtained. Mechanistic NMR studies showed that a η^2-π-complex was formed between a terminal alkyne and an uranium-acetylide intermediate. This latter complex had been characterized only spectroscopically.

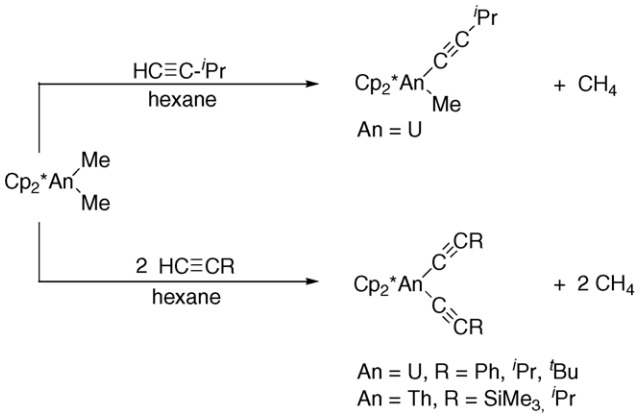

Scheme 54.

3.4. Organoactinide complexes as polymerization catalysts

Eisen and co-workers also used the $Cp^*_2AnMe_2$ (An = Th, U) system for the synthesis of short oligomers [88]. They described a novel strategy for the catalytic synthesis of short oligomers, dimers and/or trimers, of terminal alkynes. The method allows control of the extent of, and, in some cases, the regiospecifity in the catalyzed oligomerization of terminal alkynes promoted by bis(pentamethylcyclopentadienyl)actinide dimethyl complexes. These metallocene precursors are known to promote the simultaneous production of a large number of differently sized oligomers in the presence of terminal alkynes. However, the addition of specific amines ensures the selective synthesis of short oligomers. Catalytic "tailoring" to dimers, or a mixture of dimers and trimers could be achieved by using non-bulky or bulky amines, respectively. Kinetic, spectroscopic and mechanistic data argue that the turnover-limiting step involves the formation of the mono(amido)thorium acetylide complex with rapid insertion of the alkyne and protonolysis by the amine.

Various organoactinides of the type $Cp^*_2An(CCR)_2$ (An = Th, U) have been synthesized by Eisen and co-workers from the corresponding $Cp^*_2AnMe_2$ complexes by addition of an equimolar amount or an excess of the corresponding terminal alkyne (Scheme 54) [89].

Attempts to trap the mono(acetylide)complex $Cp^*_2An(CCR)(Me)$ were successful only for the transient species $Cp^*_2U(CC^iPr)(Me)$. The bis(acetylide) complexes are active catalysts for the linear oligomerization

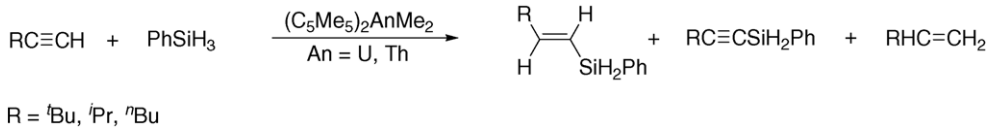

Scheme 53. Room temperature reaction of $Cp^*_2AnMe_2$ (An = Th, U) with an excess of terminal alkynes RCCH (R = ^{t}Bu, ^{i}Pr, ^{n}Bu) and $PhSiH_3$ (alkyne:silane:catalyst = 40:40:1) in either benzene or tetrahydrofuran.

of terminal alkynes HCCR. The regioselectivity and the extent of oligomerization depend strongly on the alkyne substituent R, whereas the catalytic reactivities are similar for both organoactinides. Reaction with *tert*-butylacetylene regioselectively yields the 2,4-disubstituted 1-butene-3-yne dimer, whereas (trimethylsilyl)acetylene is regioselectively trimerized to (*E*,*E*)-1,4,6-tris(trimethylsilyl)-1,3-hexadiene-5-yne, with small amounts (3–5%) of the corresponding 2,4-disubstituted 1-butene-3-yne dimer. Oligomerization with less bulky alkyl- and aryl-substituted alkynes produced a mixture of oligomers.

3.5. Theoretical calculations and electronic structure determinations

Cloke and co-workers reported the preparation of the bis(pentalene) complex $[U\{\eta^8\text{-}C_8H_4(1,4\text{-}Si^iPr_3)_2\}_2]$ and studies of the binding properties by density functional theory and photoelectron spectra [90]. Geometry optimization of $[M(\eta^8\text{-}C_8H_6)_2]$ M = Th with D_{2d} and D_2 symmetry constraints, gives structures in good agreement with the X-ray structure found for $[Th\{\eta^8\text{-}C_8H_4(1,4\text{-}Si^iPr_3)_2\}_2]$; in particular, the folded nature of the ligand is well reproduced by the calculation. Examination of the barrier of relative rotation of the two ligands only showed a significant energy rise when the two rings were eclipsed.

References

[1] T. Dubé, S. Gambarotta, G.P.A. Yap, Angew. Chem. Int. Ed. 38 (1999) 1432–1435.
[2] M. Karl, G. Seybert, W. Massa, K. Harms, S. Agarwal, R. Maleika, W. Stelter, A. Greiner, W. Heitz, B. Neumüller, K. Dehnicke, Z. Anorg. Allg. Chem. 625 (1999) 1301–1309.
[3] H.-R. Zhang, K.K. Wang, J. Org. Chem. 64 (1999) 7996–7999.
[4] O.N. Druzhkova, N.A. Pimanova, L.N. Bochkarev, Russ. J. Gen. Chem. 69 (1999) 784–787.
[5] T.A. Zheleznova, L.N. Bochkarev, A.V. Safronova, S.F. Zhil'tsov, Russ. J. Gen. Chem. 69 (1999) 784–787.
[6] A.Y. Ermilov, A.V. Nemukhin, V.M. Kovba, Mendeleev Commun. 9 (1999) 88–90.
[7] Z. Xie, K. Chui, Q. Yang, T.C.W. Mak, Organometallics 18 (1999) 3947–3949.
[8] Z. Xie, S. Wang, Z.-Y. Zhou, T.C.W. Mak, Organometallics 18 (1999) 1641–1652.
[9] Z. Xie, S. Wang, Q. Yang, T.C. Mak, Organometallics 18 (1999) 2420–2427.
[10] S. Wang, Q. Yang, T.C.W. Mak, Z. Xie, Organometallics 18 (1999) 4478–4487.
[11] D. Stellfeldt, G. Meyer, G.B. Deacon, Z. Anorg. Allg. Chem. 625 (1999) 1252–1254.
[12] D.L. Clark, J.C. Gordon, B.L. Scott, J.G. Watkin, Polyhedron 18 (1999) 1389–1396.
[13] W.-P. Leung, F.-Q. Song, F. Xue, Z.-Y. Zhang, T.C.W. Mak, J. Organomet. Chem. 582 (1999) 292–300.
[14] Q. Liu, J. Huang, Y. Qian, A.S.C. Chan, Polyhedron 18 (1999) 2345–2350.
[15] A. Trifonov, F. Ferri, J. Collin, J. Organomet. Chem. 582 (1999) 211–217.
[16] A.A. Trifonov, E.N. Kirillov, A. Fischer, F.T. Edelmann, M.N. Bochkarev, J. Chem. Soc. Chem. Commun. (1999) 2203–2204.
[17] R.J. Butcher, D.L. Clark, J.C. Gordon, J.G. Watkin, J. Organomet. Chem. 577 (1999) 228–237.
[18] W.T. Klooster, L. Brammer, C.J. Schaverien, P.H.M. Budzelaar, J. Am. Chem. Soc. 121 (1999) 1381–1382.
[19] J. Lin, Z. Wang, J. Organomet. Chem. 589 (1999) 127–132.
[20] I. Lopes, G.Y. Lin, A. Domingos, R. McDonald, N. Marques, J. Takats, J. Am. Chem. Soc. 121 (1999) 8110–8111.
[21] W.J. Evans, M.A. Greci, M.A. Johnston, J.W. Ziller, Chem. Eur. J. 5 (1999) 3482–3486.
[22] S. Tian, V.M. Arredondo, C.L. Stern, T.J. Marks, Organometallics 18 (1999) 2568–2570.
[23] X. Zhou, Z. Huang, R. Cai, L. Zhang, L. Zhang, X. Huang, Organometallics 18 (1999) 4128–4133.
[24] S. Anfang, T. Gröb, K. Harms, G. Seybert, W. Massa, A. Greiner, K. Dehnicke, Z. Anorg. Allg. Chem. 625 (1999) 1853–1859.
[25] D. Pfeiffer, I.A. Guzei, L.M. Liable-Sands, M.J. Heeg, A.L. Rheingold, C.H. Winter, J. Organomet. Chem. 588 (1999) 167–175.
[26] A.V. Khvostov, B.M. Bulychev, V.K. Belsky, A.I. Sizov, Russ. Chem. Bull. 48 (1999) 2162–2166.
[27] A.A. Trifonov, E.N. Kirillov, M.N. Bochkarev, H. Schumann, S. Mühle, Russ. Chem. Bull. 48 (1999) 382–384.
[28] L.-X. Zhang, X.-G. Zhou, Z.-E. Huang, R.-F. Cai, X.-Y. Huang, Polyhedron 18 (1999) 1533–1537.
[29] T. Labahn, A. Mandel, J. Magull, Z. Anorg. Allg. Chem. 625 (1999) 1273–1277.
[30] H. Schumann, K. Herrmann, J. Demtschuk, S.H. Mühle, Z. Anorg. Allg. Chem. 625 (1999) 1107–1112.
[31] W.J. Evans, G.W. Nyce, R.D. Clark, R.J. Doedens, J.W. Ziller, Angew. Chem. Int. Ed. 38 (1999) 1801–1803.
[32] C.G. Pernin, J.A. Ibers, Inorg. Chem. 38 (1999) 5478–5483.
[33] M.C. Cassani, Y.K. Gun'ko, P.B. Hitchkock, M.F. Lappert, F. Laschi, Organometallics 18 (1999) 5539–5547.
[34] H. Schumann, M.R. Keitsch, J. Demtschuk, G.A. Molander, J. Organomet. Chem. 582 (1999) 70–82.
[35] Z. Xie, Z. Liu, K. Chui, F. Xue, T.C.W. Mak, J. Organomet. Chem. 588 (1999) 78–82.
[36] M. Visseaux, D. Baudry, A. Dormond, C. Qian, J. Organomet. Chem. 574 (1999) 213–218.
[37] H. Schumann, F. Erbstein, J. Demtschuk, R. Weimann, Z. Anorg. Allg. Chem. 625 (1999) 1457–1465.
[38] W.J. Evans, D.A. Cano, M.A. Greci, J.W. Ziller, Organometallics 18 (1999) 1381–1388.
[39] A.V. Khvostov, V.V. Nesterov, B.M. Bulychev, A.I. Sizov, M.Y. Antipin, J. Organomet. Chem. 589 (1999) 222–225.
[40] H. Schumann, K. Zietzke, R. Weimann, J. Demtschuk, W. Kaminski, A.-M. Schauwienold, J. Organomet. Chem. 574 (1999) 228–240.
[41] S. Al-Juaid, Y.K. Gun'ko, P.B. Hitchcock, M.F. Lappert, S. Tian, J. Organomet. Chem. 582 (1999) 143–152.
[42] J. Guan, J. Stehr, R.D. Fischer, Chem. Eur. J. 5 (1999) 1992–2003.
[43] M. Niemeyer, S.-O. Hauber, Z. Anorg. Allg. Chem. 625 (1999) 137–140.
[44] G.B. Deacon, C.M. Forsyth, P.C. Junk, B.W. Skelton, A.H. White, Chem. Eur. J. 5 (1999) 1452–1459.
[45] G.E. Herberich, U. Engler, A. Fischer, J. Ni, A. Schmitz, Organometallics 18 (1999) 5496–5501.
[46] C. Qian, H. Li, J. Sun, W. Nie, J. Organomet. Chem. 585 (1999) 59–62.
[47] H. Schumann, F. Erbstein, D.F. Karasiak, I.L. Fedushkin, J. Demtschuk, F. Girgsdies, Z. Anorg. Allg. Chem. 625 (1999) 781–788.
[48] A.T. Gilbert, B.L. Davis, T.J. Emge, R.D. Broene, Organometallics 18 (1999) 2125–2132.
[49] A.V. Khvostov, B.M. Bulychev, V.K. Belsky, A.I. Sizov, J. Organomet. Chem. 584 (1999) 164–170.

[50] C. Qian, G. Zou, J. Sun, J. Chem. Soc. Dalton Trans. (1999) 519–520.
[51] C. Qian, W. Nie, J. Sun, J. Chem. Soc. Dalton Trans. (1999) 3283–3287.
[52] M.H. Lee, J.-W. Hwang, Y. Kim, J. Kim, Y. Han, Y. Do, Organometallics 18 (1999) 5124–5129.
[53] Z. Xie, S. Wang, Q. Yang, T.C.W. Mak, Organometallics 18 (1999) 1578–1579.
[54] S. Wang, Q. Yang, T.C.W. Mak, Z. Xie, Organometallics 18 (1999) 5511–5517.
[55] G.-X. Jin, Y. Cheng, Y. Lin, Organometallics 18 (1999) 947–949.
[56] W.J. Evans, M.A. Johnston, M.A. Greci, J.W. Ziller, Organometallics 18 (1999) 1460–1464.
[57] G.A. Molander, E.D. Dowdy, J. Org. Chem. 64 (1999) 6515–6517.
[58] V.M. Arredondo, F.E. McDonald, T.J. Marks, Organometallics 18 (1999) 1949–1960.
[59] V.M. Arrendo, S. Tian, F.E. McDonald, T.J. Marks, J. Am. Chem. Soc. 121 (1999) 3633–3639.
[60] G.A. Molander, C.P. Corrette, J. Org. Chem. 64 (1999) 9697–9703.
[61] Y. Kawasaki, A. Fujii, Y. Nakano, S. Sakaguchi, Y. Ishii, J. Org. Chem. 64 (1999) 4214–4216.
[62] D. Baudry-Barbier, E. Camus, A. Dormond, M. Visseaux, Appl. Organometal. Chem. 13 (1999) 813–817.
[63] D. Barbier-Baudry, A. Dormond, P. Desmurs, C.R. Acad. Sci. Ser. IIc: Chim. 2 (1999) 375–378.
[64] S. Kaita, Z. Hou, Y. Wakatsuki, Macromolecules 32 (1999) 9078–9079.
[65] K. Koo, P.-F. Fu, T.J. Marks, Macromolecules 32 (1999) 981–988.
[66] S. Agarwal, N.E. Brandukova-Szmikowski, A. Greiner, Macromol. Rapid Commun. 20 (1999) 274–278.
[67] M. Nishiura, Z. Hou, T.-A. Koizumi, T. Imamoto, Y. Wakatsuki, Macromolecules 32 (1999) 8245–8251.
[68] H. Yasuda, M.-S. Aludin, N. Kitamura, M. Tanabe, H. Sirahama, Macromolecules 32 (1999) 6047–6057.
[69] S.N. Ringelberg, A. Meetsma, B. Hessen, J.H. Teuben, J. Am. Chem. Soc. 121 (1999) 6082–6083.
[70] N. Koga, Theor. Chem. Acta 102 (1999) 285–292.
[71] S.A. Kulkarni, N. Koga, Theochemistry 461–462 (1999) 297–310.
[72] R. Boaretto, P. Roussel, N.W. Alcock, A.J. Kingsley, I.J. Munslow, C.J. Sanders, P. Scott, J. Organomet. Chem. 591 (1999) 174–184.
[73] M. Zhou, L. Andrews, J. Li, B.E. Bursten, J. Am. Chem. Soc. 121 (1999) 12188–12189.
[74] Z. Xie, C. Yan, Q. Yang, T.C.W. Mak, Angew. Chem. Int. Ed. 38 (1999) 1761–1763.
[75] R.G. Peters, B.P. Warner, C.J. Burns, J. Am. Chem. Soc. 121 (1999) 5585–5586.
[76] R.G. Peters, B.J. Warner, B.L. Scott, C.J. Burns, Organometallics 18 (1999) 2587–2589.
[77] R.G. Peters, B.L. Scott, C.J. Burns, Acta Cryst. C55 (1999) 1482–1483.
[78] L. Ventelon, C. Lescop, T. Arliguie, P.C. Leverd, M. Lance, M. Nierlich, M. Ephritikhine, J. Chem. Soc. Chem. Commun. (1999) 659–660.
[79] C. Lescop, T. Arliguie, M. Lance, M. Nierlich, M. Ephritikhine, J. Organomet. Chem. 580 (1999) 137–144.
[80] S.M. Cendrowski-Guillaume, M. Ephritikhine, J. Organomet. Chem. 577 (1999) 161–166.
[81] W.W. Lukens Jr., S.M. Beshouri, L.L. Blosch, A.L. Stuart, R.A. Andersen, Organometallics 18 (1999) 1235–1246.
[82] W.W. Lukens Jr., S.M. Beshouri, A.L. Stuart, R.A. Andersen, Organometallics 18 (1999) 1247–1252.
[83] W.W. Lukens Jr., P.G. Allen, J.J. Bucher, N.M. Edelstein, E.A. Hudson, D.K. Shuh, T. Reich, R.A. Andersen, Organometallics 18 (1999) 1253–1258.
[84] R.C. Schnabel, B.L. Scott, W.H. Smith, C.J. Burns, J. Organomet. Chem. 591 (1999) 14–23.
[85] M. del, M. Conejo, J.S. Parry, E. Carmona, M. Schultz, J.G. Brennann, S.M. Beshouri, R.A. Andersen, R.D. Rogers, S. Coles, M. Hursthouse, Chem. Eur. J. 5 (1999) 3000–3009.
[86] A.K. Dash, J.Q. Wang, M.S. Eisen, Organometallics 18 (1999) 4724–4741.
[87] J.Q. Wang, A.K. Dash, J.C. Berthet, M. Ephritikhine, M.S. Eisen, Organometallics 18 (1999) 2407–2409.
[88] A. Haskel, J.Q. Wang, T. Straub, T.G. Neyroud, M.S. Eisen, J. Am. Chem. Soc. 121 (1999) 3025–3034.
[89] A. Haskel, T. Straub, A.K. Dash, M.S. Eisen, J. Am. Chem. Soc. 121 (1999) 3014–3024.
[90] F.G.N. Cloke, J.C. Green, C.N. Jardine, Organometallics 18 (1999) 1080–1086.